Schweizerische Eidgenossenschaft
Confédération suisse
Confederazione Svizzera
Confederaziun svizra

Department of the Environment, Transport, Energy and Communication DETEC

Swiss Federal Office of Energy SFOE
Energy Research

Final report

Latent Heat Storage for Industrial Processes

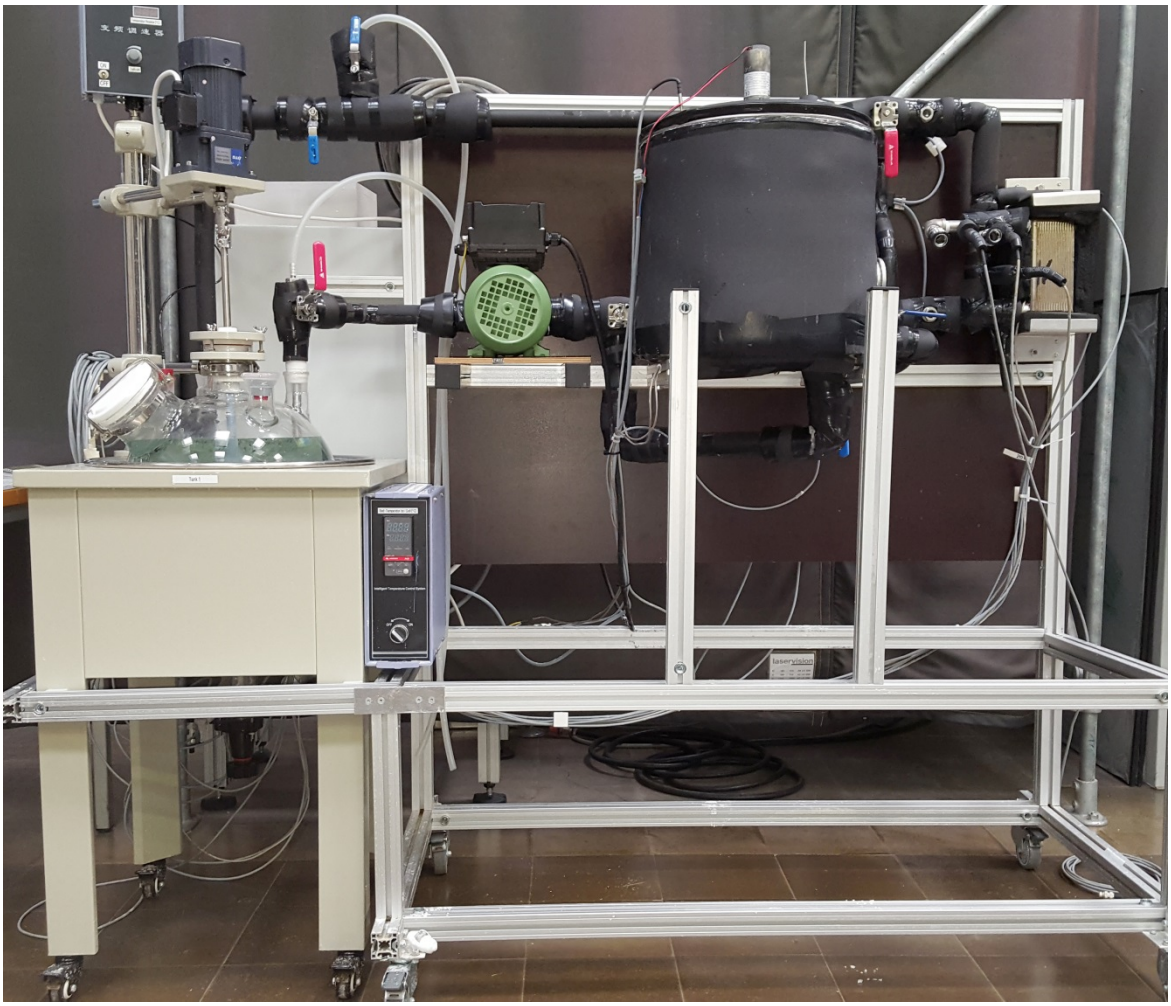

Lucerne University of
Applied Sciences and Arts

HOCHSCHULE
LUZERN

Date: 28.09.2017
Town: Horw

Publisher:
Swiss Federal Office of Energy SFOE
Research Programme Industrial Processes
CH-3003 Bern
www.bfe.admin.ch

Agent:
Lucerne University of Applied Sciences and Arts - Technik & Architektur HSLU T&A
CC Thermal Energy Storage
Technikumstrasse 21
6048 Horw
www.hslu.ch/tes

Authors:
Anastasia Stamatiou, Lucerne University of Applied Sciences and Arts, anastasia.stamatiou@hslu.ch
Remo Waser, Lucerne University of Applied Sciences and Arts, remo.waser@hslu.ch
Stefan Frehner, Lucerne University of Applied Sciences and Arts, stefan.frehner@hslu.ch
Jörg Worlitschek, Lucerne University of Applied Sciences and Arts, jörg.worlitschek@hslu.ch

SFOE head of domain: Carina Alles, Carina.Alles@bfe.admin.ch
SFOE programme manager: Rolf Schmitz
SFOE contract number: SI/501389-01

Swiss Federal Office of Energy SFOE
Mühlestrasse 4, CH-3063 Ittigen; postal address: CH-3003 Bern
Phone +41 58 462 56 11 · Fax +41 58 463 25 00 · contact@bfe.admin.ch · www.bfe.admin.ch

Zusammenfassung

Das Bewertungsgremium des SCCER hat den Stellenwert der Integration von thermischen Energiespeichern in Industrieprozessen in der Schweiz erkannt. Latentwärmespeicher haben im Vergleich zu konventionellen, sensiblen Speichern eine höhere Energiedichte bei konstantem Temperaturniveau. Das vorliegende Projekt untersucht das Konzept von Phasenwechsel-Slurries (PCS), welche durch eine partielle Kristallisation von Phasenwechselmaterialien (PCM) erzeugt werden. PCS-Systeme versprechen im Vergleich zu sensiblen Systemen sowohl als Wärmeträgerfluid wie auch als Speichermaterial höhere Energiedichten. Gleichzeitig bleiben sie pumpbar, wodurch sie bessere Wärmeübertragungseigenschaften als herkömmlichen PCM-Technologien aufweisen. Zudem können durch die Technologie hohe thermische Leistungen bei grosser Temperaturstabilität in kompakter technischer Ausführung mit konventionellen Komponenten erreicht werden. Das Hauptziel des Projektes ist die Ausarbeitung eines Proof-of-Concept Teststandes zur Demonstrierung der Machbarkeit einer kontinuierlichen, kontrollierten Kristallisation eines PCS im relevanten Temperaturbereich für Schweizerische Industrieanwendungen.

Durch eine Evaluierung wichtiger Batch Prozesse in der Industrie wurde der Fokus auf Materialien mit einer Schmelztemperatur im Bereich 60-90°C gelegt. Eine Kombination aus gemessenen und aus der Literatur entnommenen thermophysikalischen Eigenschaften führten zur Auswahl von Aluminiumammoniumsulfat Dodecahydrat ($NH_4Al(SO_4)_2 \cdot 12H_2O$) (AAH) als vielversprechendstes PCM. Die Hauptkriterien waren die hohe Phasenwechselenthalpie und die Möglichkeit, den Schmelzpunk durch die Beigabe von Wasser im gesamten, relevanten Temperaturbereich zu variieren. Wichtige thermophysikalische Eigenschaften des Materiales, wie zum Beispiel Phasenwechselenthalpie und Schmelzpunkt, wurden experimentell untersucht. Die Verwendung von Additiven wurde geprüft, um die Fluidität zu verbessern, sowie die Segregationsrate von soliden Kristallen im PCS zu verringern.

Ein funktionstüchtiger, modularer, hochtemperatur-PCS Teststand bestehend aus herkömmlichen Industriekomponenten und einem modularen Edelstahl-Rohrsystem wurde entwickelt und erfolgreich in Betrieb genommen. Weiter wurde eine experimentelle Versuchsreihe mit AAH mit einer Konzentration von 35wt% AAH in Wasser (Schmelzpunkt 52°C) und 45wt% AAH (Schmelzpunkt 63°C) durchgeführt. Die Machbarkeit für kontinuierliches Erstarren wie auch Schmelzen der PCS konnte im Teststand wurde demonstriert. Zusätzlich wurde die ununterbrochene, kontinuierliche Pumpbarkeit der AAH-Slurry mit einem Feststoffanteil von bis zu 30% aufgezeigt. Kritische Aspekt der Technologie, wie das Segregationsverhalten der PCS und di Initiierung der Kristallisation an einem kontrollierten Ort, wurden identifiziert.

Eine techno-ökonomische Analyse hat ergeben, dass es ein hoher Feststoffanteil der Slurry während des Laden und Entladens kristallisiert, beziehungsweise geschmolzen werden muss, damit die Attraktivität der Technologie gegeben ist. Es zeigte sich, dass mit einem Feststoffanteil von 25% eine Volumenreduktion von bis zu 50% im Vergleich zu Wasser erreicht wird.

Im Rahmen des Projektes wurde das hohe Potenzial von Phasenwechsel-Slurries als Wärmeträgerfluid und Speichermaterial demonstriert. Um die Herausforderungen bezüglich Segregation sowie unkontrollierte Kristallisation zu lösen, sollten weitere Untersuchungen durgeführt werden. Die Vorteile, welche PCS in Bezug auf die Temperaturstabilität bieten, sollten in nachfolgenden techno-ökonomischen Studien berücksichtigt werden, da diese eine Schlüsselrolle zur Marktdurchdringung der Technologie in Industrieprozessen spielen könnten.

Summary

The evaluation panel of SCCER has emphasized the importance of the integration of thermal energy storage in the Swiss industry. Latent heat storage technologies can offer more compact thermal storage at a constant temperature level, in comparison to conventional, sensible thermal storage technologies. In this project the concept of Phase Change Slurries (PCS) is investigated which is produced via a partial crystallization of a Phase Change Material (PCM). PCS systems promise higher energy densities both as heat transfer fluids and as storage media in comparison to sensible systems. At the same time they remain pumpable and therefore can achieve much better heat transfer characteristics than conventional latent heat storage technologies. This technology is expected to deliver high thermal power and high temperature stability in a compact design that can operate with conventional components. The main objective of this project is the development of a proof-of-concept test rig to demonstrate the feasibility of a continuous and controllable crystallization of a PCS at temperatures relevant to the Swiss Industry.

An evaluation of important batch processes in the Swiss Industry set the focus on materials with a melting point in the range of 60-90 °C. A combination of measured and literature-based thermo-physical properties pointed to aluminium ammonium sulfate dodecahydrate (AAH) (NH4Al(SO4)2·12H2O) to be the most promising PCM. Key criteria were its high phase change enthalpy and the adaptability of its melting point via the addition of water to cover the whole temperature range of interest. Important thermo-physical characteristics of the material, such as phase change enthalpy and melting point, were experimentally investigated. The use of additives was examined to increase the fluidity and decrease the sedimentation rate of the crystals in the PCS.

A functional, modular, high temperature phase change slurry test-rig based on standard industrial components and a modular stainless steel piping system was developed and successfully commissioned. Experimental campaigns were conducted using AAH with a concentration of 35wt% of AAH in water (melting point of 52 °C) and 45wt% AAH (melting point of 63 °C). The feasibility of both continuous crystallization and melting of the PCS could be demonstrated in the test-rig. Furthermore, uninterrupted, continuous pumping of the AAH-slurry with a solid fraction of up to 30% could be shown. Critical characteristics of the technology were identified with respect to segregation of the PCS and initiation of the crystallization in a controlled location of the test-rig.

A techno-economic analysis revealed that a high fraction of the slurry needs to be crystallized and melted during charging and discharging of the storage to enable a good performance of the technology. It was demonstrated that a volume reduction of up to 50% with respect to water storage can be achieved if the cycled fraction is 25%.

In the framework of this project Phase Change Slurries have demonstrated their high potential as advanced heat transfer fluids and storage media. Further work needs to be undergone to tackle the challenges of material separation and unreliable triggering of crystallization. The added value that a PCS can offer in a process in terms of temperature stability needs to be considered in following techno-economic studies as it could play a crucial role for the penetration of the technology in industrial processes.

Contents

List of Abbreviations

AAH	Aluminium Ammonium Sulfate Dodecahydrate
DSC	Differential Scanning Calorimetry
HSLU	Lucerne University of Applied Sciences and Arts
PCD	Phase Change Dispersion
PCM	Phase Change Material
PCS	Phase Change Slurry
PVA	Poly –vinyl alchohol
TBAB	Tetra-n-butylammonium bromide
TMC	Trimethyl Ammonium Chloride
WP	Work Package

1. Introduction

1.1. Background and Motivation

The evaluation panel of SCCER has emphasized the importance of the integration of thermal energy storage in the Swiss industry. Latent heat storage technologies can offer more compact thermal storage at a constant temperature level, in comparison to conventional, sensible thermal storage technologies. The focus of this project is the development of latent heat storage solutions for process heat in the Swiss industry based on the Phase Change Material Slurry (PCS) concept. The term “homogeneous slurries” will be used in this study to describe “ice-slurry-like” slurries, which are the topic of the present investigation. Homogeneous slurries are based on the partial crystallisation/melting of a flow containing a Phase Change Material (PCM). Such systems promise higher energy densities both as heat transfer fluids and as storage media while presenting much better heat transfer characteristics than conventional

storage technologies. The main advantages that this technology is expected to possess in comparison to conventional heat stores are:

- Higher heat transfer rates and operational flexibility in comparison to latent heat storage due to heat transfer between two liquids.
- Higher temperature stability/constancy during the heat transfer which could have major advantages for processes that operate optimally in a narrow temperature range.
- Cost-efficient construction in comparison to latent heat storage via the use of standard heat exchangers (e.g. plate heat exchangers) and other components.
- Higher energy density and lower volume in comparison to sensible storage

1.2. Project Definition and Goals

The deliverables of the project as they were defined in the proposal can be summarized as follows:

- Identification and evaluation of Phase Change Material (PCM) to be used for the slurry
- Development of an experimental crystallization process in the laboratory that can can demonstrate continuous and controllable PCS production.
- Realization of a cost-estimation for the PCS technology.

2. Choice of Relevant Temperature Level for the Swiss Industry

In order to select the focus - temperature of this study, a report of processes that are relevant to the Swiss industry and could profit from the implementation of latent heat storage was created. A part of the report is included in the present document while the whole report can be found as a separate attachment. The following criteria were applied when considering the processes that could profit the most from the integration of a latent heat storage.

- Processes with a high energy consumption on a national level (High energy saving potential for Switzerland)
- Processes with a low or no difference between inlet and outlet temperature (match with the melting/solidification temperature profile of Phase Change Materials)
- Discontinuous processes (Batch processes) which are suitable for indirect heat recovery via thermal energy storage.

The industrial heat demand of different Swiss industries is shown in Figure 1. An especially high demand exists in the chemical-, pharma-, cement-, food- and paper/printing industry.

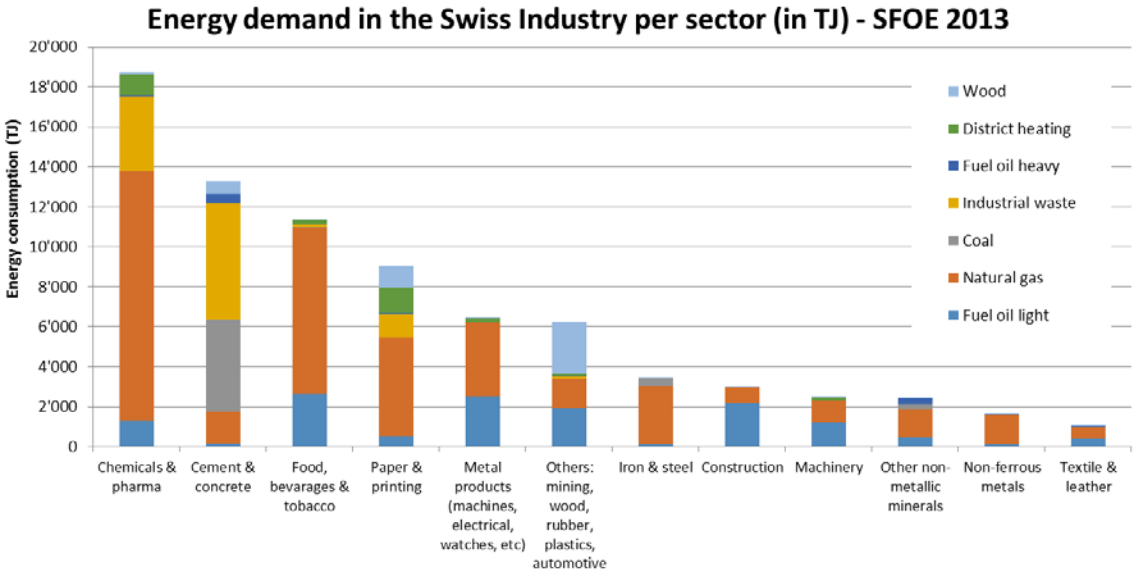

Figure 1. Industrial heat demand in Switzerland [1]**.**

Heat is used in various industrial processes in a wide temperature range. German industry shows a similar distribution of heat demand as Switzerland (see Figure 2). A lot of energy in the upper temperature range is consumed for metals, cement and chemical products [2]. If the industrial heat for hot water and space heating is included, a relatively high energy demand at low temperatures is revealed(< 100 °C) .

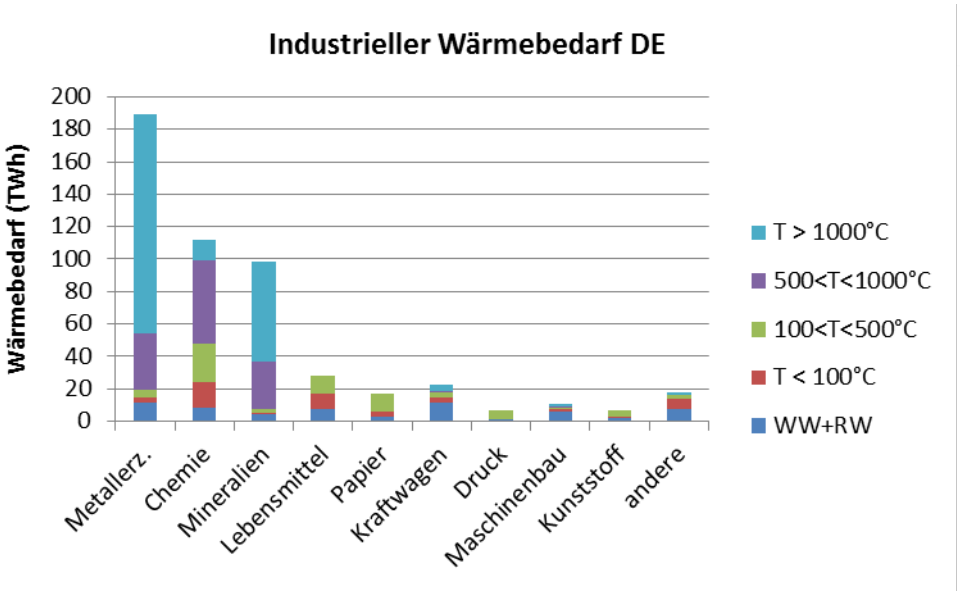

Figure 2. Industrial heat demand in Germany [2]

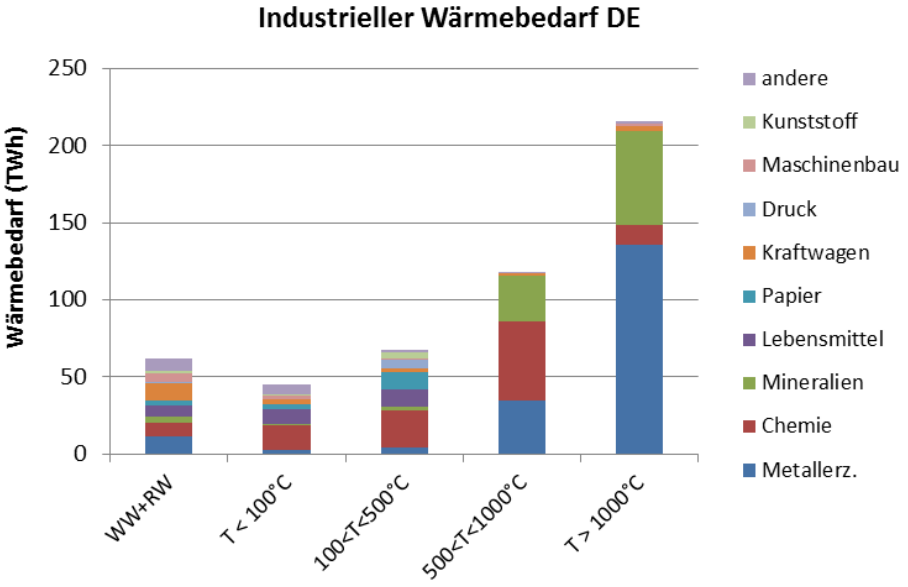

Figure 3. Industrial heat demand in Germany : process heat, warm water heat (WW) and space heating (RH) [2]**.**

The EU-27 also attributes a high energy consumption to the chemical-, food-, and paper industry, of which a substantial part is at a low temperature level (see Figure 4).

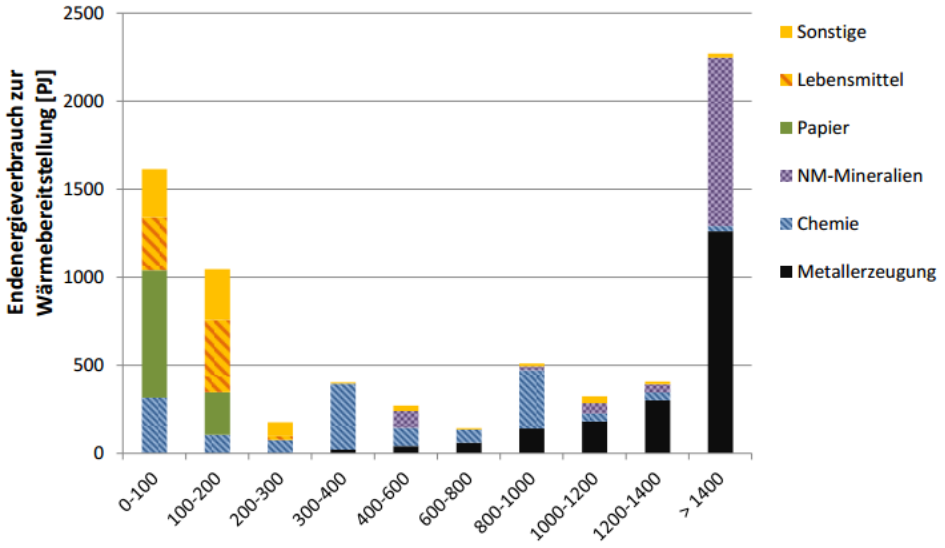

Figure 4. Industrial heat supply at differen temperature levels (°C) of the EU-27 [3]**.**

Industrial heat demand of temperatures T<250°C in Germany is also dominated by the chemical-, food- and paper industry [4] (see Figure 5).

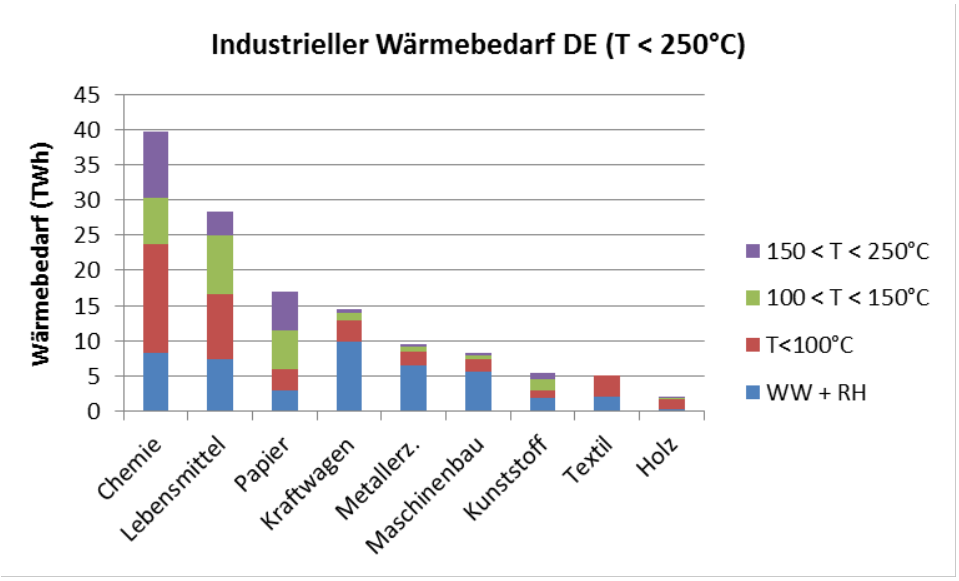

Figure 5. Industrial heat demand in germany T<250°C : process heat, warm water heat (WW) and space heating (RH) [4]**.**

A closer examination shows that the process heat is especially needed at temperatures below 100 ° C . The heat demand of T < 100 ° C is 60 % higher compared to the temperature interval 100 < T < 150 ° C and 100 % higher compared to the temperature interval 150 < T < 250 ° C - not counting heat for hot water and space heating (see Figure 6).

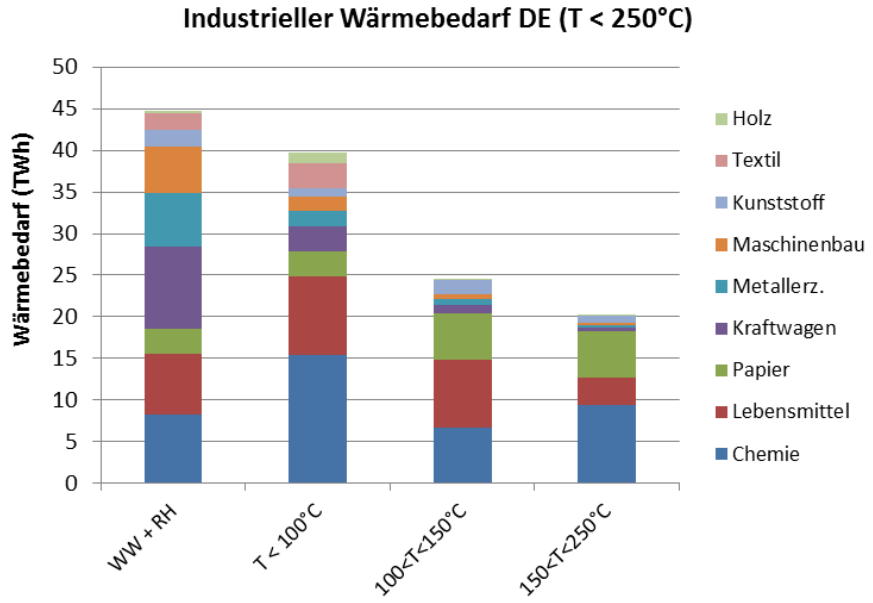

Figure 6. Industrial heat demand in germany T<250°C : process heat, warm water heat (WW) and space heating (RH) [4]

The illustration bellow (Figure 7) gives a comprehensive overview of the most common temperature levels of various industrial processes. Data shows that the temperature interval needed in the majority of industrial processes is between 20°C to 100°C which also reflects in the higher heat demand of said interval shown in Figure 6.

For temperatures higher than 100°C, it is to be expected that a big part of thermal energy demand is covered by chemical processes for drying and distilling due to their high temperature difference (100-250°C). This heterogeneity of different chemical processes is a deciding factor for the observed temperature spread (see attached report). This spread also has as a consequence, that the process heat available for a given temperature level is relatively small.

A higher potential regarding process heat is to be found in the temperature interval from 60-100°C since a majority of the processes operates in that range. Especially various pasteurizing processes in the food industry (dairy, beer and beverage production) require heat at temperatures from 60 to 100 °C. The pasteurization processes are also often associated with heat recovery resulting in a low difference between inlet and outlet temperature. Under these circumstances, latent heat storage presents a very high energy density compared to sensible heat storage and can be particularly interesting. It should also be noted that food industry utilizes semi-continuous or batch processes (see attachment), which is relevant for indirect heat recovery by means of heat storage. Hot water and space heating can be partially covered by the temperature range 60-100°C which increases the potential even further.

A thermal storage can be attractive not only from the perspective of the process but also for heat supply. By using a heat-pump heat and cold can be generated simultaneously very efficiently. The integration of thermal storage in such systems allows for the operation of the heat pump under fluctuating heat and cold loads. Storage solutions in the range of 50-90°C appear to be particularly relevant for such applications since this is the temperature output

range of industrial heat pumps. Additionally, solar heat can be implemented as a heat source as seen in examples from the brewing industry [5]. The efficiency of solar thermal collectors decreases with increasing temperature. Therefore the solar process heat should be integrated at the lowest possible temperature level [2]. This means that for system integration, a storage temperature below 100 °C is recommended.

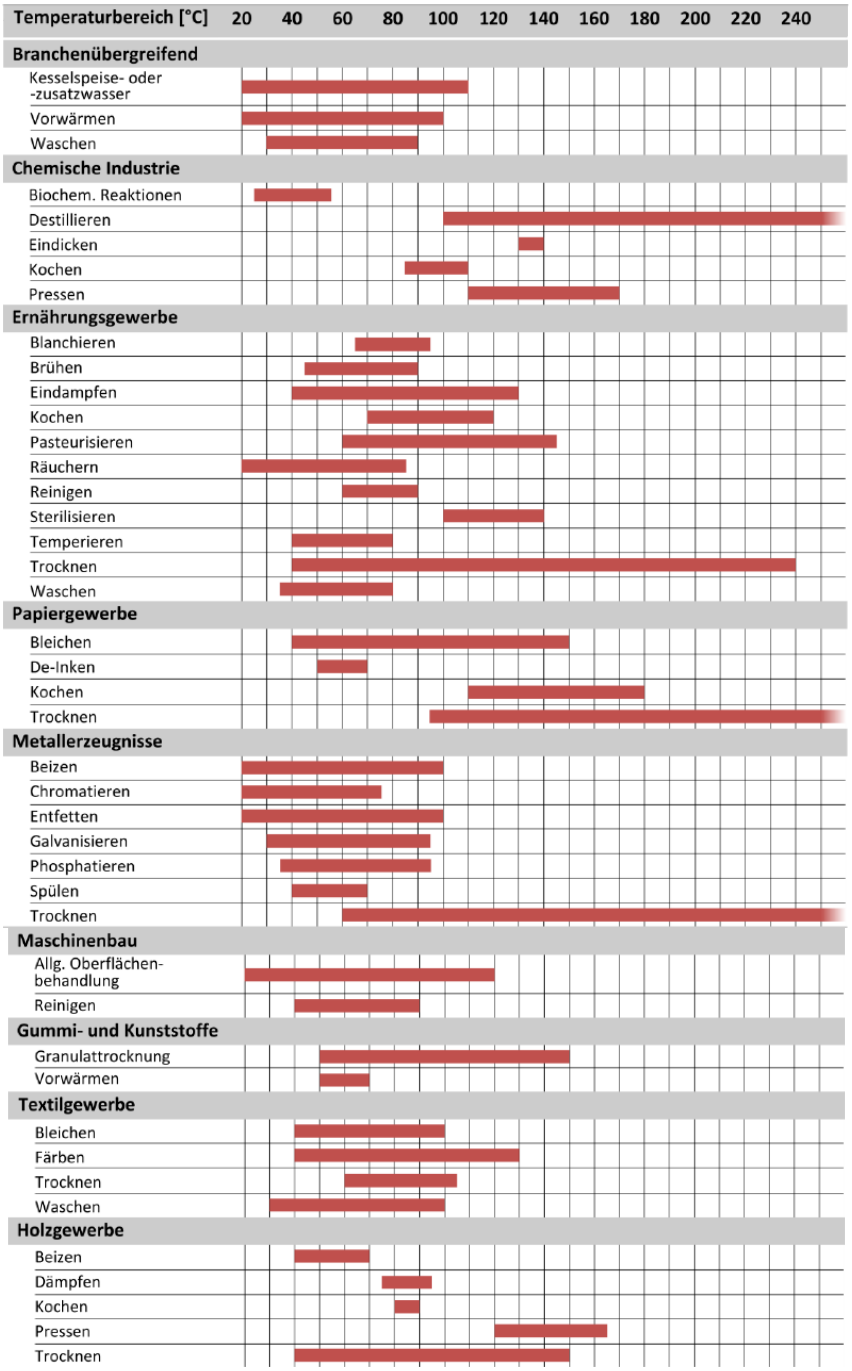

Figure 7. Overview of temperature levels in industrial processes [4]

Overall, the available data of the industrial processes show, that the temperature range of 60-90 ° C is of great interest for the use as latent heat storage. In particular, the food industry with

its high energy demand, pasteurizing processes with low inlet and outlet temperatures and semi-continuous or batch processes, can be referred to as relevant. Storage technology is an attractive addition for heat supply via heat pump or in combination with solar heat. **The focus temperature of this study is therefore set to 60-90°C**.

3. Literature Review on Phase Change Slurries (PCS)

In this chapter an extensive literature review on Phase Change Slurries (PCS) is presented. The largest part of the relevant literature is dedicated to ice slurries and was used as the basis for this work. A separate section is dedicated to the few but very relevant publications concerning PCSs with other PCM apart from water.

3.1. Definition of PCM Slurries

No clear term could be found, that describes the type of PCM slurries that are the topic of the present study (PCM slurries similar to ice slurries). The term slurry generally includes any fluid that consists of a continuous fluid phase with a dispersed solid phase. This comprises not only quasi one-component systems (e.g. water with a small amount of additives) such as ice slurries but also other types of fluids. The types of fluids that are relevant to latent heat storage and are characterised as slurries can be categorised as follows:

– Microencapsulated PCS (MPCS): Solid-liquid suspensions where the PCM is encapsulated in a polymeric capsule forming, particles with a diameter between 0.001-1 mm [6]. MPCS have the advantage that they don't agglomerate and are mechanically protected by the encapsulation but are quite expensive and also present some stability issues.

– Phase Change Dispersions (PCD) are typically paraffin droplets which are dispersed in a continuous water phase by the use of surfactants. In contrast to ice slurries, they are characterised by very small particle/droplet diameter (< 10 µm). Additionally, in contrast to ice-type slurries, the fluid remains a 2-phase fluid both when the dispersed phase is melted and when is frozen.

– Homogeneous slurries: This term which will be used in this study to describe "ice -like" slurries, which are the topic of the present investigation. Similarly to PCDs, homogeneous slurries are 2-phase fluids below the melting point of the dispersed phase. However they form a homogeneous solution above the melting point of the dispersed phase. This slurry type includes: ice slurries, clathrate slurries and salt hydrate slurries. In contrast to Phase Change Dispersions (PCD), such slurries form larger particles with a diameter between 0.1 and 1 mm.

As described in the project proposal, the focus of this project is set to slurries that have a similar behaviour as ice slurries, defined in the report as "homogeneous slurries".

3.2. Ice Slurries

3.2.1. Motivation

The industrial application of ice slurries began approximately 35 years ago [7]. The initial trigger was the implementation of legislations promoting the use of secondary refrigeration loops in industrial applications in order to reduce the mass of primary refrigerants and therefore

the associated greenhouse gas emissions [8]. Ice slurries were proposed as advanced secondary fluids for such applications. Some advantages of ice slurries are [7,9]:

- They have a higher energy density than conventional secondary refrigerants leading to reduction of equipment size (up to 50% reduction in the piping diameter, reduction in pump size) and cost saving. This also leads to lower pumping energy consumption (down to 60% of the initial consumption).
- 50-100% higher heat transfer coefficients in comparison to conventional heat transfer fluids.
- They can be used also for direct product cooling (e.g. fish), in contrast to conventional ice storage media.
- High temperature stability (especially if no freezing depressants are used).
- Possibility to decouple thermal power from storage capacity in contract to conventional latent storage technologies.
- They can be directly combined with compact thermal energy storage in a more straight forward manner than conventional single phase working fluids.

3.2.2. Production Methods

Ice slurries are the most widely investigated type of slurry. They are a mixture of water and small ice particles (diameter: 0.1 – 1 mm). The melting point of pure ice slurries is 0°C but it can be lowered down to -40°C with the addition of freezing point depressant [10]. The most widespread production method of ice slurries is their direct solidification of part of the water on the walls of a heat exchanger and the use of some sort of **mechanical surface scraper or brush** to release the particles in the water flow. The main disadvantages of this method are its high investment, operation and maintenance costs [8,10]. Another popular method for ice generation is the **supercooling (cooling down below the freezing point) of the water in a conventional heat exchanger with subsequent crystallisation**. After the water exits the heat exchanger it is physically disturbed to generate ice crystals in the bulk volume of the water transforming the sensible heat to latent. The crystallization can take place in the storage tank or in the pipes. No record has been found of ice particles being produced directly in the heat exchanger, apparently because even in low solid mass fraction, some ice particles will inevitably get stuck on the heat exchanger wall [11]. In contrast to freezing/charging, the melting/discharging of ice slurry is possible in conventional heat exchangers, such as tube-shell or plate heat exchangers [12]. This method is simpler and has lower operation costs than the mechanical scraper method. However the supercooling or initiation of crystallization cannot be fully controlled which leads to blockage incidents in the heat exchangers [8].

Supercooling is an inherently stochastic effect but many factors influence probability of a crystallization incident under specific conditions [8,11]:

– Degree of supercooling; The higher the difference between the freezing point and the PCM temperature, the higher the probability of the occurrence of a crystallization incident. In fact studies have shown that a supercooling degree of 2 K for water is the highest that can be applied without too many incidents of uncontrolled crystallisation occurring inside the heat exchanger.

– Surface characteristics of heat exchanger: Rough surfaces tend to induce more crystallisation incidents in comparison to polished surfaces.

– Sudden increase/decrease of the flow rate.

– Collision and friction of solid against solid.

– Application of electrical charge, using ultrasonic irradiation/vibration, seeding with small ice crystals.

– Bubbling of a fluid through the water.

Additional ice slurry production methods include: (a) **direct contact heat exchange** where a primary or secondary refrigerant bubbles directly through the water and exchanges heat without an intermediate heat exchanger surface [13] and (b) **vacuum ice systems** [7].

The main obstacle to the wider spreading of ice slurries is the high cost [10]. In the case of production using supercooling, another hindrance is the unstable operation that can lead to blockage of heat exchangers and pipes [8]. According to [8], some crystallisation incidents are inevitable and therefore a defrosting system had to be foreseen in each ice slurry production site. Additionally the water to be supercooled must be preheated to 0.5 °C before entering the heat exchanger to ensure that no small ice crystals exist in the flow which could serve as nucleation sites.

3.2.3. Solid Mass Fraction and Flow Properties

The slurry flow properties are of crucial importance to ensure good heat transfer characteristics, stable operation and energetic efficiency. The fraction of solid particles in the flow is one of the most decisive factors for the flow properties of the ice slurries. It has been shown that when the ice mass fraction ranges between 0-30%, the slurry is still considered pumpable [10]. Generally, high solid mass fraction leads to higher energy densities and therefore smaller piping systems and heat exchangers. Furthermore higher solid mass fractions lead to higher viscosities, higher pressure drops and therefore higher pumping power. Additionally slurries with high solid fractions require lower temperatures for their production which also has an energetic penalty for the process [10].

Particle geometry (size, globular shape, smoothness) is also decisive when it comes to slurry flow properties. Particularly it was shown that ice slurries with dendritic and globular shapes resulted in plugging even for low solid mass fractions. On the contrary, particles which were initially globular but were smoothed thermally or chemically (with freezing point depressants) presented good flow characteristics even at high fractions of solids [9]. Additives such as glycol generally increase the viscosity but they can also cause chemical smoothing of the particles resulting better flow characteristics. It has been shown that ice slurries produced with the supercooling method contain rougher particles which cannot be properly smoothened even by using chemical or thermal smoothing [9].

3.2.4. Additives

The most common additives used in the generation of ices slurries, are freezing point depressants such as alcohols, glycols and salts [7]. They cause the freezing point of the water/additive solution to decrease below 0°C. The freezing point continues to decrease with an increasing amount of additive until it reaches the eutectic point of the solution (if such a point exists) where the solution solidifies uniformly in one constant temperature. When the solution temperature drops below the freezing temperature of the specific mixture, pure ice crystals start to form causing the concentration of additive in the solution to increase and the

freezing point to decrease. In case the temperature is further reduced, this process continues further until the eutectic point is reached. If the crystallization doesn't take place entirely, exactly at the eutectic point, then the crystallization process ceases to be isothermal. Therefore additives should be avoided in PCM applications which require isothermal charging and discharging, unless the initial concentration matches the eutectic concentration.

As mentioned in the previous section, particles which were initially globular but were smoothed thermally or chemically (with freezing point depressant) presented good flow characteristics even at high fractions of solids [9]. Therefore chemicals such as glycol can also be added to the water, to chemically smoothen the ice particles and enhance the flow properties of the slurry.

Other additives that have been used to enhance the performance of ice slurries are [14]: (a) supercooling-supressing additives (e.g. Polyvinyl alcohols (PVA), sodium oleate etc) and (b) anti-agglomeration additives. Investigations of other PCM slurries have also employed the use of drag reducing agents [15].

3.2.5. Storage

Ice slurry typically shouldn't contain more than 30% solid mass fraction when being pumped but can contain up to 60% when stored [10]. There are four main concepts for the ice slurry storage [11].

- Continuous homogeneous mixing of the slurry in the storage tank. It guarantees a homogeneous operation but is very energy consuming.
- Intermittent mixing. The stirring doesn't take place at hours where the storage is not used (e.g. night)
- No mixing – chilled water storage. The storage is completely stratified. Cold water is extracted from the bottom of the storage to be used for the cooling applications
- No mixing – screw particle transportation. The storage is completely stratified. A homogeneous slurry with a controlled, pre-defined ice fraction is created for the cooling applications by mechanically removing ice particles from the top of the storage using a screw and mixing them with ice water.

3.3. Other "Homogeneous" PCM Slurries

Very few substances have been evaluated for their suitability to create "homogeneous" slurries apart from water. Furthermore, most of the investigated slurries were considered for cooling applications and therefore have a freezing point below 30°C. The most investigated substance after water is Tetra-n-butylammonium bromide (TBAB) clathrate hydrate [16–18]. TBAB hydrates have good thermo-physical properties and high enthalpy of fusion. The melting point depends on the concentration of TBAB in water but most of the studies focus on the aqueous solutions with a concentration of 36.5 wt% TBAB and a melting point of 12.5 °C. In contrast to ice slurry generation, some investigators tried to generate the TBAB crystals directly in the heat exchanger. However some formation of crystals was observed in the walls of the heat exchanger which resulted to an increased pressure drop [17]. A few other clathrate hydrate candidates have been tested, including trimethylolethane hydrate slurries [19–21]. Clathrate

hydrates are only suitable for refrigeration applications at ambient pressure and will not be further considered in this work.

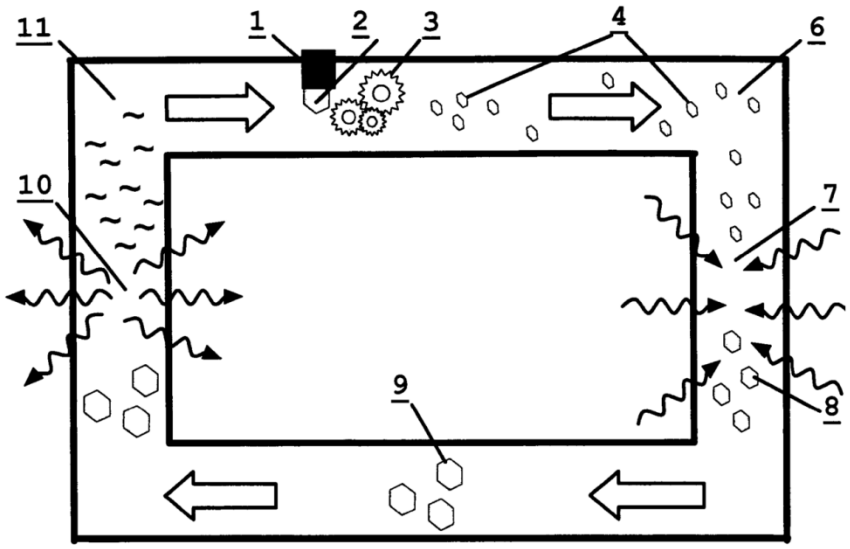

Figure 8. Example of a K_2HPO_4 $6H_2O$ slurry generation unit [22]

The other class of PCM that has been considered for its application in PCM slurries are salt hydrates. Mehling et al. [22] proposed the use of salt-hydrates with low crystallisation rates (e.g. $K_2HPO_4 \cdot 6H_2O$, m.p. 14°C, $Ca(NO_3)_2 \cdot 4H_2O$ m.p. 43°C, $KAl(SO_4)_2$ $12H_2O$, m.p. 91°C, $NH_4Al(SO)_4 \cdot 12H2O$, m.p. 94.5°C) in PCM slurries. He proposed bringing the salt hydrate melt in a supercooled state and seeding with crystals of the same substance to initiate the freezing process. According the same patent because of the low crystallization rates of salt hydrates their particles are not expected to grow more than 1 mm in diameter. According to the authors, this should prevent the agglomeration problems that are observed in other slurries like ice slurries. Figure 8 shows an example of a proposed unit to create $K_2HPO_4 \cdot 6H_2O$ slurry. $K_2HPO_4 \cdot 6H_2O$ is flowing through a tube and passes through a point where $K_2HPO_4 \cdot 6H_2O$ crystals are generated via a Peltier element (1). The crystals are detached via ultrasound and crushed in a mechanical device and are released in the mixture as it flows to the heat sink where the $K_2HPO4 \cdot 6H_2O$ is crystallized. The control of the crystallization is achieved by the natural limitation of the $K_2HPO_4 \cdot 6H_2O$ particles in not growing more than 1 mm in diameter.

Schmit et al. [23] further investigated potassium hydrogen phosphate hexahydrate ($K_2HPO_4 \cdot 6H_2O$, m.p. 14°C) slurry. The feasibility of generating $K_2HPO_4 \cdot 6H_2O$ slurries in a plate heat exchanger was reportedly demonstrated in a student thesis conducted in ZAE Bayern. Some difficulties were encountered with respect to: (a) large supercooling, (b) semi-congruent melting (c) difficulty in preparing a stoichiometrically correct sample and (d) small volume change between solid and liquid (problem in determining the charging degree). The material properties were determined and a turbidity sensor was employed and calibrated to measure the % of charging of the storage. A T-history device was used to provide the mass fraction data for the calibration. An electric heater was used to melt the slurry before the PCM entered the heat exchanger but not all solid particles could be melted. This was attributed to the very high viscosity of the slurry with up to 30% solid fraction (0.0072 Pa s at 14°C) which induces a

laminar flow and low heat transfer. It is also attributed to the formation of $K_2HPO_4 \cdot 3H_2O$ which has a higher melting temperature as well as to the low heat conductivity of the $K_2HPO_4 \cdot 6H_2O$. To initiate solidification of the PCM, the flow was seeded with existing $K_2HPO_4 \cdot 6H_2O$ crystals which the researchers prepared by cooling down the hydrate to -30 °C.

Suzuki et al. [24] investigated $Na_2HPO_4 \cdot 12H_2O$ slurries for applications in combination with an absorption chiller at 35 °C. Pure $Na_2HPO_4 \cdot 12H_2O$, has a phase change enthalpy of 281 kJ/kg. As the freezing point is above room temperature, the particular hydrate would form one solid block at room temperature, rendering the cold start-up of the system very difficult. Therefore the solution of $Na_2HPO_4 \cdot 12H_2O$ with water/glycol mixtures was investigated. Glycol decreases the solubility of salt hydrates at high temperatures and at the right concentrations can provide a fluid slurry mixture at room temperature. In this study, the weight ratio of ethylene glycol to solvent mixture, ξ (ξ = w_{glycol}/ (w_{H2O+} $w_{glycol)}$) was varied from 0 to 0.7. A mixture ratio, ξ of 0.4 and a hydrate concentration of 50 wt% in glycol/water were found to be the most appropriate for the application in question. At this concentration the slurry has a 16.5 wt% solid fraction at the phase change temperature and 40 wt% solid fraction at room temperature (see Figure 9). The authors considered this to be a low enough crystal fraction to enable a problem-free, cold start-up. The latent heat available at these conditions was measure in a Differential Scanning Calorimeter (DSC) to be 45 kJ/kg, which was considered to be sufficiently high for the purpose of the application. In addition, the particle size was found to be 0.1 mm right after the slurry production and 0.2 mm after 1 h of storage which was considered small enough to flow through the heat exchangers and tubes without causing blocking.

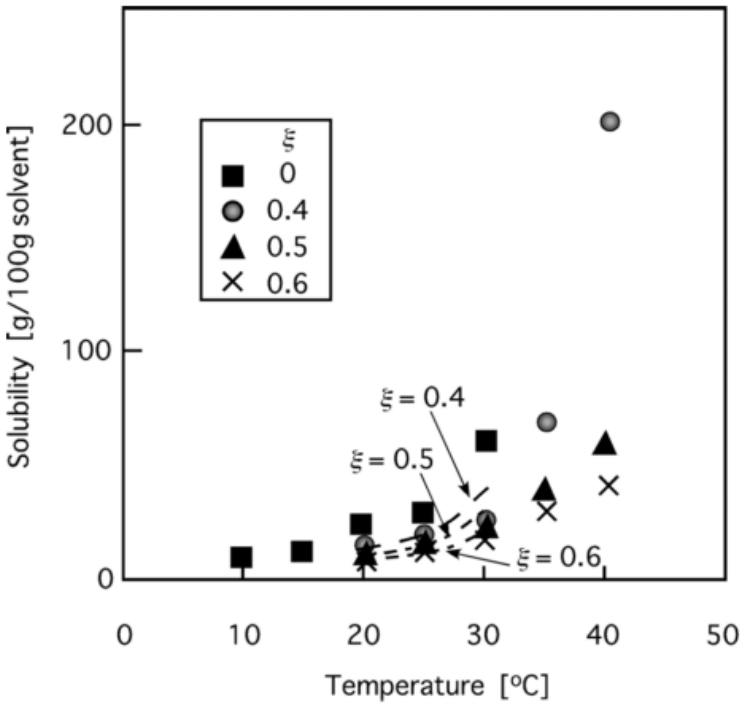

Figure 9. Solubility of 50 wt% $Na_2HPO_4 \cdot 12H_2O$ in water/glycol solvent mixtures as a function of temperature and solvent composition. ξ is defined as the weight ratio of ethylene glycol to solvent mixture (w_{glycol}/ (w_{H2O}+ w_{glycol})) [24]

The only high-temperature slurry that has been reported to this date is based on aluminum ammonium sulfate disodium dodecahydrate (ammonium alum hydrate, $NH_4Al(SO_4)_2 \cdot 12H_2O$) with a latent heat of 251 kJ/kg and a phase change temperature of 94.5 °C [25–27]. Similarly to $Na_2HPO_4 \cdot 12H_2O$, the phase change temperature of ammonium alum hydrate can be altered by varying its concentration in a solvent. In the specific study, the phase change temperature was set at 51 °C with a 35 wt% concentration in pure water, intended for domestic applications. According to [27], at this concentration, a hydrate solid fraction of 12 wt% solid fraction is present at 51°C which becomes 29 wt% at 10 °C, ensuring a smooth start-up at room temperature.

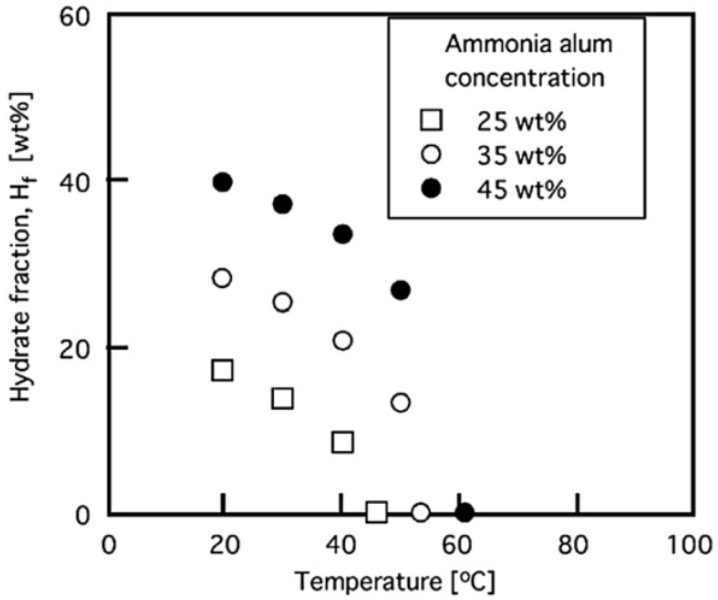

Figure 10. Solid hydrate fraction of ammonia alum as a function of temperature in different concentrations in water [27]

A major challenge with ammonium alum hydrate is the high density (1,630 kg/m^3) of the solid particles which causes very fast separation of the continuous and dispersed phase of the slurry. However it has been shown that the addition of a combination of Poly Vinyl Alcohol (PVA) as an emulsifier and cationic surfactants can reduce segregation and increase system fluidity [28].

4. Material Selection, Evaluation and Modification

In this chapter the material selection and evaluation is presented. The goal of this part of the project was the identification of a phase change material suitable for the creation of phase change slurries in the temperature range of 60-90°C. In a first step an extended literature review was performed to identify suitable PCM based on their thermo-physical properties. Promising candidates were tested experimentally at HSLU. After the PCM was chosen a second phase was initiated, investigating the use of surfactants and thickeners to decrease the sedimentation speed of the slurry and increase its fluidity.

4.1. Phase Change Material Identification and Evaluation

The first step for the selection of a PCM candidate for the slurry production for industrial was a material screening. For this purpose, a list of criteria that assesses the suitability of a specific material for the application was considered of great use. As it is expected that no material will be able to fulfil all set criteria, a further classification of the requirements according to their importance (High, Medium, Low) was considered necessary. In this process both general criteria that render a PCM suitable for latent heat storage were considered as well as slurry-specific criteria. Whereas generally favourable PCM characteristics have been broadly discussed in literature [29,30], very little information could be found on favourable slurry-specific characteristics. After the criteria list was set, the evaluation took place based mostly on literature data. Promising candidates with missing thermo-physical data can were when necessary characterized in the HSLU analytical laboratory in terms of their melting enthalpy, freezing/melting point, heat conductivity, heat capacity.

4.1.1. List of Selection Criteria

Table 1 summarises the selection criteria for the PCM with an indication of their importance. The slurry-specific requirements were deduced from the publications mentioned in Section 3.3 and where completed with observations from the first crystallisation experiments conducted at HSLU.

Selection Criteria

1	General PCM Characteristics	Importance
1.1	Melting point at temperature relevant for the Swiss industry (60-90 °C)	H – One of the main project requirements (See chapter 2)
1.2	A high phase change enthalpy per unit volume	H – Decisive for the compactness and economics of the system
1.3	A high specific heat	M – Desired but not crucial
1.4	High thermal conductivity of both phases	M – Less important than in static storage since forced convection will take place
1.5	Low supercooling effect	N.A. Depending on the slurry production concept low supercooling can be a positive or a negative characteristic
1.6	An adequate rate of crystallization	H – Too slow crystallisation will negatively affect the effective heat transfer; too fast crystallisation could prevent the production of a stable slurry
1.7	A small volume change on phase transformation	L – Not so important in the case of slurries.
1.8	Congruent melting and solidification	M – Less important than in static applications, since mixing takes place

1.9	High density	M - The higher the density the smaller the components; good for the economics and compactness
1.10	Long-term stability	H- Very important for the economics
1.11	Compatibility with the construction materials	M- The construction materials can be adapted to the characteristics of the slurry
1.12	Non-toxic, non-flammable and non-explosive to ensure safety	M- Less important for industrial applications
1.13	Low price	H – Especially important for homogeneous slurries where only a part of the purchased PCM contributes to the storage
2	**Slurry-Specific Characteristics**	
2.1	Ability to form stable slurry	H- Not all PCMs are able to form slurries
2.2	Low viscosity	M- Important but can be regulated with additives
2.3	Controllable particle size/geometry to prevent blockage	H- Blockage incidents are decisive for the viability of slurries; additives can be used to assist particle geometry control
2.4	Fluidity at room temperature	M- Can be of importance to facilitate start-up but remains to be defined how crucial it is
2.5	Repeatable supercooling	H-Decisive for the controllability of the system

Table 1. Generic and slurry-specific criteria for PCM selection with indicated importance. H- stands for high importance, M- for medium importance and L- for low importance; N.A. not applicable in the case of PCM slurries

4.1.2. Experimental Equipment

A Differential Scanning Calorimeter (DSC) from Mettler Toledo was employed to determine the phase change temperature and phase change enthalpy of the PCM of interest. In some cases DSC was not suitable for the determination of these properties due to: (i) small sample size (in the order of µg) which enhanced supercooling effects and (ii) static conditions (no stirring) which enabled separation of the PCM or PSC in its components. In such case crystallisation experiments were conducted in an Easymax 102 – Advanced Synthesis Workstation from Mettler Toledo, available at HSLU (see Figure 11). The device comprises two identical reactors (sample holders) with a volume of 100 mL each. Their temperature is regulated by two heating jackets outside of the reactors which can deliver temperatures from -40°C – 180 °C. The temperature profile of the two reactors can be regulated independently while both the jacket and the reactor temperature are recorded continuously. Magnetic stirrers are employed to ensure a good heat transfer, homogenous temperature profile within the reactor and homogenous slurry distribution in the reactors.

Figure 11. Easymax 102 from Mettler Toledo used for melting and crystallization experiments

4.1.3. Choice of PCM

A pre-screening of PCM classes revealed that the most promising candidates for further investigations are salt hydrates. The ability of some salt hydrates to form stable slurries has been demonstrated in literature. Quite some salt hydrates exist in the temperature range of interest for this study. They are generally characterized by high melting enthalpies and low prices. In case a suitable salt hydrate can be found which can operate after being dissolved in water, the economics can become even more favourable. It is also possible that fluidity at room temperature can be ensured by addition of water/solvents. They generally present a high supercooling, which could also be advantageous depending on the slurry generation concept. Issues with corrosiveness and phase segregation can be dealt with appropriate material choice and utilisation of additives.

After salt hydrates were finalised as the PCM class of choice for this project, a literature review was conducted to search for specific materials. The relevant salt hydrates that could be found in literature are listed in Table 2. The first and most important criterion is the suitability of the melting and freezing temperature of the material (60-90 °C for this study). Since the phase change temperature can be lowered by the addition of water and other solvents and additives, also salt hydrates with melting points higher than 90°C were included. Studying of phase diagrams would be crucial for the identification of interesting mixtures but their availability is very scarce. Experimental determination of points in phase diagrams is very time consuming and will only be performed, if necessary, for PCMs that show a very promising behaviour in the crystallisation experiments.

Since the resources of the present study in terms of material research are limited, it was decided that only pure substances with a relevant phase change temperature and mixtures with known phase diagrams will be considered. It was further decided to exclude from further consideration commercial substance with unknown consistencies as well as materials that haven’t been considered as PCM to this date. DSC measurements and first crystallisation experiments were conducted for promising candidates

Name	Formula	Melting point °C	Melting Enthalpy kJ/kg	Comments
Lithium acetate dihydrate	$LiCH_3COO \cdot 2H_2O$	70	150	[31] Unlikely to be used because of Li
Sodium pyrophosphate decahydrate	$Na_2P_2O_7 \cdot 10H_2O$	70	184	[32]
Aluminium nitrate nonahydrate	$Al(NO_3)_2 \cdot 9H_2O$	72	155	[31]
Barium hydroxide octahydrate	$Ba(OH)_2 \cdot 8H_2O$	78	265	[31,33]
Aluminium sulfate octadecahydrate	$Al_2(SO_4)_3 \cdot 18H_2O$	88	218	[34]
Strontium bromide hexahydrate	$SrBr_2 \cdot 6H_20$	88	159	Own measurement, commercial PCM, with additives
Magnesium nitrate hexahydrate	$Mg(NO_3)_2 \cdot 6H_2O$	89	162.8	[35]
SP90	Unknown	89	150	Commercial PCM from Rubitherm
Strontium hydroxide octahydrate	$Sr(OH)_2 \cdot 8H_2O$	89	370	[34]
Aluminium nitrate octahydrate	$Al(NO_3)_2 \cdot 8H_2O$	89.5		[36]
Aluminium potassium sulfate dodecahydrate	$KAl(SO_4)_2 \cdot 12H_2O$	91	184	[31]
Aluminium ammonium sulfate dodecahydrate	$NH_4Al(SO_4)_2 \cdot 12H_2O$	94.5	251	[27] Feasibility for slurry production has been demonstrated
Lithium chloride hydrate	$LiCl \cdot H_2O$	99	212	[34] Unlikely to be implemented because of Li
Calcium bromide tetrahydrate	$CaBr_2 \cdot 4H_20$	110		[34] Could be relevant after dilution with water
Magnesium chloride hexahydrate	$MgCl_2 \cdot 6H_2O$	117	167	[31] Could be relevant after dilution with water
Magnesium bromide hexahydrate	$MgBr_2 \cdot 6H_2O$	164.4	150	[37] Could be relevant after dilution with water

Table 2. Salt hydrates with relevant melting points

After this evaluation procedure, it was decided to move forward with aluminium ammonium sulfate dodecahydrate ($NH_4Al(SO_4)_2 \cdot 12H_2O$) as the main PCM candidate for the next steps of this study. It is one of the best characterised salt hydrates available in this temperature range. Additionally, $NH_4Al(SO_4)_2 \cdot 12H_2O$ is not flammable or explosive and is presents no major health issues for humans apart from mild irritations. Its ability to produce slurries has been demonstrated and no degradation issues have been reported (see Section 3.3). It has been shown that segregation issues can be dealt with, by adding of small amounts of additives. A first market research indicates that the particular hydrate could be found at a rather low price. One of the main advantages of $NH_4Al(SO_4)_2 \cdot 12H_2O$ is that its melting temperature can be regulated with the addition of water to cover the whole range of chosen temperatures (60-90 °C) rather than only one specific point (see Figure 12).

4.1.4. Characteristics of Aluminium Ammonium Sulfate Dodecahydrate

Phase change temperature and phase diagram

The melting temperature of pure AAH amounts to 94.5°C and can be lowered by the addition of water. Figure 12 (a) shows the melting temperature of AAH as a function of the water concentration determined by Suzuki et al. in [21]. In the present work, slurries with an AAH concentration of 35 wt% as well as 45 wt% and a corresponding phase change temperature of approximately 52°C respectively 63°C are used.

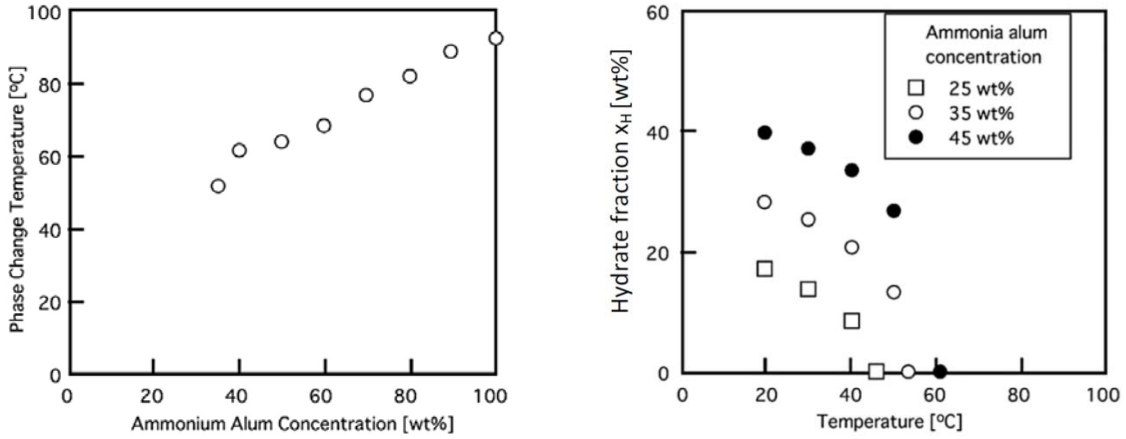

Figure 12. (a) Phase change temperature of Aluminium Ammonium Sulfate Dodecahydrate as a function of its concentration in water and (b) solid hydrate fraction for different water dilutions as a function of temperature [27]**.**

The hydrate fraction x_H in the water-AAH solution depends on the temperature of the solution as shown in Figure 12 (b). It is worth mentioning that Suzuki et al. concluded that an AAH concentration of 35% appears to be optimal for the production of PCM slurry. One reason for this is the fact that even at 20°C the solid faction is not higher than 30% and thus the PCM water solution should remain pumpable at room temperature. On the other hand, as shown in Figure 12 (b) with a concentration of 45wt%, the solid fraction at 20°C is more than twice as high as for the 35wt% solution. Hence, it can be expected that the 45wt% AAH slurry is considerable more challenging regarding blockage of the system as the 35wt% AAH.

Enthalpy and specific heat capacity

In the salt hydrate phase change slurries, heat is stored respectively released sensible in the liquid and solid phase as well as latent due to the solution or dissolution of hydrate crystals as previously described. Mathematically, the specific enthalpy of the used PCS h_{PCS} at temperature T with respect to an arbitrary chosen reference temperature T_{ref} may be written as:

$$\boldsymbol{h_{PCS}(T) = \int_{T_{ref}}^{T} cp_s \cdot x_H(T) \cdot dT + \Delta x_H(T) \cdot \Delta h_{\{PC\}} + \int_{T_{ref}}^{T} cp_l \cdot (1 - x_H(T)) \cdot dT} \qquad \textbf{(1)}$$

where the first term on the right hand side of the equation describes the sensible heat in the solid phase, the second term the latent heat and the third term the sensible heat stored in the liquid phase. $\Delta x_H(T)$ describes the change of the hydrate fraction in the solution between the two temperature levels:

$$\boldsymbol{\Delta x_H(T) = x_H(T) - x_H(T_{ref})} \qquad \textbf{(2)}$$

If an equivalent, constant heat capacity in the liquid and solid phase is assumed, Equation 1 simplifies to:

$$\boldsymbol{h_{PCS}(T) = cp_{PCS} \cdot (T - T_{ref}) + \Delta x_H \cdot \Delta h_{PC,PCS}} \qquad \textbf{(3)}$$

In theory, the heat capacity cp is the partial derivative of the enthalpy with respect to the temperature at constant pressure p [38]. Since in the present application, the storage of latent and sensible heat occurs simultaneously, the concept of the apparent specific heat capacity, which was introduced in the field of numerical simulations [39] is used. Thus, the specific apparent heat capacity can be calculated using following equation:

$$\boldsymbol{cp = \frac{\partial h_{PCS}}{\partial T}} \qquad \textbf{(4)}$$

Based on the phase change enthalpy of the dodecahydrate, liquid heat capacity and hydrate mass fraction determined in [40], the enthalpy and apparent heat capacity can be calculated as a function of the temperate T as shown in Figure 13 with a reference temperature T_{ref} of 25°C. Enthalpy and apparent heat capacity are in general considerable higher as of water. As illustrated, the heat capacity of both fluids have a peak at the melting temperature since at this point, the change of the hydrate fraction with temperature is maximal and thus a large amount of latent heat is released respectively absorbed.

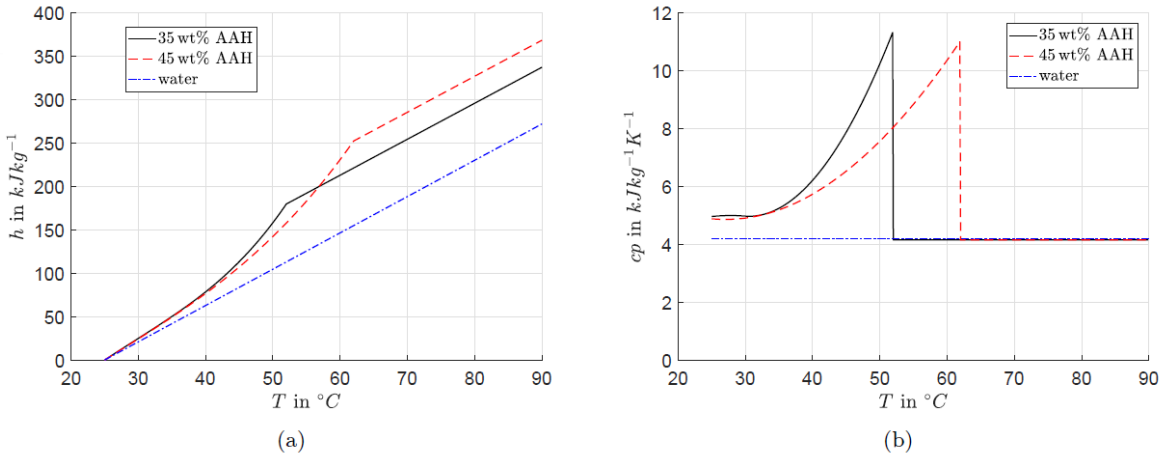

Figure 13. (a) Enthalpy of the AAH slurry for a hydrate concentration of 35% and 45% as a function of the temperature with a reference temperature of 25°C. (b) Apparent specific heat capacity as a function of the temperature. In both plots, the properties of the AAH slurry are compared with water.

4.1.5. Measurements of Thermo-physical Properties

The pure AAH was tested with DCS and showed a melting temperature of 94.67 °C and high melting enthalpy of 255 kJ/kg was measured in HSLU (see Figure 14), which is expected to decrease after the addition of water.

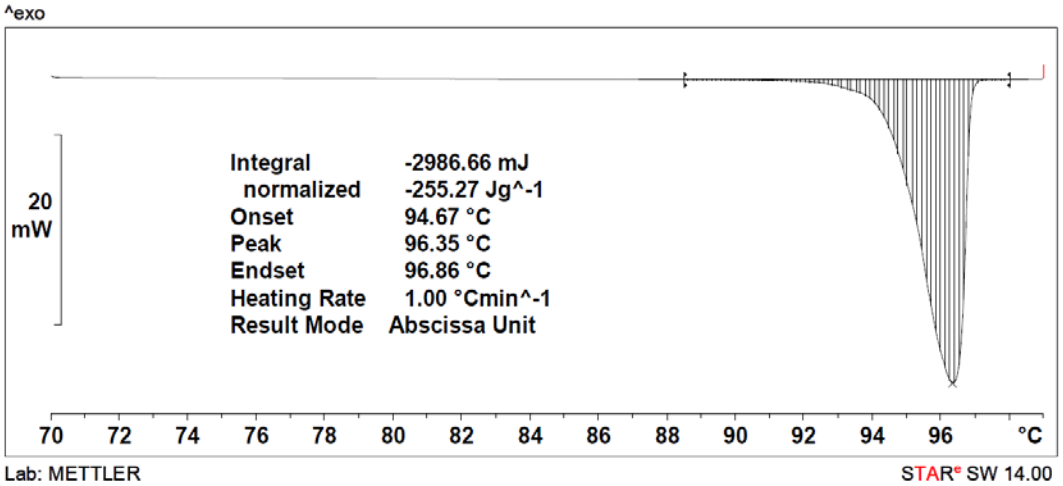

Figure 14. Result of DSC measurement of undiluted Aluminium Ammonium Sulfate Dodecahydrate, conducted at HSLU. The onset temperature and melting enthalpy agree well with the values reported in literature.

Samples containing 35% and 45% AAH in water were also tested in DSC. As seen in Figure 15, no peak could be measured in the expected temperature range. This fact points to very high supercooling and/or segregation of the mixture to its components. Therefore the DSC was

not suitable for testing of AAH/water mixtures and the Easymax was used for further experimentation.

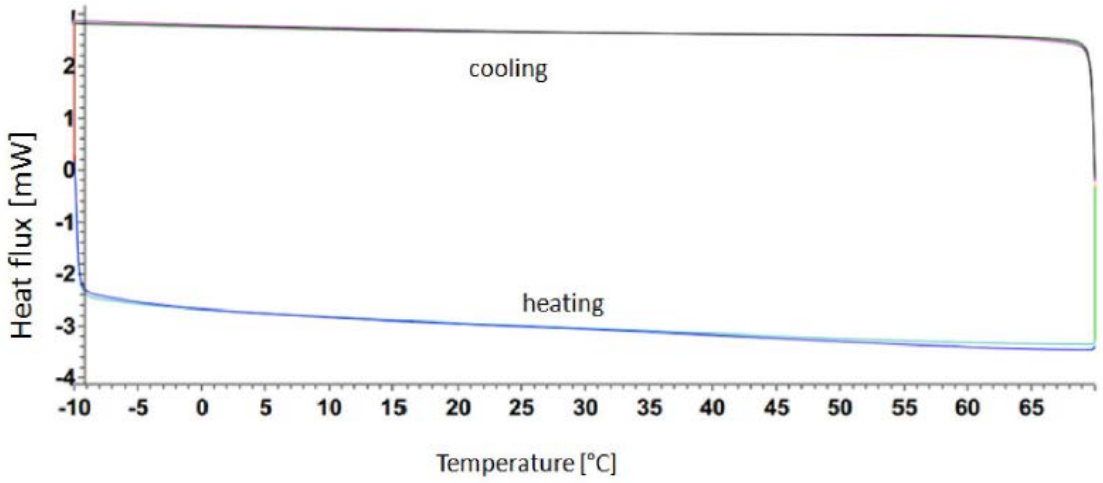

Figure 15. DSC measurement with 35% AAH in water. No peak can be observed in the temperature of interest indicating very high supercooling or segregation of the sample.

Figure 16 (a) and Figure 17(a) show several crystallization and melting cycles in the Easymax with samples of 35% and 45% AAH in water respectively. The peaks that can be observed during the cooling ramps indicate crystallization after supercooling. These peaks reveal that the supercooling degree varied strongly and crystallization temperature varied from 6.7°C to 25.7°C for the 35% AAH (expected melting point at 52°C) and from 35.8 °C to 48.1 °C for the 45% AAH (expected melting point at 63°C). In contrast to the crystallization experiments, the melting experiments showed very good agreement with literature. As seen in Figure 16 (b) and Figure 17(b), the melting points were determined using a tangential along the measured slurry temperature. With this method, the melting temperature was measure between 55.1 and 55.6 °C for the 35% AAH and between 63.6 and 64°C for the 45% AAH.

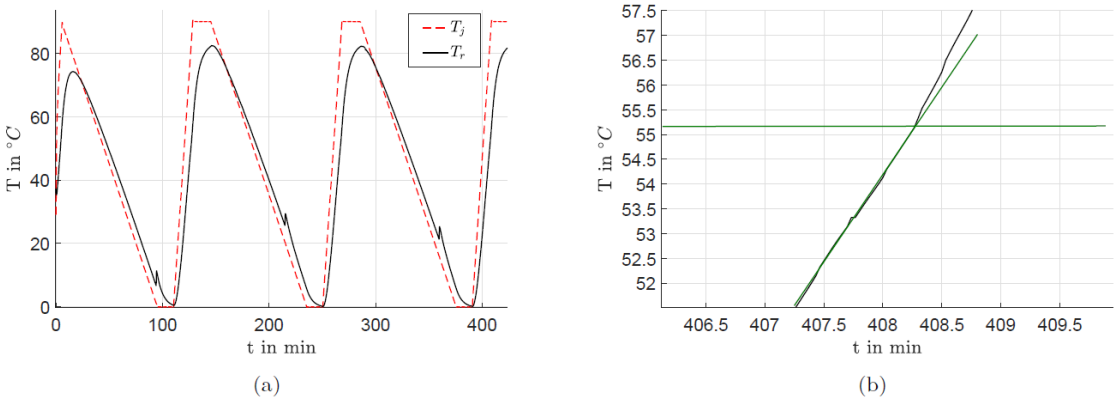

Figure 16. Jacket Tj and slurry Tr temperature versus time for the entire measurement period. (b) Determination of the melting temperature with a tangential line along the slurry temperature curve. When the heating rate of the ammonium alum sulfate water solution is increasing abruptly, it can be assumed that no more crystals are present in the sample and the liquidus

line is reached.

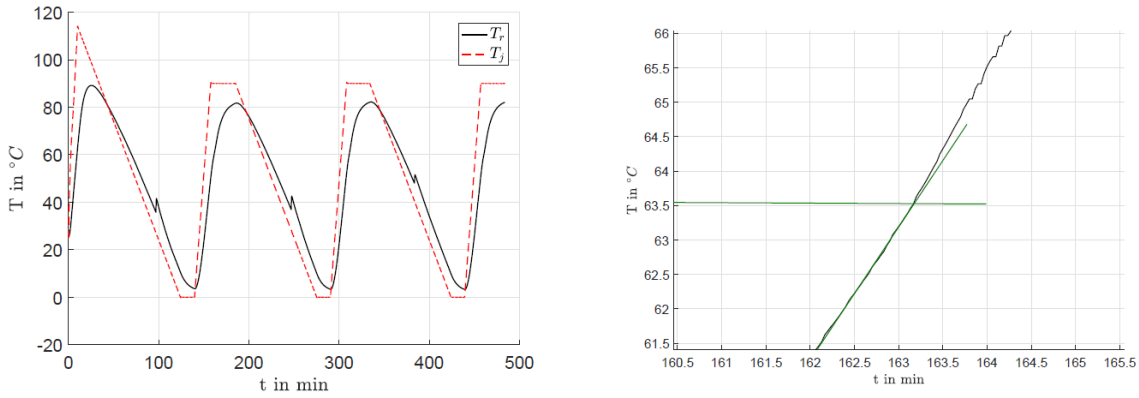

Figure 17. (a) Jacket Tj and slurry Tr temperature versus time for the entire measurement. (b) Determination of the melting temperature using the same approach as for the 35wt% slurry.

Figure 18, shows parts of a phase diagram of the Aluminium Ammonium Sulfate -water system as they were measured at HSLU and reported at [27]. In literature, only one source could be found which provides a phase diagram of the considered salt hydrate [41]. A comparison between the results obtained by HSLU/Suzuki et al. and the phase diagram published by Lane is given in Figure 18. As shown, the two plots are in relatively good agreement.

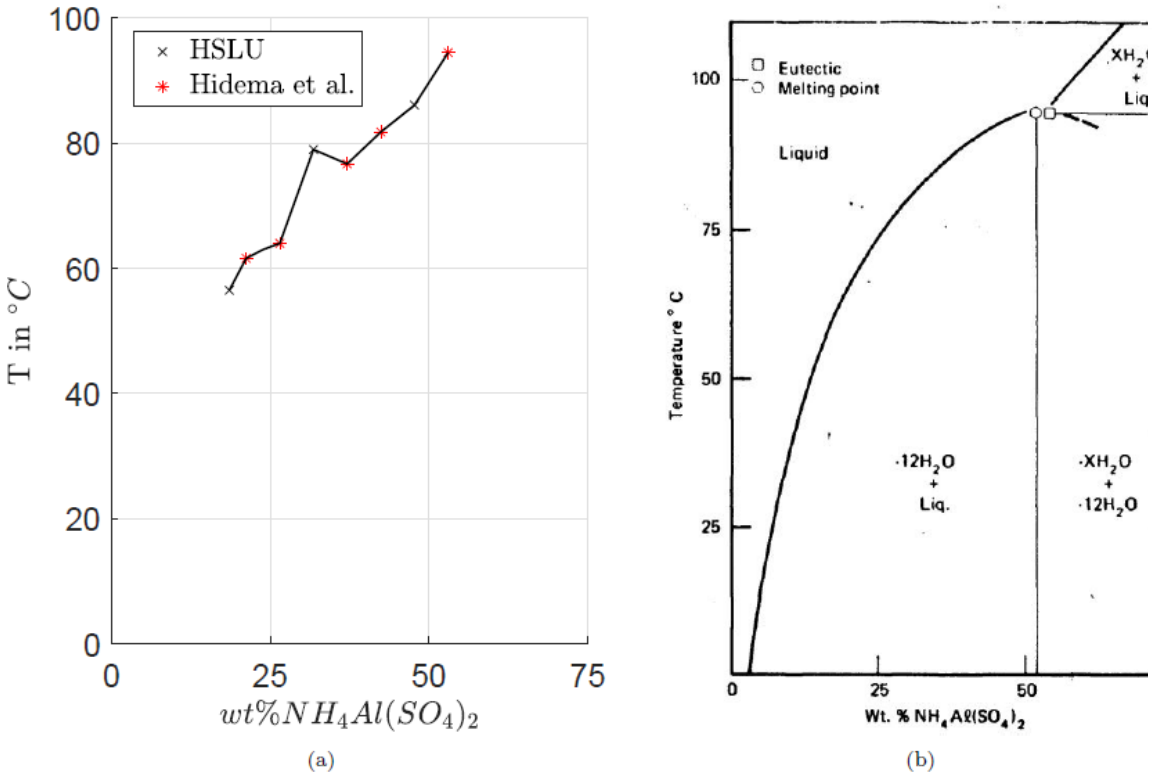

Figure 18. (a) liquidus line determined for an Aluminium Ammonium Sulfate -water system based on literature data and measurements performed in the Easymax. (b) Phase diagram of the same aluminium ammonium sulfate -water system found in literature [41]**.**

Figure 19 shows pictures taken during and after the Easymax experiments. It can be seen that the $NH_4Al(SO_4)_2 \cdot 12H_2O$ particles segregated and gathered to the bottom of the beaker a few seconds after the magnetic stirring was stopped. This has also been reported in literature and has to be treated with the mixing of additives (see Section 3.3). As expected the slurry remained a mixture of solid particles and liquid solution even at room temperature.

Figure 19. 45wt% slurry: (a) Sample with a temperature above the melting temperature, (b) crystallized PCS at approx. 15 °C shortly after the stirrer stopped, (c) the same sample after 30s without stirring.

4.2. Material Optimization

4.2.1. Motivation

As already mentioned and observed in Figure 19, a major challenge with ammonium alum hydrate is the high density (1,630 kg/m^3) of the solid particles which causes very fast separation of the continuous and dispersed phase of the slurry. This can have severe effects in the system operability, especially in the case of a power shortage or a pump failure that would cause the PCS to remain static. In such an event the crystals would segregate, and the start-up of the system would become especially challenging.

It has been shown in previous studies that the addition of a combination of additives can reduce segregation and increase system fluidity [28]. More specifically addition of a combination of three additives has been proposed: (i) Behenyl Trimethyl Ammonium Chloride as surfactant, (ii) Sodium Salicylate as counter ions and (iii) PVA with a degree of polymerization of 500 as a stabilizer. A combination of these additives in the right ratio, in a mixture containing 35% Alum Amon in water, has been shown to produce rod-like micelles which increase fluidity (see Figure 20) and can delay sedimentation for up to two days (see Figure 21) [26,28]. Additionally it was also shown that the addition of these substances, can lead to a reduced crystal size which is also desirable as smaller crystals are less likely to cause system blockage (see Figure 21).
In order to ensure a stable plant operation also in case of pump inoperability, it was decided to use try to reproduce the composition proposed by Hidema et al. The methodology and materials used are described in the following sections.

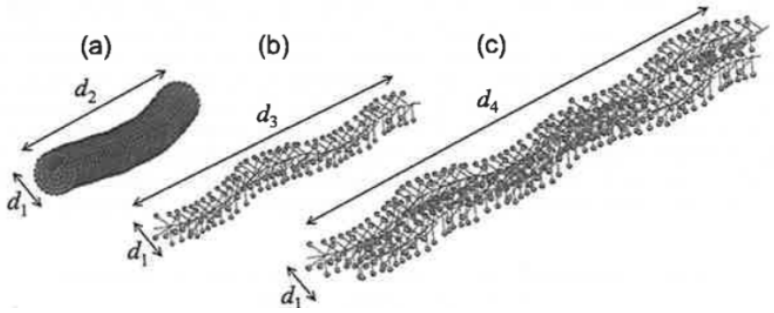

Figure 20. Illustration of formed rod-like micelles and PVA enclosed by surfactant [28]

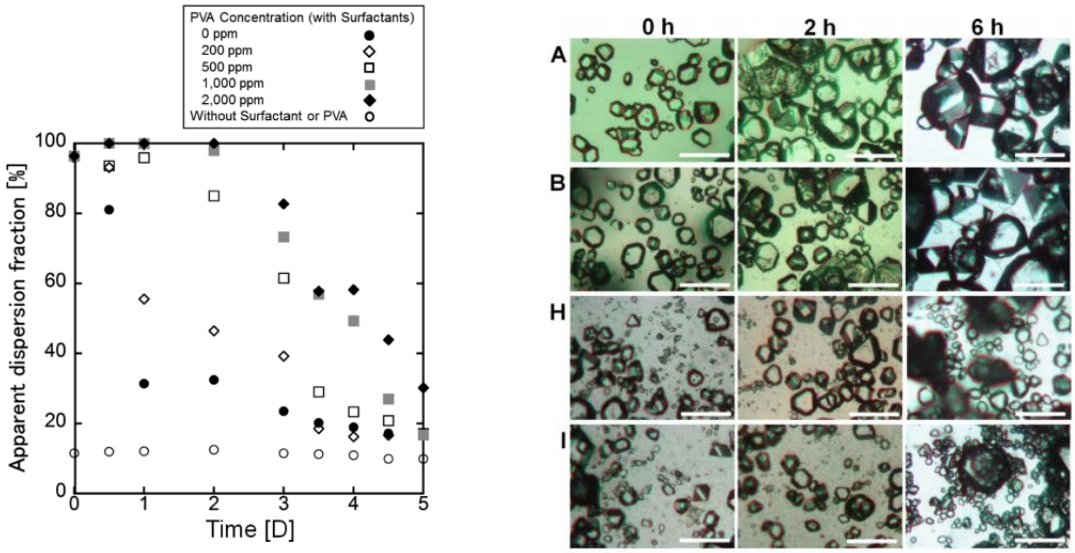

Figure 21. (left) Apparent dispersion fraction during the sedimentation experiments and (right) ammonium alum hydrate crystals after at 0, 2, and 6h, after creation and with increasing amount of PVA from top to bottom. Scale bars indicate 500 µm; [26]

4.2.2. Methodology

Materials

As mentioned in the previous section, the combination of additives proposed by Hidema et al. [28] was used in order to reproduce their reported results. The list of materials used can be seen in Table 3. Since not exactly the same PVA and the same Behenyl Trimethyl Ammonium Chloride could be purchased as the ones reported by Hidema et al., two different types of each substance where used to test the influence of the material production method on the results. Specifically, two different PVAs were used during the experiments, namely one from the manufacturer ‘Colltec’ (saponification factor ~1 and polymerization of 500) and one from the manufacturer ‘Kuraray’ (saponification factor 98.0 – 98.8 and polymerization of 500). Because thickeners are known to have a positive effect on the homogeneity of salt hydrates mixtures

also without the use of surfactants [42], the use of two additional thickeners (Silicon dioxide and Carboxymethyl-cellulose sodium salt) were tested and the results were compared with the recipe proposed by Hidema et al.

Material	Specification	Purpose
Aluminium Ammonium Sulfat Dodecahydrate	251 kJ/kg	Latent heat material
Behenyl TMC-25-MBAL-PA	in cetostearyl alcohol	Ionic surfactant
Behenyl TMC-85		Ionic surfactant
Natrium Salicylat		Counter ion
Polyvinyl alcohol (Colltec)	Sap. ~1	Thickening agent
Polyvinyl alcohol (Kuraray)	Sap. 98.0 – 98.8	Thickening agent
Aerosil	Silicon dioxide	Thickening agent
Alfa aesar	Carboxymethyl-cellulose sodium salt	Thickening agent

Table 3. Materials used in the presented investigation

Sample Preparation

The sample preparation was based on the process described in [26] and on personal correspondence with two of the paper authors (Ruri Hidema and Hiroshi Suzuki). Since the goal of the reproduction is to acquire the results obtained in (Ruri Hidema H. S., 2016), the same material compositions were used. A sample consisting of 35 wt% salt hydrate in water and no additives was used as reference. Samples containing 35 wt% salt hydrate in water, 2,000 ppm thickener, 2,000 ppm surfactant and a surfactant to counter ion molar ratio of 1.5 are the ones expected to deliver the best results ([28]).

The set-up for producing a slurry sample was optimized during the project, as issues were faced during the manufacturing process. Figure 22 shows the optimized set-up, where each slurry sample has a volume of 45 mL, in a 50 mL glass flask and closed by a cap screwed on the flask. This flask is placed in a metal bowl containing thermal oil that is heated up by an IKA RCT basic hot plate with a magnetic stirrer. A temperature sensor is installed in the thermal oil, and is connected to the hot plate to adjust the temperature automatically. The slurry sample is stirred continuously using a magnet that is added to the glass flask.

It should be noted that the sample performance proved to be particularly sensitive to factors such as sample preparation temperature, stirring speed, order of addition of components, brand of additives. Some important points were:

- Sample preparation temperature should be high enough to dissolve PVA (ca. 70°C) but lower than 90°C so that the surfactant molecules don't get destroyed
- Slow stirring speeds should be used
- PVA solution and salt solution should be produced separately and the latent heat materials should be combined later
- Surfactants should be stirred at 60 °C and low speed during an entire day

A schematic of the detailed sample preparation procedure can be found in the Appendix.

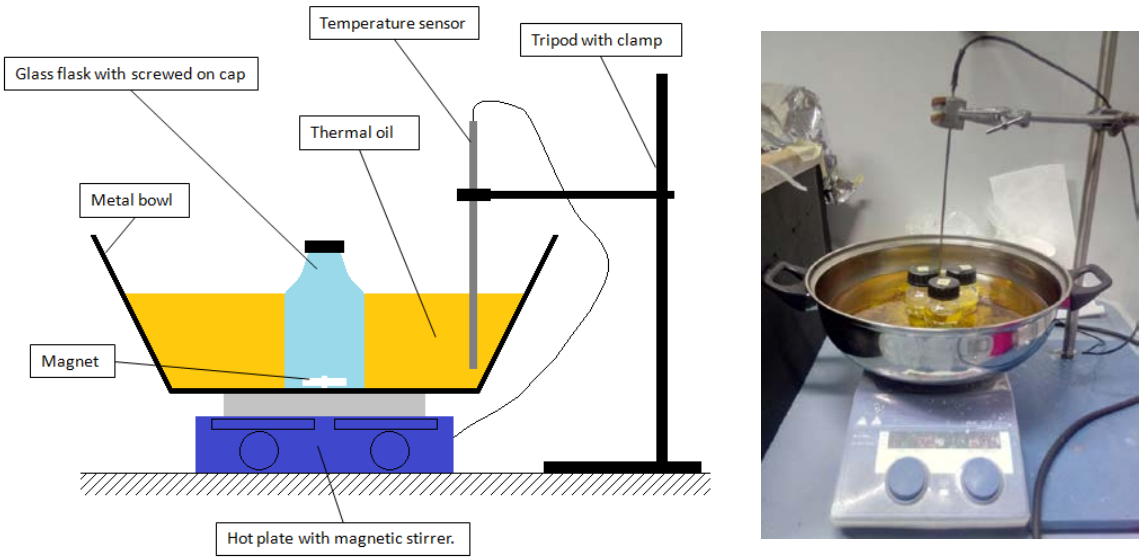

Figure 22. Set-up for PCS production; schematic overview (left) and photograph of the test set-up (right)

Evaluation of Sedimentation Speed

After the samples were prepared they were evaluated with respect to their sedimentation speed based on the methodology described in [26]. A second test set-up that is used during the experiments is similar to the set-up used in [28] and is used for measuring the sedimentation layer. The samples that were produced using the previous set-up are decanted in another glass flask, closed using a lid and are put in a water bath with a temperature of 50 °C. The water bath is connected via an external pump to the primary side of a heat exchanger, which is connected to a Huber Ministat 125 temperature regulator at its secondary side, to maintain a constant temperature in the water bath.

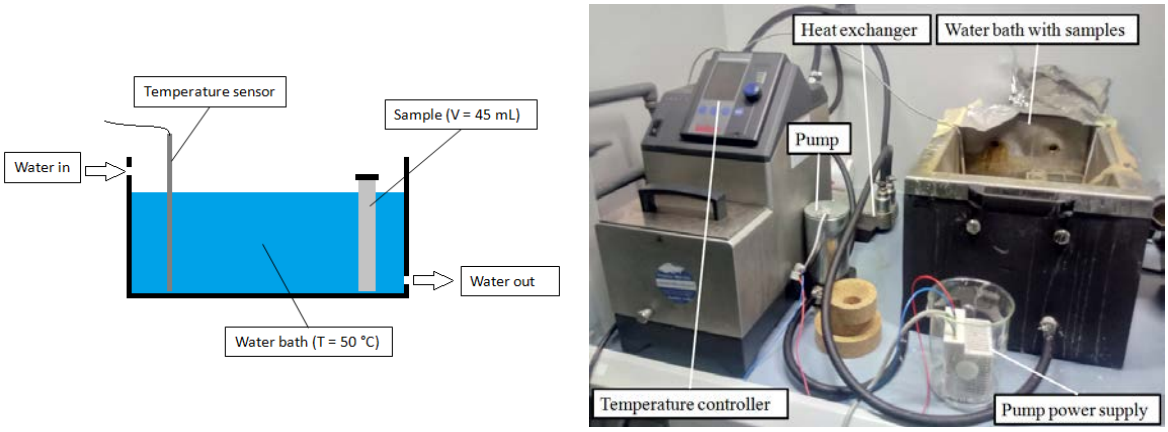

Figure 23. Set-up for evaluation of the sedimentation speed; schematic overview (left) and photograph of the test set-up (right)

The sedimentation velocity is determined by measuring the height of the sedimentation layer and the initial height of the solution over time. The apparent dispersion fraction 'δ' of the solution is defined as the ratio between the liquid content after sedimentation and the total at the start of the measurement. It is assumed that the sedimentation layer forms a uniform barrier on the bottom, due to gravitational forces on the PCS. The height of the sedimentation layer 'h_{sed}' and the height of the solutions 'h_{init}' are measured along the height of the cylindrical container, (see Figure 24), thus the liquid percentage can be easily defined as the container diameter of the container is constant. After the initial height was determined, the sedimentation height was measured every 10 minutes, and photographs were taken from the samples. Equation 5, defines the dispersion fraction obtained from these heights. A dispersion fraction of 100% results in a homogeneous mixture, while results < 100% corresponds to a formation of a sedimentation layer.

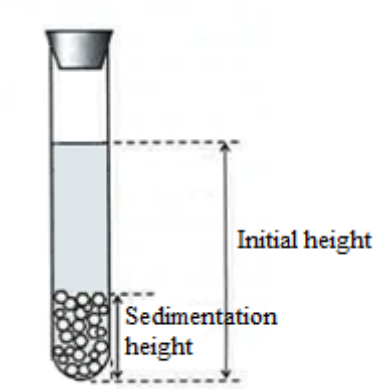

Figure 24. Definition of sedimentation height (h_{sed}) and initial (h_{in}) sample height that were used for the evaluation of the sedimentation speed.

$$\delta = \frac{h_{init} - h_{sed}}{h_{init}} \cdot 100\% \qquad (5)$$

4.2.3. Results

Experiments with Behenyl Trimethyl Ammonium Chloride (25%)

In this experimental series a total of 14 experiments were conducted, varying the amount of surfactant from 2000 ppm to 8000 ppm and two types type of PVA. All experiments were conducted using Behenyl TMC 25 with exact compositions that are listed in Table 4. The measurements were performed at room temperature and after shaking both samples to counter the supercooling effect. Although this effect is not studied, from this experiment is concluded that additives have a positive influence on the sedimentation velocity.The sedimentation velocity of sample 4.II and the reference sample 4.I can be seen in Figure 25.

#	Sample	Water [mL]	Salt Hydrate [g]	PVA_C [ppm]	PVA_k [ppm]	Surfactant [ppm]	Counter ions [mg]
4	I	33.9	18.3				
	II	33.9	18.3	2,000		2,000	49.6
6	III	33.9	18.3	2,000		2,000	49.6
	IV	33.9	18.3		2,000	2,000	49.6
	V	33.9	18.3		2,000	8,000	49.6
	VI	33.9	18.3	2,000		8,000	49.6
7	VII	33.9	18.3				
	VIII	33.9	18.3	2,000		2,000	49.6
	IX	33.9	18.3		2,000	2,000	49.6
	X	33.9	18.3	2,000		6,000	49.6
	XI	33.9	18.3		2,000	6,000	49.6
	XII	33.9	18.3	2,000		6,000	49.6
	XIII	33.9	18.3		2,000	6,000	49.6
	XIV	33.9	18.3		2,000	2,000	49.6

Table 4. Material content and composition used in the reproduction experiments to make samples with V = 45 mL

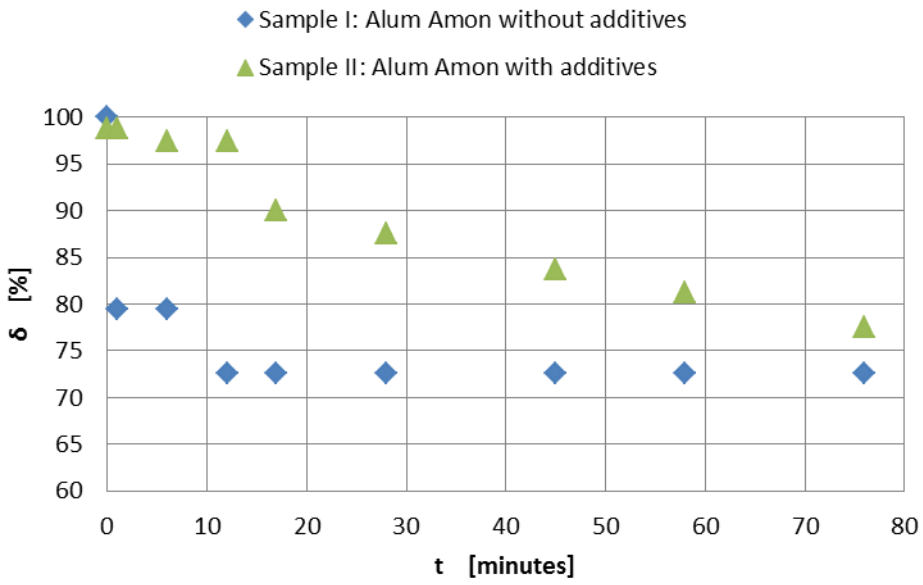

Figure 25. Apparent dispersion fraction 'δ' over time using samples containing Alum Amon (35% AAH in water) with and without additives. The measurements are performed at a room temperature and measured at the growth of sedimentation height for the first 80 minutes

In Figure 25, a clear improvement in the dispersion fraction over time can be observed in the sample containing additives. However the delay in sedimentation is in the order of minutes instead of days as reported by [26]. Photographs of the samples can be seen in Figure 26. Both solutions contain a clear homogeneous mixture at the start of the measurement, showing that it is possible to produce a homogeneous mixture with this experiment set-up. After 75 minutes, sedimentation was visible in both samples. The sedimentation layer of the AAH without additives consists of smaller crystals than the solution with additives which doesn't agree with literature observations. A reason for this difference is explained by the thickening effect of the PVA, because it creates a suspension. The formation of a suspension leads gravitational agglomeration, meaning that the surfactant with counter ions hardly influences the prevention of crystal growth by collision. Another reason that might happen is that due to the suspension, the crystals have more time to grow in size.

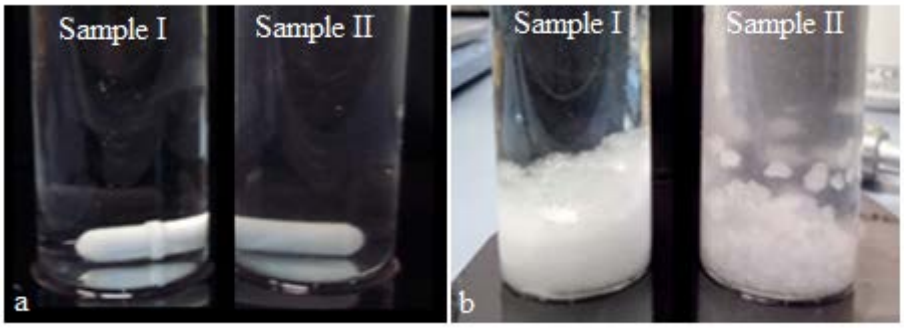

Figure 26. Photographs taken at (a) the start and (b) the end of the measurement. At the start both samples, AHH without (sample I) and with additives (sample II), are a clear homogeneous mixture. A sedimentation layer has formed at the end of the measurement, which shows small crystals for sample I and large crystals for sample II in the sedimentation layer

Experiments with different types and amounts of PVA were performed to see the effect of these factors on the sedimentation speed. The results of these experiments (experiments 6, Table 4) can be seen in Figure 27. In the Figure it can be observed that even though both PVA types have a polymerization grade of 500, they have a different effect on the samples. More specifically PVA from company Colltec presents in this case a better performance in delaying the sedimentation than PVA from company Kuraray. It should be however noted that the repeatability of the experiments should be further investigated to confirm these conclusions. In all cases however the delay in sedimentation speed was in the order of minutes rather than days.

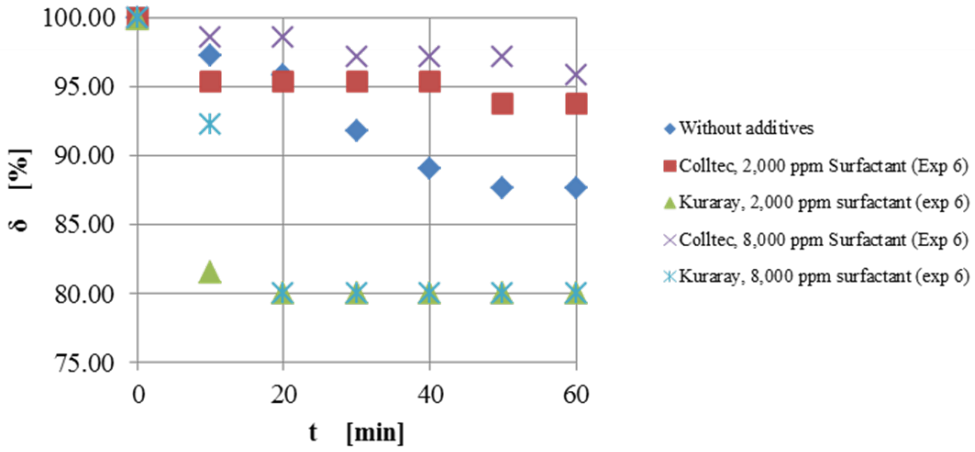

Figure 27. Apparent dispersion fraction obtained from the measurements of experiment 6 using different types and amounts of PVA

Another issue that was revealed with these experiments is a creation of a foam layer which was not reported in literature and be observed in Figure 28 for samples of experiment 6. The foam makes the use of such samples prohibitive in a real experimental setup were pumping of the slurry is required, as it can cause system blockage. It was suspected that the foam was attributed to the solvent existing in the Behenyl TMC 25 material (cetostearyl alcohol) which lead to the purchase and testing of Behenyl TMC 85.

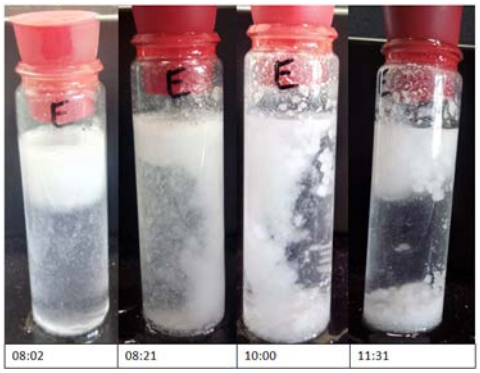

Figure 28. Change in solution composition for sample 6 VI in the first 2.5 hours. The solution consist of 8,000 ppm of surfactant with counter ions and PVA of Colltec in a AAH – water solution

Experiments with Behenyl Trimethyl Ammonium Chloride (85%)

As mentioned in the previous section it was suspected that the cetostearyl alcohol contained in the Behenyl TMC 25 was responsible for the undesired foaming of the samples. Therefore Behenyl TMC 85, which contained 85% active substance instead of 25% was purchased and examined to test this assumption. The compositions of the tested samples can be found in Table 5. It should be noted that the amount of active substance (behenyl trimethyl ammonium chloride) in the samples was kept constant at 2000 ppm. Since the concentration of active substance was higher in Behenyl TMC 85, less of the substance was added to the samples in comparison to the samples containing Behenyl TMC 25.

These results are compared with the experiments of Table 4 that comprised the same composition but were prepared with Behenyl trimethyl ammonium chloride of 25%. The results are shown in Figure 29. It can be seen that the use of the Behenyl TMC-85 has a positive influence on the delay of sedimentation velocity in comparison to the sample containing behenyl TMC-25. Additionally, the difference between the samples containing PVA of manufacturers 'Colltec' and 'Kuraray' do not present such a large deviation in performance as observed in Figure 27. Both of the samples could maintain a dispersion fraction of almost 100% for 20 minutes which is a significant increase in performance compared to the unmodified sample.

Sample	Water [mL]	Salt Hydrate [g]	PVA_C [ppm]	PVA_k [ppm]	Surfactant [ppm]	Counter ions [mg]
I	33.9	18.3	2,000		2,000	49,6
II	33.9	18.3		2,000	2,000	49.6

Table 5. Material content and composition used in the experiment using a new surfactant (behenyl trimethyl ammonium chloride 85%)

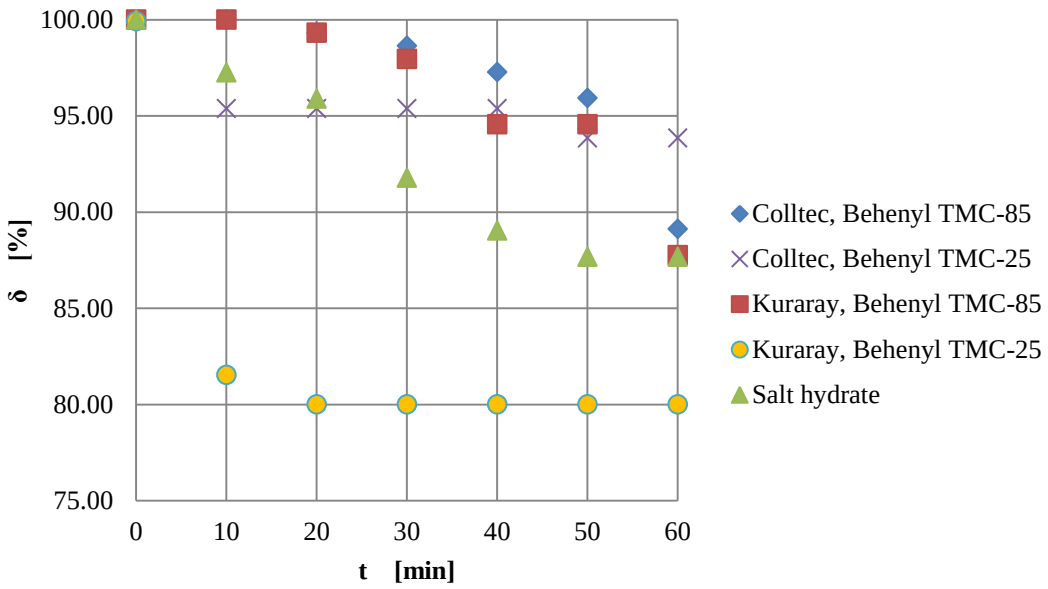

Figure 29. Apparent dispersion fraction for two different types of surfactants and two different types of PVA

The photographs that were taken during the measurements are shown in Figure 30. They show, at a first observation, that there is no foam formed in and on top of the solution. From this it can be concluded that the foam was formed due to the high cetostearyl alcohol concentration in Behenyl TMC-25. Another observation is that the crystals formed in both types of PVA (after 1 hour) remain in the order of size from the salt hydrate. This means that there is no gravitational agglomeration anymore and no growth in crystal size. After 2 days the solutions became cloudier and a larger sedimentation layer was formed, however there was no growth in crystal size observed.

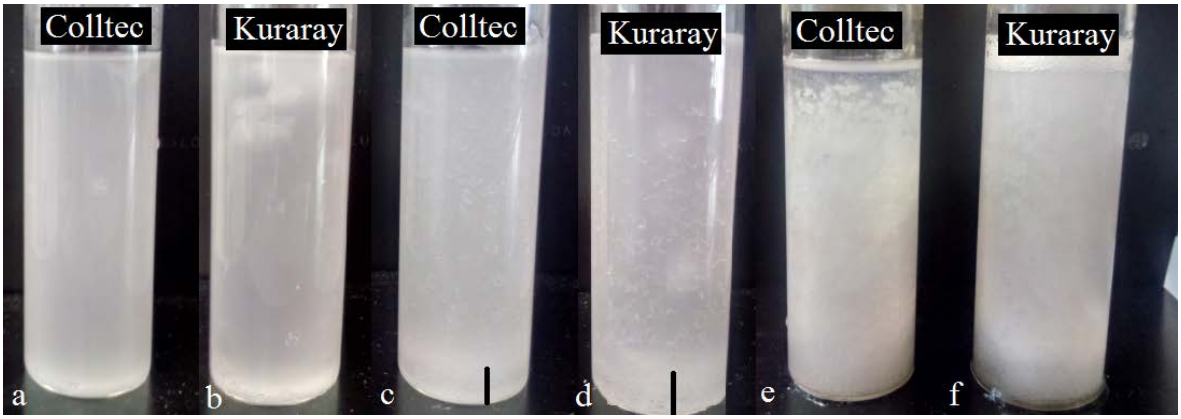

Figure 30. Photographs taken during the measurement. Photograph a and b are taken at the start of the measurement, photograph c and d after 1 hour and e and f after 2 days.

Experiments with other thickeners

The effect of thickeners carboxymethylcellulose sodium salt and silicon dioxide on the sedimentation velocity was also investigated and compared with the samples containing Benehyl TMC-85 and surfactants. A different procedure is used for the sample preparation. First a salt hydrate/ water solution is made and after the salt hydrate is dissolved the thickener is added directly. The samples were stirred for 2 days to be sure that the thickener was completely solved in the solution. The exact compositions of the samples examined are shown in Table 6 and Table 7. Figure 31 shows that the use of carboxymethylcellulose sodium salt increases the sedimentation velocity instead of decreasing it. This behaviour could be attributed to the addition of a non-optimal amount of thickener in the solution or a faulty sample preparation method for making slurry should be used.

Sample	Water [mL]	Salt Hydrate [g]	Thickener [mg]
I	33.9	18.3	66.8
II	33.9	18.3	137.2
III	33.9	18.3	207.0

Table 6. Material content and composition used in the experiment using carboxymethylcellulose sodium salt from Alpha Aesar as a thickener

Sample	Water [mL]	Salt Hydrate [g]	Thickener [mg]
I	33.9	18.3	36.5
II	33.9	18.3	67
III	33.9	18.3	134
IV	33.9	18.3	201
V	33.9	18.3	268

Table 7. Material content and composition used in the experiment using silicon dioxide from Aerosil as a thickener

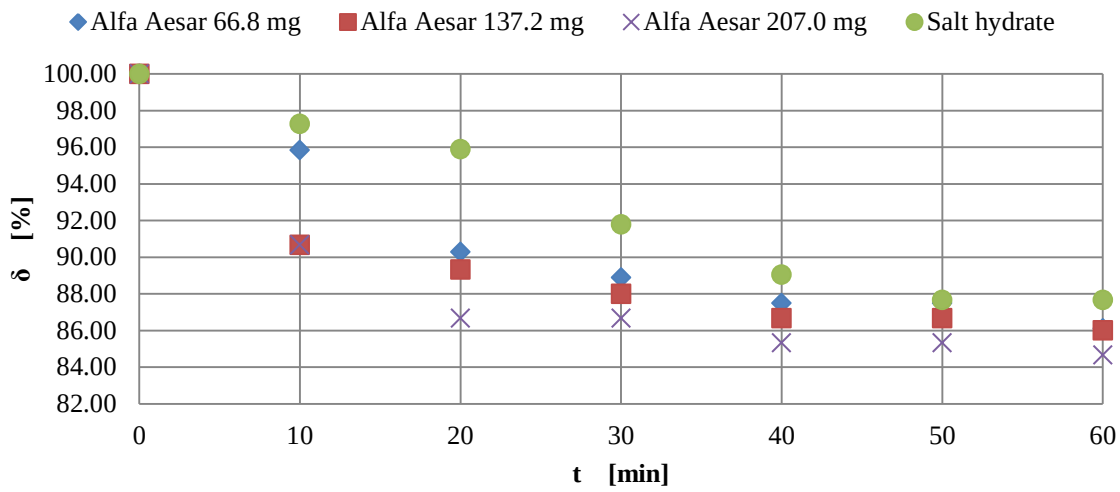

Figure 31. Measurements of the effect of using carboxymethylcellulose sodium salt on the sedimentation velocity, by defining the apparent dispersion fraction

On the contrary, Figure 32 shows a significant reduction of the sedimentation velocity for all samples containing silicon dioxide as thickener. The best performance is observed for the samples containing 67 and 134 mg. The increase in performance for these samples are comparable with the best performance recorded for the Behenyl TMC – 85/PVA mixtures. However, the preparation effort of the sample containing silicon dioxide is significantly lower, making the use of such a thickener an attractive alternative to the surfactant PVA mixture.

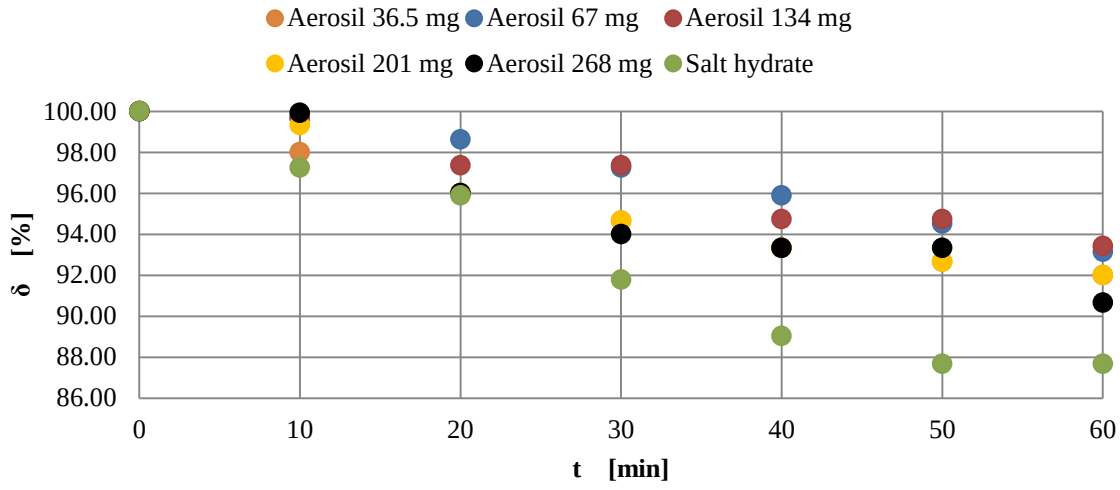

Figure 32. Measurements of the effect of silicon dioxide on the sedimentation velocity, by defining the apparent dispersion fraction

4.3. Summary and Conclusions

For the selection of the most suitable PCM for the project, an extensive literature review was performed of the research conducted in the field of PCM technologies, summarising their properties and critical characteristics. Based on the literature review, a list of criteria was put together to enable classification of the PCMs and identification the most promising candidates for this project. A combination of measured and literature-based thermo-physical properties was gathered for interesting PCM candidates. In the course of this process, aluminium ammonium sulfate dodecahydrate ($NH_4Al(SO_4)_2 \cdot 12H_2O$) was chosen as the main PCM candidate for the next steps of this study. This material was chosen because its ability to produce slurries has been demonstrated and no degradation issues have been reported. Another great advantage is that its melting temperature can be regulated with the addition of water to cover the whole range of chosen temperatures (60-90 °C) rather than only one specific temperature point. Differential Scanning Calorimetry (DCS) was used for the characterization of pure AAH but was proven unsuitable for measurements with mixtures of mixtures of AAH in water due to high supercooling and/or phase separation. Instead the melting and crystallization temperatures could be determined in an Easymax at higher sample volumes and under constant stirring. The melting points were determined for samples containing 35% and 45% AAH in water (average melting points at 55.5 and 63.8 °C respectively) and were found to be consistent with literature.

In a second step the materials were modified using additives to decrease crystal sedimentation and increase slurry fluidity. The methodology and materials were based on [26,28]. Most of the modified samples exhibited a much better performance in terms of sedimentation than the unmodified AAH/water samples. However the increase in performance remained for all samples, orders of magnitude away from the values reported in literature (sedimentation delay of hours instead of days). Additionally, the performance of the modified material was proven to be very sensitive to the type of surfactant and PVA used, and to the temperatures used during sample preparation. Therefore, serious doubt was raised as to whether such a sensitive process would be suitable for an industrial application. For comparison reasons, two standard thickeners were used for the material modification (carboxymethylcellulose sodium salt and silicon dioxide). The former induced no increase in dispersion performance whereas samples containing the latter exhibited an increase in performance similar to the best sample modified with Benehyl TMC-85/PVA. Since the sample preparation when using silicon dioxide as additive was much simpler and more robust, this method could be proposed as an alternative to the method proposed by Hidema et al. However, the effect of the thickener on the overall performance of the slurry and especially on the fluidity should be investigated before further conclusions are drawn. It should be noted that the modified samples were not tested in the proof of concept test rig which would be an interesting next step to evaluate their performance.

5. Proof-of-Concept Test-rig

Within the scope of the presented project, a proof-of-concept test-rig for the continuous production of a high temperature phase change material slurry was developed and successfully commissioned in the thermal laboratory of HSLU. I a first step, a flexible, modular preliminary test-rig was built to gain experience with the used salt hydrate. Based on the findings obtained using the preliminary test-rig, the final version of the rig was designed.

5.1. Test-rig Concept

A simplified schematic of the basic concept of the test-rig developed in the present project is shown in Figure 33. The PCS is supercooled in the heat exchanger and crystallization is subsequently triggered in a releaser. The concept is based on the production of ice-slurries.

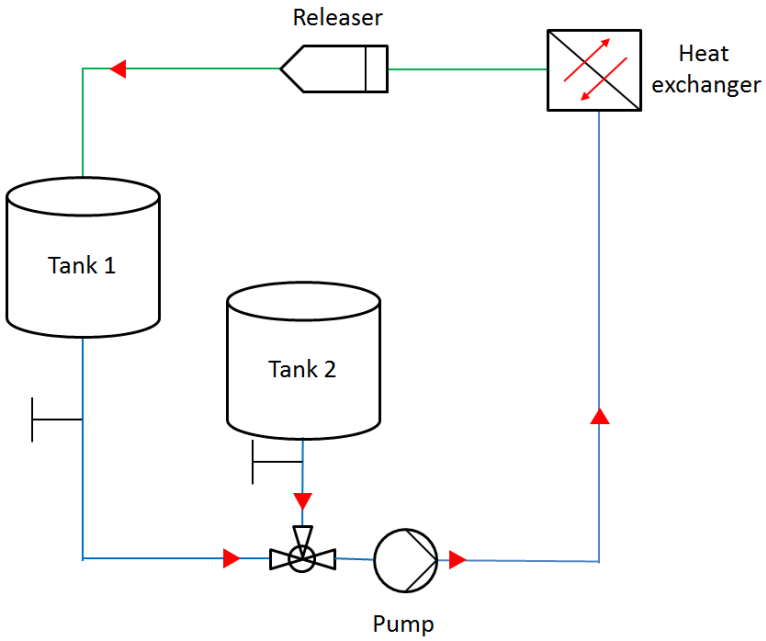

Figure 33: Simplified schematic of test-rig basic concept.

5.2. Requirements List

Totally eight requirements regarding the test-rig were defined. The list of requirements of the slurry test-rig is shown in Table 8.

Nr	Name	Description/Quantification
1	Production of PCS	PCS should be produced in batch (steady state conditions) and continuous mode.
2	Storage of PCS	After PCS is produced, the test-rig should allow to store it in a separated storage.
3	Melting of PCS	The test-rig should allow to melt the PCS in the same HEX.
4	Modular construction of setup	Heat exchanger, crystallization releaser, pump and other components should be easily exchangeable.
5	Temperature range	50-90 °C
6	Optical observation	The test-rig should allow to optically inspect the flowing PCS, most importantly before and after the HEX.
7	Controlled crystallization and melting in the test-rig	The test-rig should allow a crystallization of the (supercooled) PCS in a defined section of the piping system. Furthermore, in case of melting, the phase change should take place as well in a defined section of the rig.
8	Determination of crystal fraction	In case of crystallization, the test-rig should allow to determine the hydrate fraction x_H within the slurry after crystallization.

Table 8: List of requirements of the to be developed PCS test-rig.

5.3. Design and Components

A schematic of the hydraulic circuit of the final setup is shown in Figure 34. The test-rig is composed of two PCM tanks, a flexible vane pump, a plate heat exchanger which are connected with a modular piping system. The piping is made of stainless steel tubes with an inner diameter of 12mm. The usage of two tanks allows the conduction of batch mode experiments with constant inlet conditions of the PCS. Furthermore, continuous experiments can be conducted by directly pumping the PCS back into tank 1. As required, the rig is constructed modularly to achieve a simple modification and cleaning of the piping system in case of a blockage. A water supply connection in combination with a drain allows the flushing of the entire piping system with water after shutdown to avoid a blockage due to crystal sedimentation.

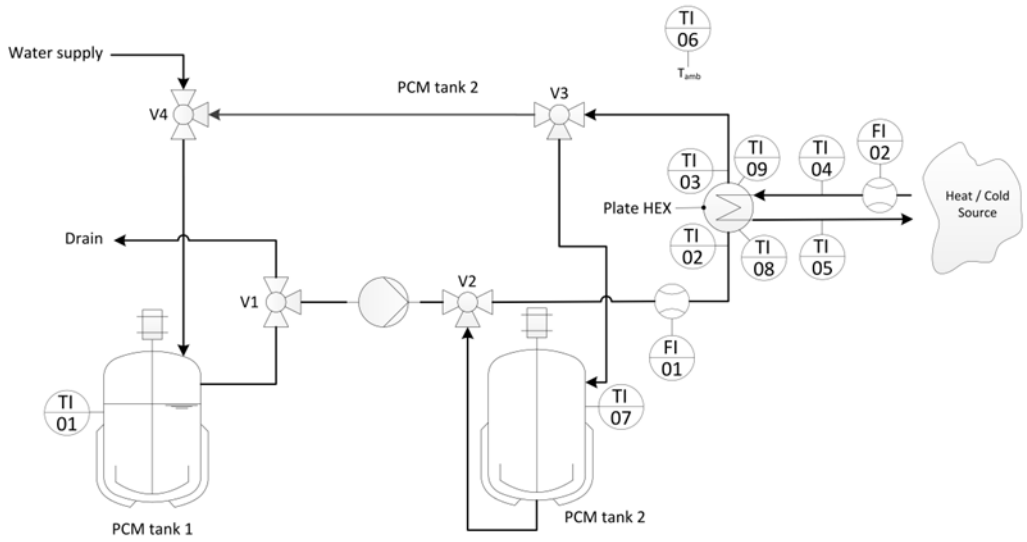

Figure 34: Schematic of the hydraulic circuit of the final setup.

A photograph of the final setup developed in the scope of the present project is shown in Figure 35. The system is insulated with at least 1cm of polyethylene insulation. Two sight windows, one before and one after the heat exchanger are installed to allow an optical observation of the flowing slurry. The total dimension of the rig is approximately 2.5m x 1m x 1.5 m (L x W x H).

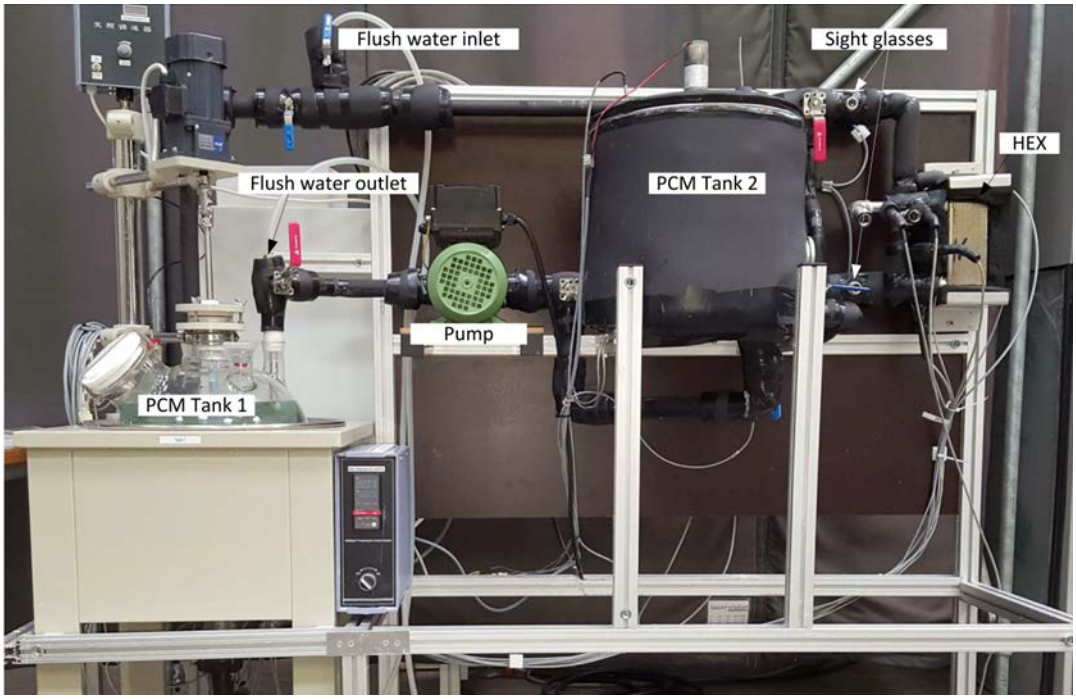

Figure 35. Final setup and important components.

5.3.1. Dimensioning

Regarding the dimensioning of the test-rig, following technical issues were taken into consideration:

- Minimal batch time/ maximal flow rate: As described in Table 8, the test-rig should allow batch mode experiments under steady-state conditions. To achieve steady-state conditions, a minimal batch time which is dependent on the maximal flow rate chosen is required.
- Minimal flow velocity: A minimum flow velocity is required to avoid crystal sedimentation within the flowing slurry.
- Pressure drop: The pressure drop within the piping system should match the pump characteristics to achieve the desired flow rates.

A detailed description of the test-rig dimensioning may be found in the appendix.

5.3.2. Piping and PCM tanks

Piping

The piping of the test-rig is realized using *Optipress-Aquaplus* DN15 fittings of manufacturer *Nussbaum* with an inner diameter of 12mm. Manual ball valves were used in the entire setup. To allow an efficient dis- and reassembly of the test-rig in case of a blockage, all straight pipe sections are independently removable using screw connected press-fittings as shown in Figure 36.

Figure 36: (a) Photograph of a press fitting used for the piping of the system. (b) Photograph of a viewing window which is used for an optical inspection of the flowing slurry.

Based on the experiments performed, it could be observed that the design of the piping system is crucial concerning blockage of the system. Following technical results regarding the piping system design using unmodified AAH slurry can be listed:

- Long vertical sections should be avoided or consequently emptied after the shutdown of the system. Otherwise, due to sedimentation, the pipe section may block. If the solid layer built due to sedimentation is cooled to room temperature, large, mechanically very robust crystals are formed. In the present project, these crystals, if present, could only be removed mechanically and not by a heating of the piping system.
- Heat bridges due to insufficient insulation should strictly be avoided since crystals might be built on the pipe walls which then can lead to a blockage of the system.
- It could be shown that the preheating of the pipes is not necessary using an inner pipe diameter of 12mm for the 45wt% slurry.

In Figure 37, an example of a blocked pipe is shown. Two effects lead to this incident: Firstly, the pipe elbow was not insulated which enhances the creation of solid crystals. Second, the blockage occurred on the bottom of a vertical tube section due to crystal sedimentation. Based

on this incident, the vertical section was shortened (as far as possible) and the further the manifold was insulated.

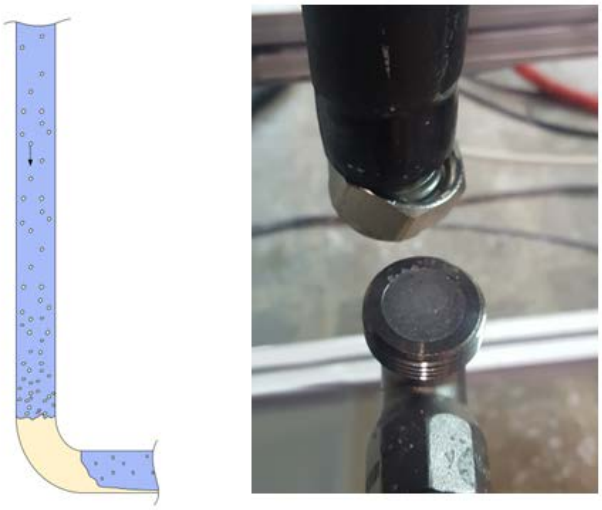

Figure 37: Due to sedimentation of the material, a solid layer (drawn yellow in (a)) may be created on the bottom of long vertical tube sections. The effect is illustrated in (a) and a photograph of a pipe blockage caused by this effect is shown in (b).

PCM tanks

PCM tank 1 is a commercial glass reactor with approximately 15L volume and an integrated stirrer. The reactor is surrounded by a heatable stainless steel frame. In the present project, the frame was filled with water to heat the PCS in the reactor. PCM tank 2 is a modified stainless steel pan. Following modification were made: installation of an electrical heating wire and thermal insulation, installation of a stirrer to inhibit sedimentation, installation of a drain at the bottom of the tank to avoid a cumulation of solid, sedimented hydrate crystals.

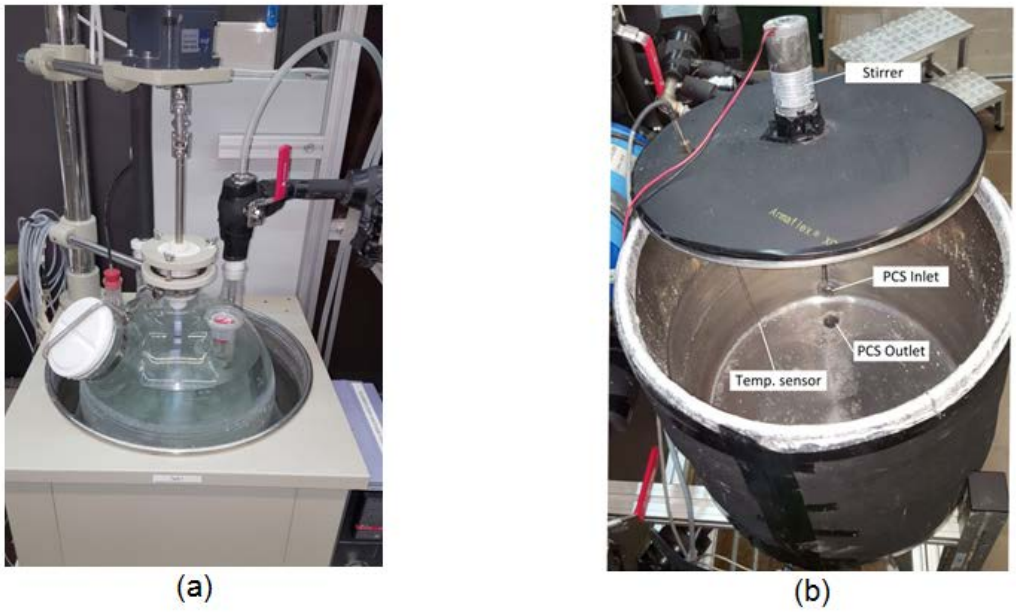

Figure 38: Photograph of PMC tank 1 (a) and PCM tank 2 (b).

5.3.3. Pump

The pump may be considered as a key component of the slurry test-rig due to the high mechanical (solid particles) and thermal requirements. Two different pump types were tested in the preliminary setup, a gear pump as well as a flexible vane pump. Although the gear pump is theoretically capable of pumping small solid particles, observations made during the experiments showed that larger particles created due to sedimentation in the pipes cause considerable abrasion in the pump. Hence, in the final setup, the flexible vane pump (impeller pump) which has been tested in the preliminary setup was used as the main pump. In flexible vane pumps, the rotor is mounted eccentrically in the pump casing as shown in Figure 39. Similar to gear pumps, the liquid is drawn into the pump by an increasing volume between the vanes on the suction side. The slurry is then transported to the outlet while trapped between the flexible vanes and forced out by a decreasing volume between the vanes [43]. The main advantage of this pump type is its ability to pump a wide range of liquids including emulsions. Suction lifts of up to 5m are possible. The rotor is made of a synthetic elastomer (e.g. Neoprene, Nitrile rubber or fluoroelastomers) depending on the liquid pumped. The main drawback of vane pumps is the usually limited temperature range (max. 90°C) due to the impeller material and the limited pressure difference of typically 5bar. Furthermore, it is worth mentioning that the dry operation of the pump may lead to severe wear of the impeller. Within the present project, a flexible vane pump of supplier *ZUWA*, type *Nirostar 2001-A* with an integrated frequency inverter was used in the preliminary setup and is used in the final setup.

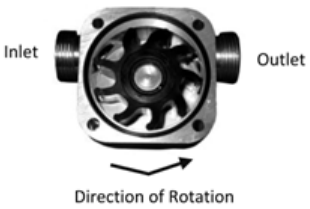

Figure 39: Side view of the pump case with removed pump cover [44].

The pump characteristics curves can be found in the appendix.

Impeller material and abrasion
In the present project, acrylonitrile-butadiene-rubber (NBR) as well as fluor-rubber (FKM) impellers were tested. Former shows in general higher chemical resistance than latter, however, the mechanical strength of NBR is a key advantage in comparison to FKM impellers. In the present project it was observed, that NBR impellers clearly surpass FKM impellers in terms of pumpability of the PCS. Using an FKM impeller, the 45wt% could repeatedly not be pumped. It appeared as solid particles slipped between the impeller and the pump case and thus the performance of the pump was significantly inhibited. Furthermore, as shown in Figure 40, after approximately 15 experiments (including few blockages of the system), the FKM impeller (left) used showed clear signs of abrasion in comparison to a new impeller (right).

Figure 40: Comparison between a used FKM impeller (left) and a new FKM impeller (right). The impeller on the left shows clear signs of abrasion.

In conclusion, it can be stated that the usage of a flexible vane pump in combination with a NBR impeller showed the most promising technical results regarding pumbability of the PBS.

5.3.4. Heat Exchanger

As mentioned, the same heat exchanger was used in both, the preliminary as well as the final setup. In Figure 41, a photograph of the used plate HEX with removed insulation on the front side is presented. As shown, the HEX consists of 15 plates and has a total area of approximately 0.18m^2. At both outlets, a rectangular manifold is placed to avoid systematic measurement uncertainties. The HEX is packed in approximately 5cm of polyethylene insulation to minimize the thermal losses. In all experiments, the HEX was operated in countercurrent flow conditions.

Figure 41: Side view of the installed heat exchanger in the final test-rig. For a better orientation, the front insulation has been removed.

On basis of the experiments performed to verify the heat exchanger energy balance by the use of water, important findings regarding the design of the heat exchanger outlet pipes were made. Using straight HEX outlets, a large dependency of the measured temperature on the position of the sensor in vertical direction could be observed. This effect leads to deviations within the energy balance of up to 30%. Due to this observation, it can be assumed that a high stratification regarding temperature in vertical direction might be present in the flow leaving the HEX. As a consequence, a 90° bend directly after the HEX outlet was installed to achieve a mixing of the stratified flow as illustrated in Figure 42.

Furthermore, the bending guarantees that the sensor is always surrounded by the fluid (this might not be the case in a straight, horizontal outlet where air pockets can be present). Finally, regarding the energy balance of the HEX, it was observed that the thermal insulation of the temperature sensors is of high importance.

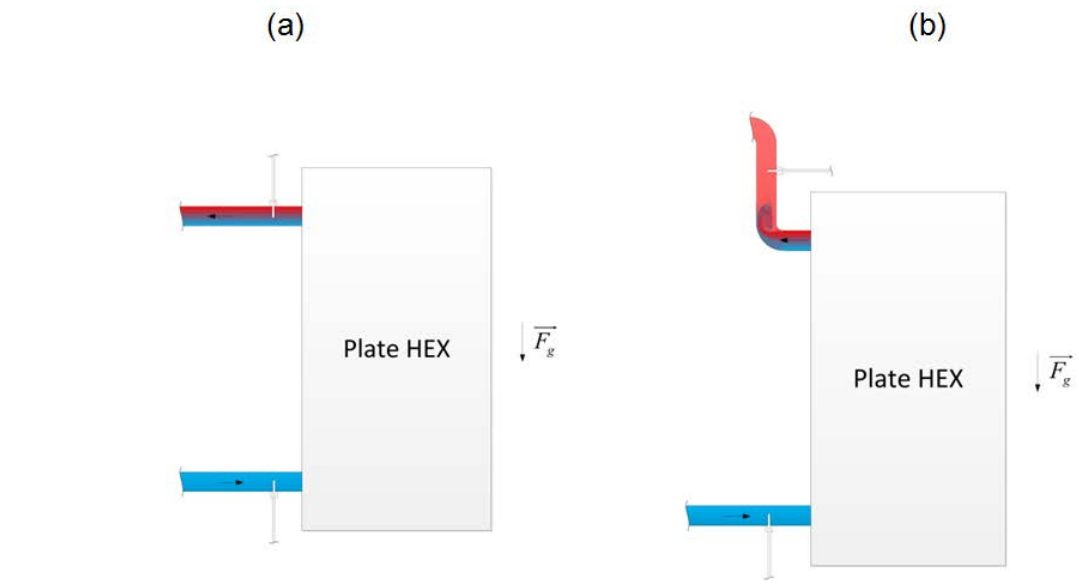

Figure 42: Illustrative comparison between a straight heat exchanger outlet pipe and a 90° vertically bent outlet.

5.3.5. Crystallization releaser

Two different methods to increase the crystallization probability of the supercooled PCS leaving the heat exchanger were investigated. Both approaches are of type *dynamic nucleation* which means that external stimuli are used to induce the creation of crystals. Manual seeding methods were due to time reasons not considered.

In the first approach investigated, mechanical stresses are induced by a sudden expansion of the inner tube diameter from 6 mm to 21mm (throttle valve). The valve is placed downstream of the heat exchanger. A schematic and photograph of can be found in Figure 43. As illustrated, a temperature sensor is placed closed to the outlet of the throttle valve. If crystallization occurred in the valve, an increased temperature in comparison to the HEX outlet temperature would be observed due to the phase change enthalpy released (if thermal losses to ambient are small). The throttle valve is well insulated to reduce thermal losses and environmental influences. Furthermore, as illustrated in Figure 43 (b), a short, transparent tube section made of borosilicate glass was installed before and after the valve.

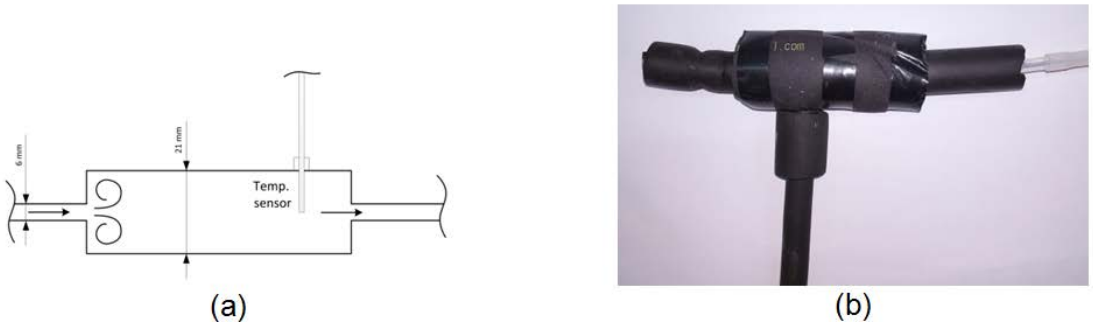

Figure 43: (a) Schematic drawing of the throttle valve used to increase the probability of crystallization to occur. (b) Photograph of the installed valve.

The second approach to increase the crystallization probability is based on an induction of ultrasonic waves into the flowing PCS. As shown in Figure 44, the approach was technically implemented by the use of an ultrasonic bath, usually utilized for cleaning and sterilization purposes. The supercooled PCS is transported in a u-shaped tube through the bath. To enhance the propagation of the waves, the tube is pressed on the bottom of the bath, as close as possible to the ultrasonic emitter. Furthermore, in order to minimize the heat transfer from the bath to the PCS or vice-versa, the bath temperature was set in advance to the expected PCS temperature which was available from previous experiments. Again, the bath was placed downstream of the HEX and a temperature sensor was placed at the outlet of the bath. As illustrated in Figure 44 (b), the temperature sensor was well insulated to improve the accuracy and minimize the thermal impact of the environment.

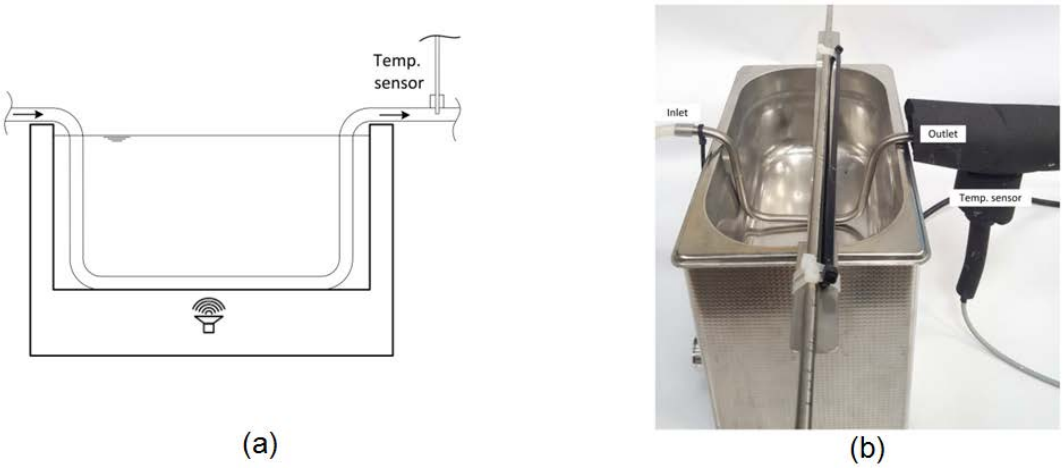

Figure 44: (a) Schematic drawing of the setup to increase the crystallization probability using an ultrasonic bath. (b) Photograph of the setup.

5.3.6. Measurement equipment and data aquisition

Pt 100 resistance sensors are used exclusively for all temperature measurements. All temperature sensors involved to determine energy balance within the heat exchanger are of Class DIN 1/5 with a considerable low measurement uncertainty. Both flow meters are based on the inductive method which will be briefly explained after this. A list of the measurement sensors used is shown in Table 20 in the appendix. The symbols described in the table correspond to all hydraulic schemes of the final setup presented within this report.

Resistance temperature sensors

Resistance temperature detectors (RTD) use the temperature dependency of the electrical resistance R_s of a metal to determine its temperature. In case of a Pt 100, the metal used is platinum. In the present work, a 4-wired connection, as illustrated in Figure 45, is used to measure the resistance. In a 4-wired circuit, the electrical current through the resistance I_r is kept constant and the voltage drop over the resistance is measured with two separated connectors. Using this approach, the effect of the internal resistance of the wires on the measurement result is minimized. A detailed description of the measurement method may be found in [45].

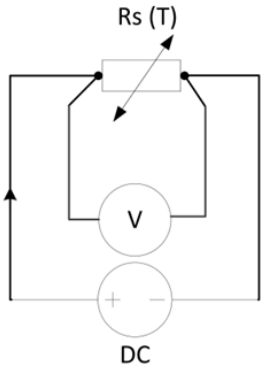

Figure 45: Simplified schematic of the 4-wire circuit used in the present work to measure the temperature dependent resistance R_s of the Pt 100 sensor.

The callendar-van dusen equation, which is a linearization curve, is used to determine the temperature based on the measured resistance [46]:

$$R_s = R_0(1 + A \cdot T + B \cdot T^2) \quad (6)$$

where R_0 is the nominal resistance at 0°C (100Ω in case of a pt100) as well as A and B coefficients depending on the used sensor type (in this case A=3.9083 * 10^{-3} B=-5.775 * 10^{-7}). The correct operation of all sensors mounted at the HEX (TI02-TI05) was verified using a water/ice slurry (deionized water).

Flow meter

Both flow meters, FI01 for the determination of the slurry flow rate as well as FI02 for water are based on the inductive measurement method. As shown in Figure 46, the sensor is composed of a lined flow tube, two electromagnetic coils and two opposed electrodes [43]. A magnetic field B which is perpendicular to the flow direction is created by the coils. Based on the Faraday's law of induction, the voltage induced between the two electrodes is proportional to the mean flow velocity v_m and can be described with following equation:

$$U = B \cdot v_m \cdot D \qquad (7)$$

The measurement principle works for electrically conductive fluids only. However, it is applicable for fluids containing solid particles [43]. Again, it is worth mentioning that the same technology was used in [47] for a salt-hydrate low temperature test-rig. In the present test rig, a flow meter of supplier *Wisag*, tpye *FLOMID 0 FX* with an nominal diameter of 6mm is used to measure the PCS flow rate. The sensor and inverter are integrated in one device. Regarding the installation of the flow meter it is important to ensure that the minimal straight sections up- and downstream (5 * d_i upstream, 3 * d_i downstream) of the device are kept.

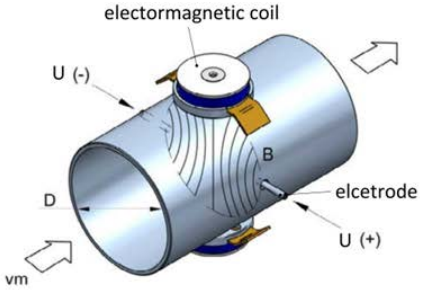

Figure 46: Schematic illustration of inductive flow rate measurement principle (taken from Wisag FlOMID documentation).

Data Aquisition

The data aquisition is achieved with a *cDAQ-9184* compact data aquisition ethernet chassis of supplier *National Instruments* (see Figure 47). The chassis is used in combination with input modules which can independently be combined. A list of the used modules can be found in Table 9. Commercial software *LabVIEW* is used to collect the data. The further processing of the data is done in *Matlab*.

Type	Quantity	Description
NI 9219	3	Module for RTD sensors in combination with 3-wired or 4-wired connection. Used for all temperature measurements.
NI 9203	1	Module for electrical current measurement $4 - 20\,mA$. Used for both flow meters.

Table 9: NI modules used for data aquisition.

Figure 47: Photograph of the used chassis cDAQ-9184 of National Instruments with all connected wires.

5.4. Experimental Campaigns

The experimental campaign to provide a proof-of-concept for the continuous production as well as melting of a PCS slurry with a phase change temperature between 60°C and 90°C may be divided into three groups:

1. Batch mode solidification experiments: Experiments with the objective to trigger crystallization either directly in the heat exchanger or in a crystallization releaser were performed for the 35wt% as well as the 45wt% slurry.
2. Continuous experiments: A continuous experiment with the 45wt% slurry was performed in which the PCS was cooled down step-wise and crystallized in the rig and subsequently heated up and melded.
3. Batch mode melting experiments: Finally, melting experiments in batch mode with the 45wt% slurry were performed.

5.4.1. Materials

As documented above, three different materials were used, namely a 35wt% AAH water solution, a 45wt% slurry as well as water. The available materials properties can be found in Table 10. All data regarding the PCS are taken from [40].

Property	35wt% AAH slurry	45wt% AAH slurry	Water
Phase change temp. (liquidus line), T_{Pc}	52 °C	63 °C	0 °C
Specific heat capacity solid, cp_s	n.a.	n.a.	$2.060\,kJkg^{-1}K^{-1}$
Specific heat capacity liquid, cp_l	$4.143\,kJkg^{-1}K^{-1}$ (60-80 °C)	n.a	$4.183\,kJkg^{-1}K^{-1}$ (60 °C)
Phase change enthalpy (liquid/solid), Δh_{Pc}	$251\,kJkg^{-1}$ (hydrate only)	$251\,kJkg^{-1}$ (hydrate only)	$333.5\,kJkg^{-1}$
Density liquid, ρ_l	$1160\,kgm^{-3}$	n.a.	$0.9831\,kgm^{-1}$
Density solid, ρ_s	$1640\,kgm^{-3}$	$1640\,kgm^{-3}$	$918\,kgm^{-3}$
Kin. viscosity η	approx. $4'000\,\mu Pas$ at 60 °C ($x_H = 0\%$) $9'000\,\mu Pas$ at 50 °C ($x_H = 12\%$) $11'000\,\mu Pas$ at 10 °C ($x_H = 29\%$)	n.a.	$466.6\,\mu Pas$ at 60 °C

Table 10: Properties of the used materials.

Both, the 35wt% as well as the 45% slurry were prepared directly in PCM tank 1 of the experimental setup. Deionized water available in the HSLU thermal lab was heated 10K above the expected melting temperature of the PCS. Under continuous stirring, the correct amount of pure hydrate was slowly added.

5.4.2. Batch Solidification Experiments

This experimental series focused on the feasibility of a controlled supercooling and subsequent crystallization of the PCS slurry with the final goal to produce PCS slurry with a predefined solid fraction. The experimental procedure may be divided into following steps:

1. Initially the water salt hydrate solution is heated up in PCM tank 1 to 10K above the expected phase change temperature. Again, to avoid sedimentation, the PCS is continuously stirred.
2. The temperature and flow rate of water which enters the heat exchanger as shown in Figure 48 are adjusted.
3. After steady state conditions within the heat exchanger are reached (after approx. 5min), the main experimented is started: The data acquisition is activated and the volume flow rate of PCS is adjusted. PCS is pumped through the flow meter and heat exchanger into PCS tank 2 as shown in Figure 48 (a).
4. When PCS tank 1 is empty, the data acquisition is stopped and hence main experiment is stopped. Afterwards, the PCS is pumped back to tank 1 by inversing the flow direction of pump 1 and changing the position of valve V2 as shown in Figure 48 (b).

5. When PCS tank 2 is empty, the piping system is emptied as far as possible by pumping remaining PCS in the piping system back into PCM tank 1.
6. The piping system is flushed with approx. 5 L of pure water to avoid a blockage of the system due to crystallization and sedimentation in the rig.

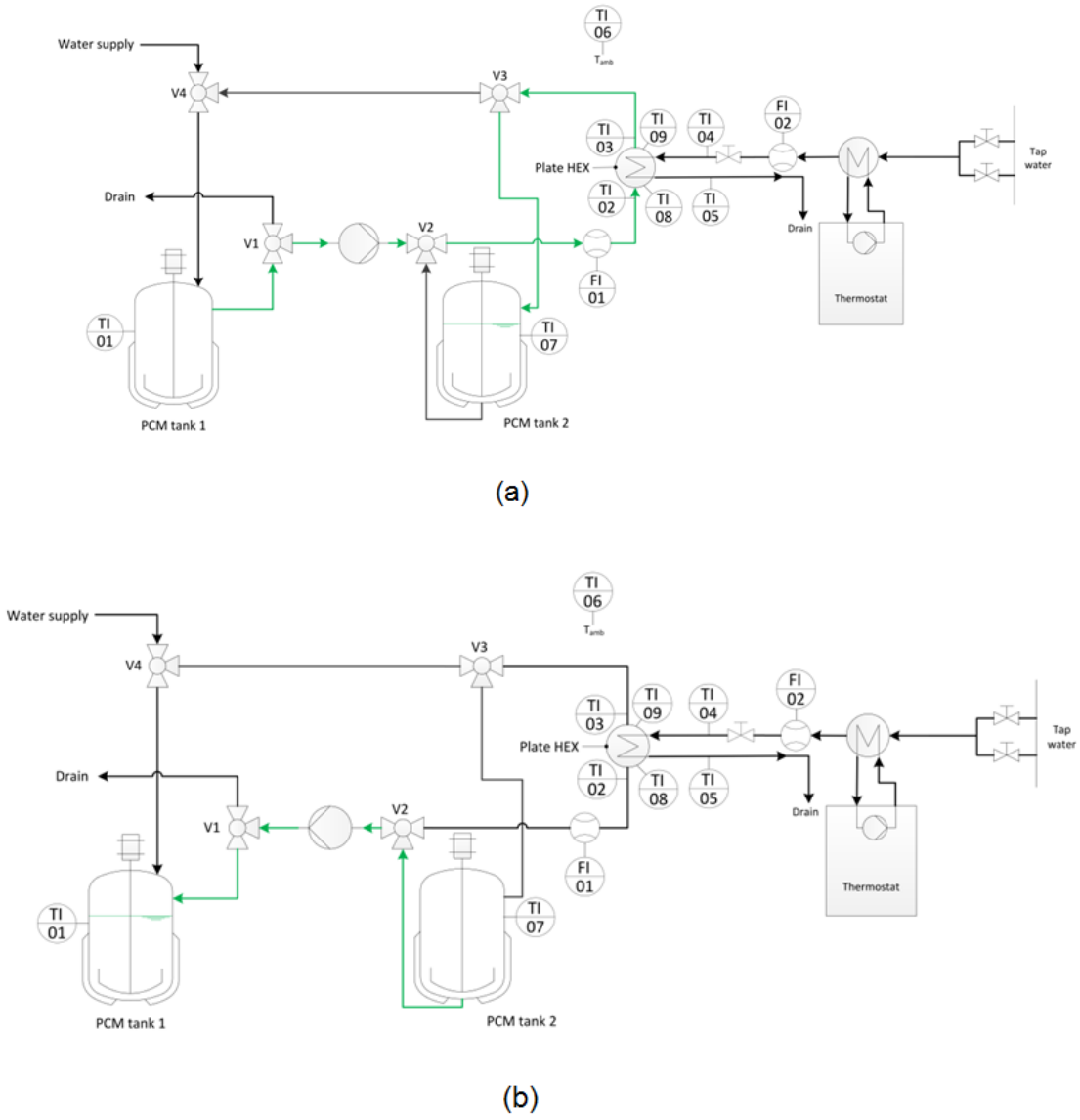

Figure 48: (a) Batch mode operation: PCS is pumped from tank 1 through the HEX to tank 2 where it is stored. (b) The bidirectional pump allows a direct pumping back of the PCS from tank 2 to tank 1.

As mentioned, batch mode solidification experiments were performed with a 35wt% as well as a 45wt% slurry. Using the 35wt% slurry, a comprehensive study with both crystallization releasing methods previously described as well as a direct crystallization in the heat exchanger was performed for different water inlet temperatures.
In Figure 49, as an example, the obtained measurement results of an experiment with a water inlet temperature of 40°C and a 45wt% slurry are shown. The measured HEX inlet- and outlet

temperatures (a) and volume flow rates (b) are plotted as a function of time. The flow rates measured were filtered using a rational transfer function implemented in Matlab (see [48]) due to the relatively large fluctuations observed in the raw data. In contrary, the temperature curves have not been filtered.

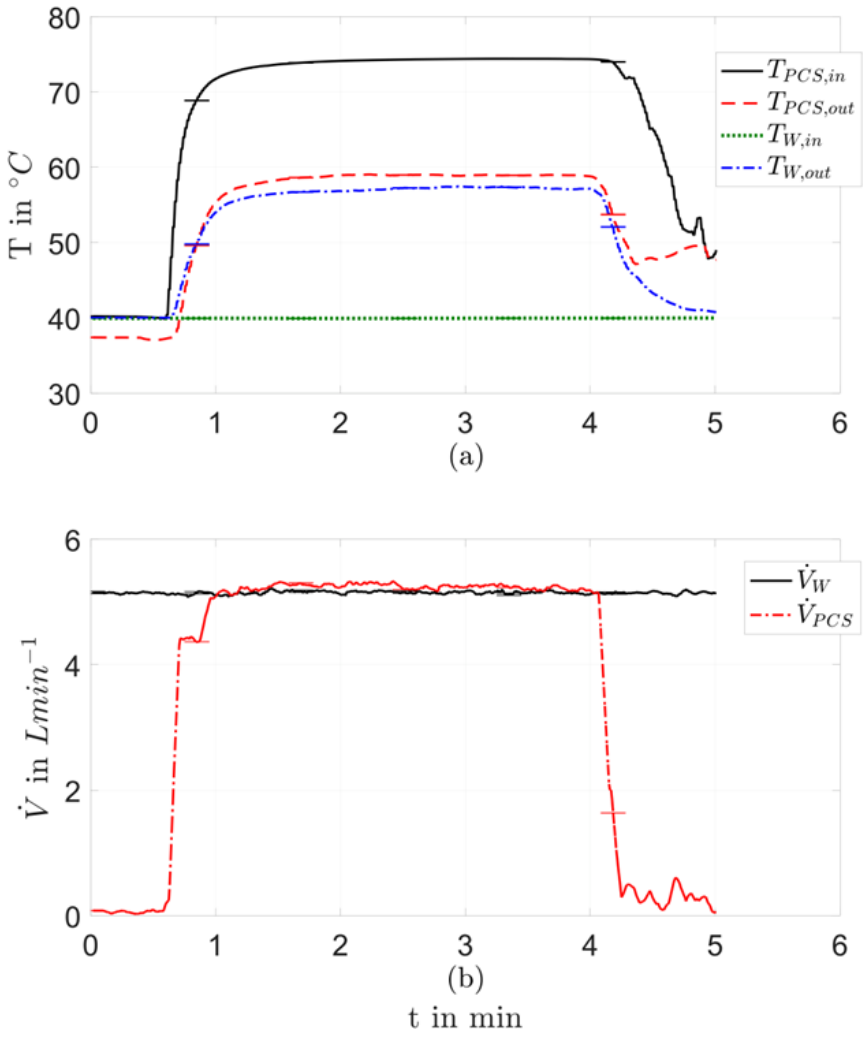

Figure 49: Heat exchanger in- and outlet temperatures (a) and flow rates (b) as a function of time for experiment C2 with a 45wt% PCS and 40°C water inlet temperature.

In Figure 50, the thermal losses in the heat exchanger as well as the heat flow rate transferred by the water are plotted versus time. The thermal losses were estimated based on the HEX surface and ambient temperature. A measurement uncertainty analysis according to GUM has been conducted for all quantities shown.

$$\dot{Q}_W = \dot{V}_W \cdot \rho_W \cdot (T_{W,out} - T_{W,in}) \quad (8)$$

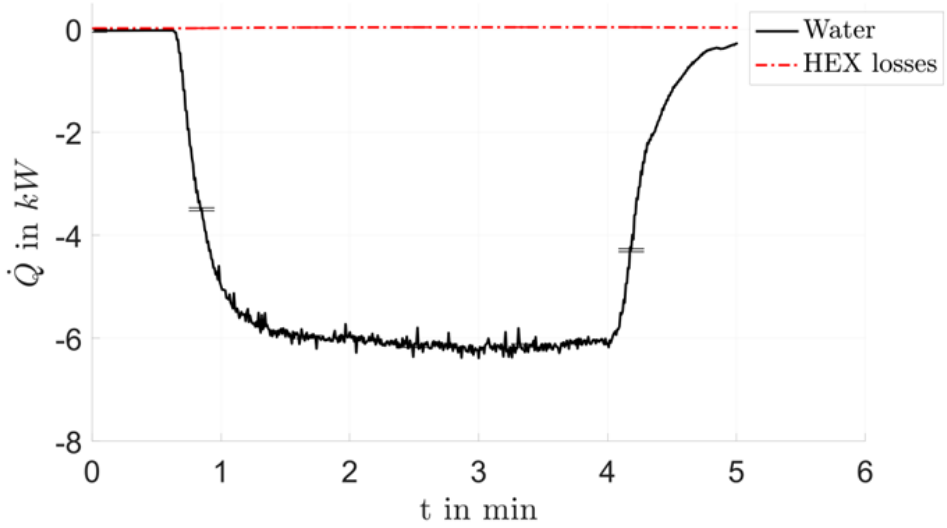

Figure 50: Heat flow rate determined by the water temperature change and flow rate in the HEX as well as heat losses in the heat exchanger as a function of time for experiment C2.

It is worth mentioning that all but one experiments performed showed qualitatively similar results in comparison to the example shown in the previous two plots. These are:

- Steady-state conditions are reached after approx. 2 min. After 2 min no significant temporal change of the measured quantities can be observed.
- There is no evidence for the freezing of the heat exchanger or blockage of the piping system similar to the experiments with the 35wt% slurry.
- The thermal losses in the heat exchanger are in comparison negligible as shown in Figure 50. A similar conclusion can be made for all other experiments of experimental series C.
- The creation of crystals could not be observed in the glass window installed at the HEX outlet in all crystallization experiments.

In the experimental results obtained with 30°C water inlet temperature and a 45wt% slurry shown in the appendix, the volume flow rate of the PCS and the heat flow rate decreased with time. Furthermore, the PCS and water temperature differences between in- and outlet dropped. These effects may be explained by the freezing of the heat exchanger or the beginning blockage of a pipe section. During the experiment, no crystals could be observed in the window placed downstream of the HEX. Hence, it can be assumed that crystallization occurred due to cold spots or the presence of solid crystals from previous experiments in the pipe section between the glass window and PCM tank 2.

To determine whether crystallization occurred (in the HEX or releaser), the specific enthalpy change of the PCS between HEX in- and outlet was determined based on a simple energy balance. The heat exchanger energy balance may be written as:

$$\mathbf{0} = \dot{\boldsymbol{V}}_{\boldsymbol{W}} \cdot \boldsymbol{\rho}_{\boldsymbol{W}} \cdot \boldsymbol{cp}_{\boldsymbol{W}} \cdot \left(\boldsymbol{T}_{\boldsymbol{W,in}} - \boldsymbol{T}_{\boldsymbol{W,out}}\right) + \dot{\boldsymbol{V}}_{\boldsymbol{PCS}} \cdot \boldsymbol{\rho}_{\boldsymbol{PCS}} \cdot \left(\boldsymbol{h}_{\boldsymbol{PCS,in}} - \boldsymbol{h}_{\boldsymbol{PCS,out}}\right) + \dot{\boldsymbol{Q}}_{\boldsymbol{Loss}} \qquad \textbf{(9)}$$

where $h_{PCS,in}$ is defined in Equation 3.The equation can be rearranged to obtain:

$$\Delta h_{PCS} = \left(h_{PCS,out} - h_{PCS,in}\right) = \frac{\dot{Q}_{Loss} + \dot{V}_W \cdot \rho_W \cdot cp_W \cdot \left(T_{W,in} - T_{W,out}\right)}{\dot{V}_{PCS} \cdot \rho_{PCS}} \qquad \textbf{(10)}$$

The enthalpy difference as a function of the PCS temperature change from HEX inlet to outlet or releaser outlet is determined for all experiments listed above and is compared with theoretical values shown in Figure 13 which are based on literature data.

The enthalpy change of the PCS from the heat exchanger inlet to the outlet has been determined for all batch experiments. A measurement uncertainty analysis based on 60-120 consecutive data points and the measurement tolerance of the used sensors according to GUM was performed. In Figure 51 the determined enthalpy change of the 35wt% slurry from in- to outlet Δh_{PCS} is plotted for the different mean PCS heat exchanger outlet temperatures $\overline{\mathrm{T}}_{\mathrm{PCS,out}}$. An equivalent inlet temperature of 65°C $T_{PCS,in}$ was adjusted in all experiments. The red straight line illustrates the expected theoretical enthalpy change for the given temperature difference based on literature data [40]. Furthermore, the theoretical enthalpy change of water is shown with the blue dashed-dotted line. The enthalpy changes determined for experiments with a crystallization trigger device (throttle valve and ultrasonic bath) are based on the energy balance in the heat exchanger. However, in contrast to the other experiments, the temperature measured downstream of the crystallization trigger device is used in the graph.

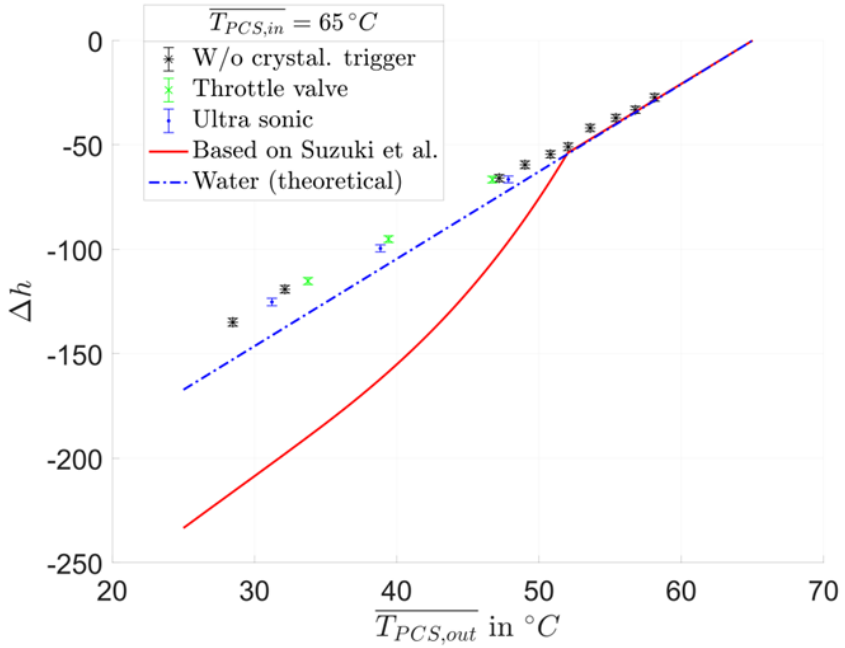

Figure 51: Enthalpy change of the PCS from the heat exchanger inlet to the heat exchanger outlet plotted against the main outlet temperature $\overline{\mathrm{T}}_{\mathrm{PCS,out}}$ for all performed experiments. The experimental data is compared with theoretical values based on literature data and the enthalpy difference of water for the same temperature difference between in- and outlet.

A similar enthalpy/outlet temperature-diagram as for the 35wt% slurry was created based on the experiments performed with the 45wt% slurry. Crystallization releasing methods were not further investigated. The results of 45wt% solidification experiments are shown in Figure 52.

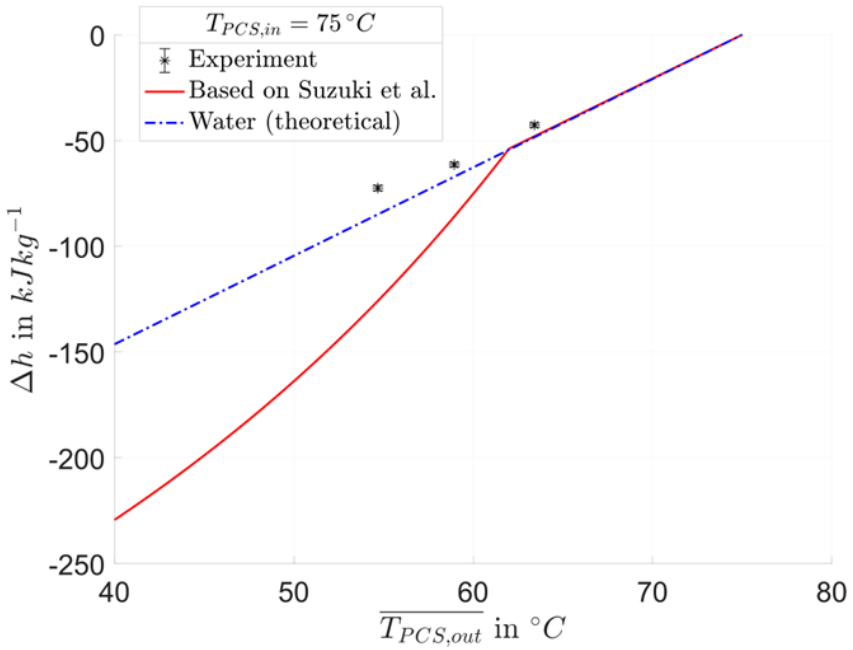

Figure 52: Enthalpy change of the PCS from the heat exchanger inlet to the heat exchanger outlet plotted against the main outlet temperature $\overline{T}_{PCS,out}$ determined for 60 subsequent data points (30s). The experimental data is compared with theoretical values based on literature data and the enthalpy difference of water.

Following results may be derived from Figure 51 and Figure 52:

- The enthalpy difference between in- and outlet of the PCS is negative due to the fact that the PCS is cooled down in the HEX.
- The experimentally determined enthalpy changes show a linear dependency on the temperature difference, similar to water.
- At PCS outlet temperatures above the expected phase change temperature, a small deviation between the theoretical enthalpy change based on literature data and the experimental data can be observed.
- PCS outlet temperatures below the phase change temperature, the deviation between the enthalpy change determined based on literature data and the experimentally determined enthalpy difference increases with decreasing outlet temperature. Therefore and based on the optical observations made during the experiments, it is assumed that in the experiments no crystallization within the piping section between HEX inlet temperature sensor and HEX outlet temperature sensor took place.
- The experiments performed with a crystallization trigger (throttle valve, ultrasonic bath) show no significant difference to the experiments without crystallization stimuli methods. Hence it is assumed that crystallization did as well not take place in the releaser.
- The experimentally determined enthalpy difference of the PCS is slightly smaller than the enthalpy difference of water for the same temperature difference.

- Crystals could optically not be observed at the heat exchanger outlet. However, it appeared that crystallization took place in several experiments in PCM tank 2 or in the pump when the PCS was pumped back into PCM tank 1.
- In general, the determined measurement uncertainty due to measurement device tolerances and the repeat accuracy of subsequent data points is very small and has no impact on the results described above.

5.4.3. Continuous Experiments

To investigate the pumpability of the 45wt% slurry over a larger period of time (more than 1h) as well as the crystallization behaviour of the PCS in continuous circulation, a continuous experiment was performed. As shown in Figure 53, in contrast to the batch mode experiments, the thermostat was connected directly to the heat exchanger which allows an automatic execution of temperature profiles which can be programmed in the thermostat. An internal thermostat temperature T_{int} curve was defined and is shown in Figure 54. As shown, the minimal temperature amounts to 50°C. Hence, the expected maximal hydrate fraction in the slurry according to Figure 12 is approx. 30% if it is assumed that the PCS temperature reaches 50°C. Both, the flow rate of the water as well as of the PCS were set to 5 $Lmin^{-1}$.

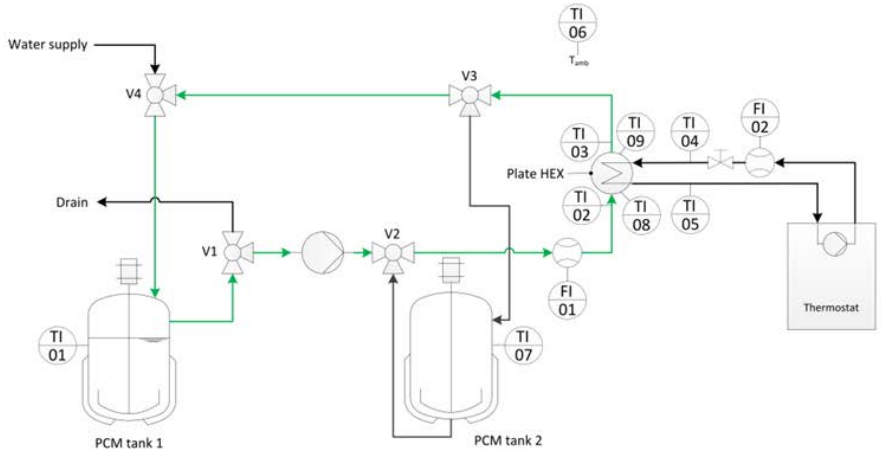

Figure 53: Continuous operation of the test-rig. The PCS is pumped directly back to PCM tank 1 and cooled respectively heated in the heat exchanger which is directly connected to the thermostat.

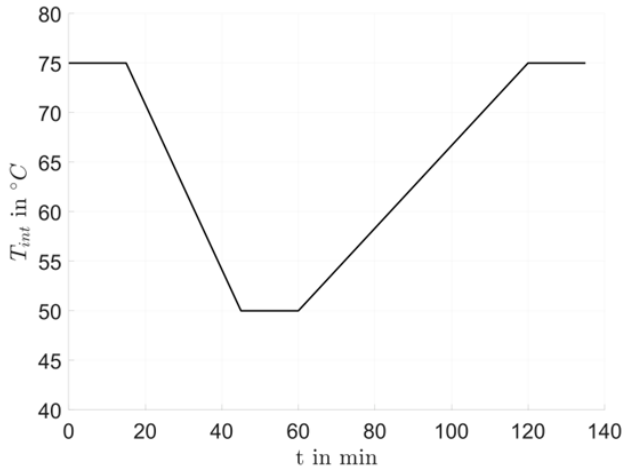

Figure 54: Internal set temperature of the thermostat T*int* as a function of time.

In Figure 55, the heat exchanger in- and outlet temperatures, flow rates as well as heat flow rate transferred to the water are plotted as a function of time. As shown, the PCS is cooled down to approx. 52°C without a blockage of the test-rig. The resulting hydrate fraction in the slurry at this temperature should theoretically amount to around 30% based literature data previously described. In the plots, five events are marked and shall be explained hereinafter:

1. At the first event (position 1, after 25 min), a peak in the slurry temperature curves is identifiable (at approximately 63°C). This peak is due to the crystallization of the PCS and the phase change enthalpy released. Hence, according to the solidification temperature determined in the easymax experiments, almost no supercooling occurred in the continuous pumping mode. After the crystallization event, the slurry which was a clear substance before, turned into a cloudy mixture of salt solution and solid hydrate particles. It is worth mentioning that the location of the first crystallization event in the test-rig could not be clearly identified. It is likely that the first crystal was created on a cold spot or a location with considerable high mechanical stresses (e.g. in the pump). After the first event, a further decrease of the PCS temperature leads to a larger hydrate concentration in the slurry which is connected with the release of latent heat. Consequently, the thermostat cooling rate represented by $\dot{Q}_W$ subsequently increased after event 1 as shown in Figure 55 (c). It is furthermore remarkable that the fluctuation observed in the measured PCS flow rate increased after solid particles were created (after event 1).
2. At the second event, the minimal thermostat temperature was reached. Thus, as shown in Figure 55 (c), the cooling rate of the thermostat decreased afterwards and became zero after approx. 55min absolute experimental time.
3. At the third event marked in Figure 55, the heating process was initiated. Consequently, the water temperature started to increase, and with a delay of around 5min the PCS temperature raised as well.
4. At point 4, the temperature gradient of the water inlet temperature suddenly decreases. Furthermore, as shown in Figure 55 (c), the thermostat heating power did not further increase. This event cannot fully be explained but might be caused by an error in the thermostat control system or program.
5. At the last point, a slight increase of the PCS temperature gradient can be observed. This event might be explained by the fact that no more solid crystals are present in thus heat is only absorbed sensibly (and no longer as well latent due to the melting of crystals).

It is worth mentioning that due to the transient nature of this continuous experiment, the determination of the enthalpy change within the slurry lead to unsatisfactory results. Due to time reasons, the continuous experiment hence was not further analyzed.

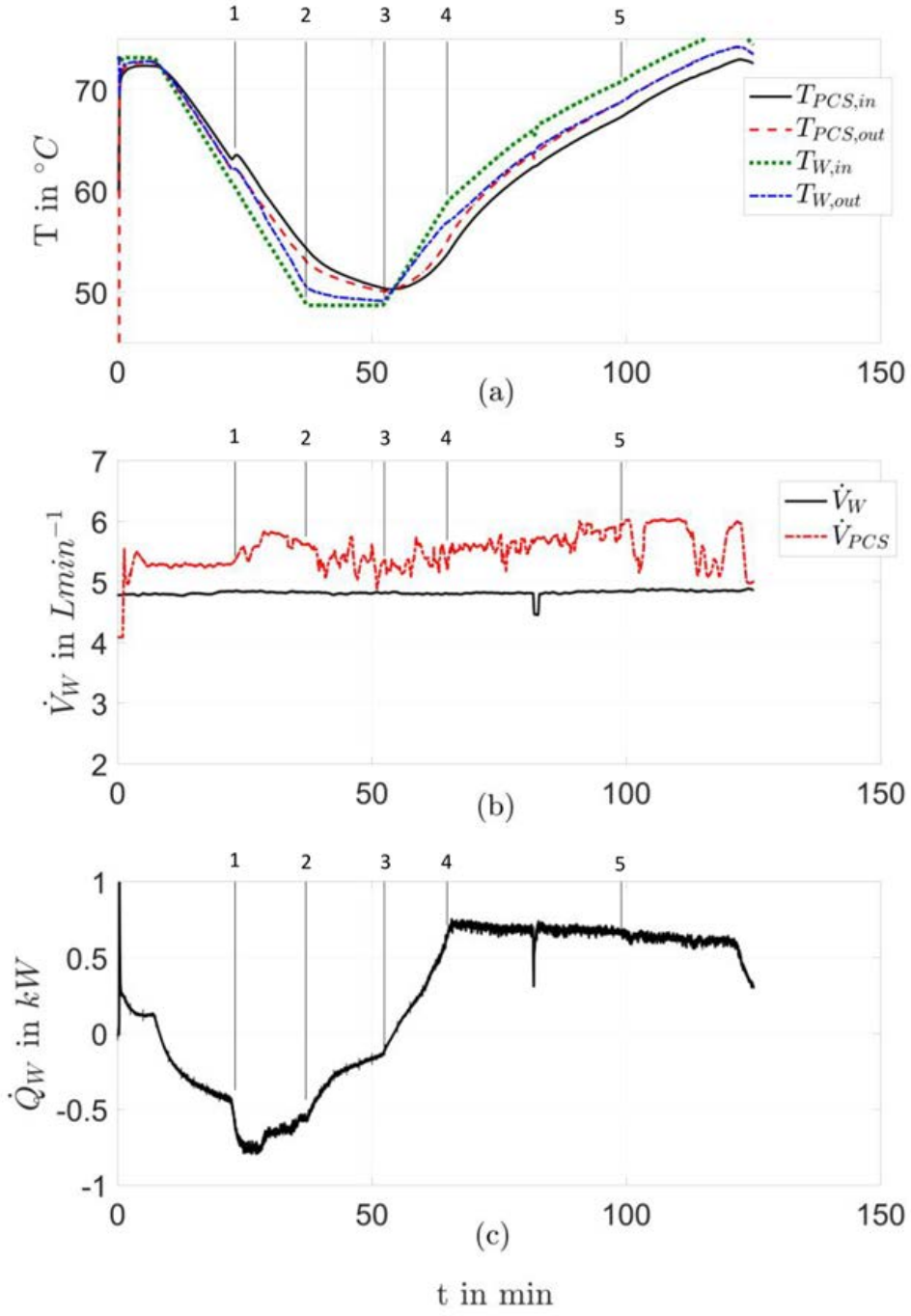

Figure 55: (a) Heat exchanger in- and outlet temperatures of PCS and water, (b) flow rates as well as thermostat heating/cooling power (c) represented by $\dot{Q}_W$ as a function of time for the continuous experiment performed with 45wt% slurry.

5.4.4. Batch Melting Experiments

In order to determine the enthalpy change of the PCS when hydrate crystals are melted, melting experiments for the 45wt% slurry were conducted using the final test-rig. The experiments were conducted with the 45wt% slurry using an initial temperature of 55°C and a hydrate fraction of approx. 25% according to Suzuki et al.[40]. The crystals were produced in a continuous pumping mode as previously described. The experimental procedure is similar to the procedure described in the previous subsection for solidification experiments but with different temperature levels.

In Figure 56, again, the temperature and flow rate profiles of experiment C5 with an water inlet temperature of 80°C are shown. Furthermore, in Figure 57, the measured heat flow rate from the PCS to the water as a well as the heat losses in the heat exchanger as a function of time are plotted.

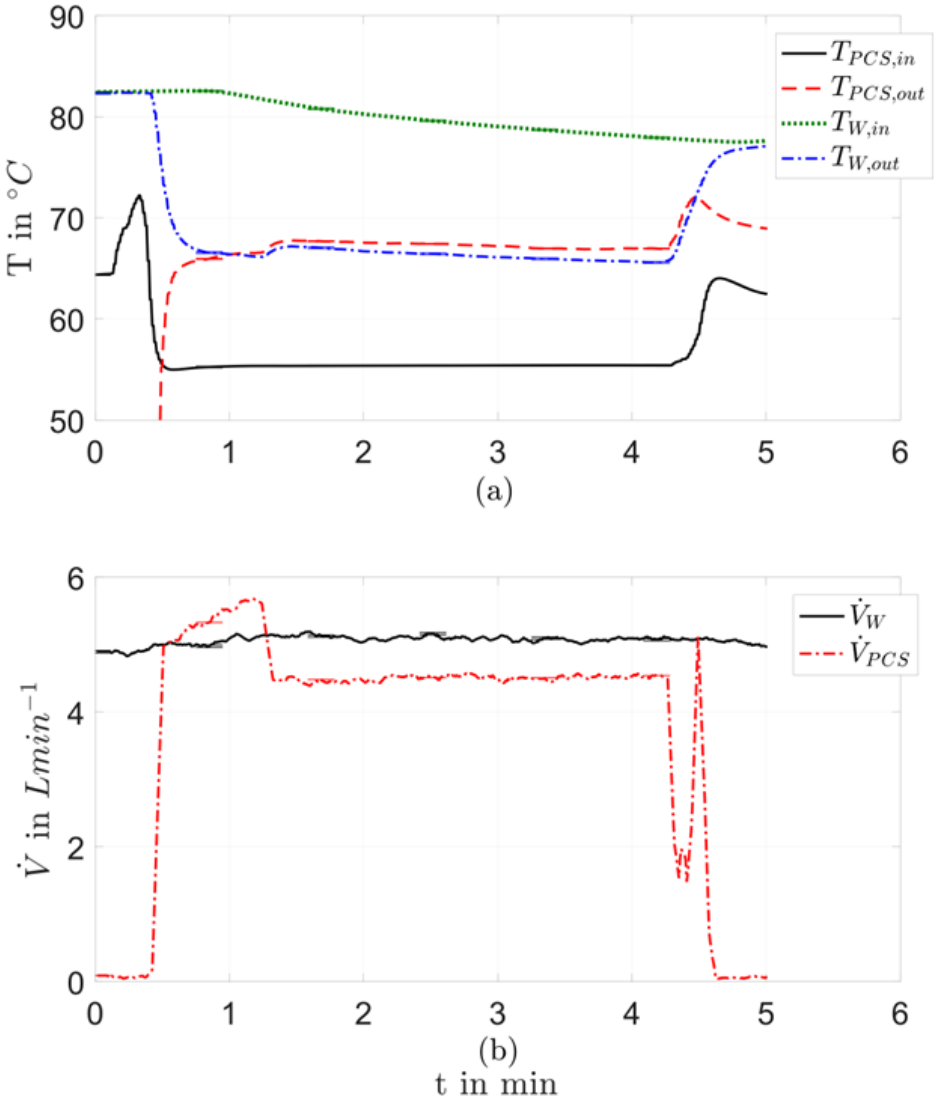

Figure 56: Heat exchanger in- and outlet temperatures (a) and flow rates (b) as a function of time for the 45wt% melting experiment with 80°C water inlet temperature. The water inlet temperature slowly drops with time due to the limited thermal output of the thermostats.

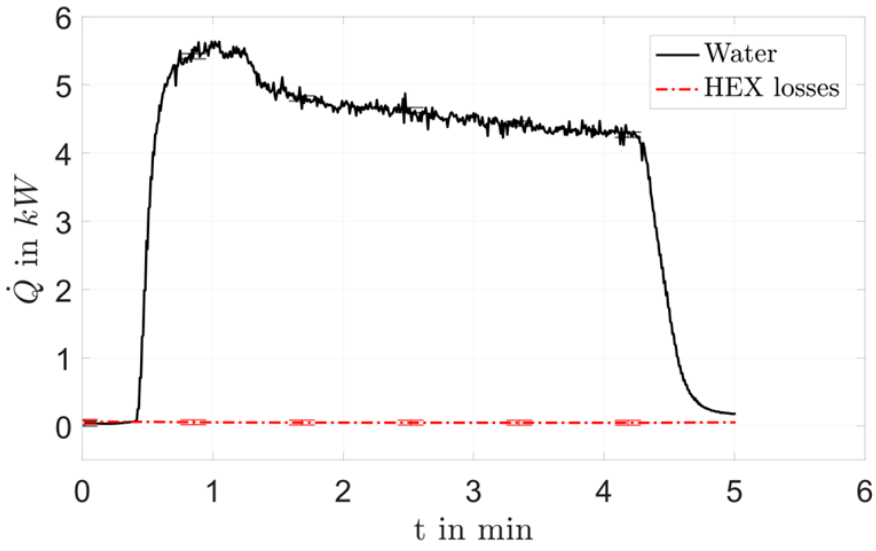

Figure 57: Heat flow rate determined by the water temperature change and flow rate in the HEX as well as heat losses in the heat exchanger as a function of time for experiment C5.

Again, based on the previous plots, following conclusions can be made:

- At the beginning of the experiment (approx. after 30s) the circulation pump was activated. In the experiments it could be observed that a relatively high risk of blockage exists if PCS with a considerable high solid fraction (25%) is pumped into the cold piping system. Hence, it was decided to flush and preheat the piping system initially with an higher PCS flow rate than the finally desired rate. Using this approach, a blockage could be avoided in all melting experiments.
- A constant PCS temperature of 55°C could be kept during the entire batch. However, the water inlet temperature dropped from approximately 82°C to 77°C. This is due to the limited thermal output and high inertia in terms of control system of the used thermostats. Nevertheless, the experiment allows a determination of the PCS enthalpy difference with quasi steady-state conditions.
- By the use of the glass windows installed before and after the HEX, it appeared that solid crystals were melted within the heat exchanger. However, due to the lack of turbidity sensors, this observation could not be quantified.

The enthalpy change, is plotted against the mean outlet temperature of the PCS for all melting experiments. In contrast to the solidification experiments, the enthalpy change in the melting experiments is positive since the PCS outlet temperature is higher than the inlet temperature. The inlet temperature was set to 55°C for all experiments. As shown in Figure 58, a significant deviation between the experimentally determined enthalpy difference and the expected values based on literature can be observed. The measured enthalpy differences are in the range of the enthalpy difference which would results with water and an equivalent temperature difference. This result is astounding since a reduction of solid particles in the HEX could optically be observed. Possible explanations are:

1. Crucial error in experimental procedure: The melting experiments were the last experiments performed of experimental group C of the campaign. Hence it could be

possible that the hydrate concentration in the used PCS at that point of time was significantly smaller than the initial 45wt%.

2. Systematic measurement error: A possible explanation could be the occurrence of a systematic measurement error in the final setup.
3. Material properties: Finally, there is a possibility that the material properties of the used AAH-water solution differ from literature data.

It is furthermore possible that a combination of the three effects may cause the deviation observed.

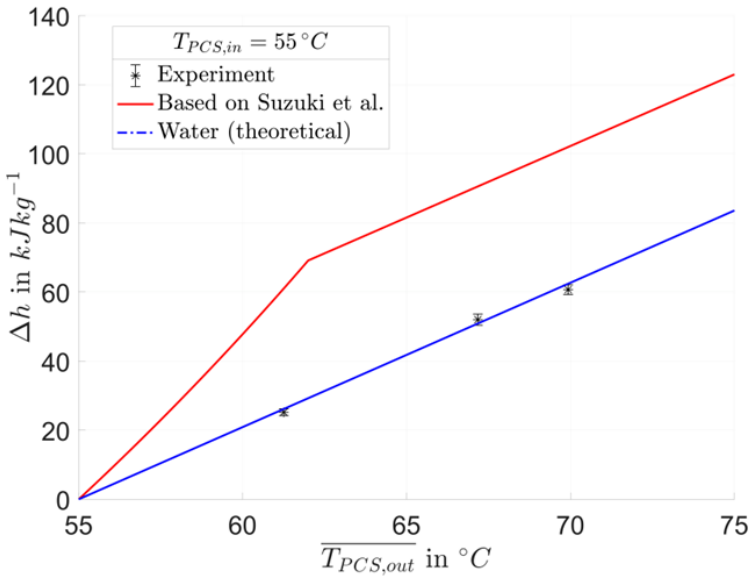

Figure 58: Enthalpy change of the PCS from the heat exchanger inlet to the heat exchanger outlet plotted against the main outlet temperature $\overline{T}_{PCS,out}$ determined for 60 subsequent data points (30s). The experimental data is compared with theoretical values based on literature data and the enthalpy difference of water.

5.5. Summary and Conclusions

In the present project, a functional, modular, high-temperature phase change material test-rig based on industrial standard components was developed and successfully commissioned. The test-rig allows an investigation of the physical and thermal properties of PCS with a fluid temperature of maximum 90°C. Batch mode, as well as continuous experiments, can be conducted and the energy flows within the heat exchanger can accurately be determined. The test-rig was developed by the usage of a flexible, provisional preliminary test-rig which allowed gaining essential findings regarding the behaviour of the used AAH slurry in a piping system regarding pumpability and blockage. The entire heat exchanger in- and outlet design remained unchanged from the preliminary to the final setup.

Basically, all but three requirements were completely achieved. As documented, it was not yet possible fully control crystallization in a defined location. Hence, a triggering of crystallization within the HEX or a crystal releaser in batch mode experiments could not be achieved. Furthermore, in melting processes, an advantage of the used PCS in comparison to water could not be proven. As discussed in this chapter, this could be either due to a

crucial error in the experimental procedure, a systematic error in the test-rig or due to unfavourable material properties.

Nr	Name	Description/Quantification	Degree of fulfillment
1	Production of PCS	PCS should be produced in batch (steady state conditions) and continuous mode.	Batch mode: crystallization could not yet be controlled. Cont. mode: production of PCS possible.
2	Storage of PCS	After PCS is produced, the test-rig should allow to store it in a separated storage.	Fulfilled.
3	Melting of PCS	The test-rig should allow to melt the PCS in the same HEX.	Fulfilled.
4	Modular construction of setup	Heat exchanger, crystallization releaser, pump and other components should be easily exchangeable.	Fulfilled.
5	Temperature range	50-90 °C.	Fulfilled.
6	Optical observation	The test-rig should allow to optically inspect the flowing PCS, most importantly before and after the HEX.	Fulfilled.
7	Controlled crystallization and melting in the test-rig	The test-rig should allow a crystallization of the (supercooled) PCS in a defined section of the piping system. Furthermore, in case of melting, the phase change should take place as well in a defined section of the rig.	Crystallization could not yet be controlled in a defined section of the rig with the used PCS. Slurry can be melted in the HEX, however, in terms of enthalpy change from in- to outlet, melting enthalpy absorbed could not be identified.
8	Determination of crystal fraction	In case of crystallization, the test-rig should allow to determine the hydrate fraction x_H within the slurry after crystallization.	Since crystallization could not yet be controlled, the determination of solid fraction could not yet be achieved.

Table 11: List of requirements for the PCS test-rig and degree of fulfillment of the final rig.

Within the project, a comprehensive experimental campaign was performed using three different types of experiments (i) batch mode solidification experiments (ii) continuous experiments and (iii) batch mode melting experiments. The first series was performed with a 35wt% slurry whereas the second and third series was performed with 45wt% only.

The batch mode solidification experiments showed that a controlled crystallization of the PCS without additives in the HEX is challenging. Furthermore, the two different crystallization releasing methods investigated did not show satisfactory results.

The continuous experiment performed with the 45wt% slurry in the final rig showed that the PCS can be pumped with hydrate fractions of up to 30% in a warm piping system. Furthermore, it could be shown that the material crystallizes almost without supercooling a continuous pumping mode. However, the location of crystallization could not be clearly identified. Furthermore, in batch mode experiments, a controlled crystallization of the PCS in the HEX could not be achieved.
Finally, melting experiments were performed. Unfortunately, an advantage of the used PCS in comparison to water in terms of enthalpy change in melting experiments could not yet be identified. This could either be caused by a deviation between the actual material properties and the expected properties due to a possible creation of low-degree hydrates, crucial errors in the experimental procedure or an unidentified systematic measurement error.

Using the 45wt% slurry in the final test-rig it could be observed that the blockage of the piping system becomes an issue if slurry with a high hydrate fraction is pumped with low flow rates into a cold (room temperature) piping system or if the PCS is cooled with low water inlet temperatures (<30°C). Furthermore, an unexpected shutdown of the system can lead to a blockage of the piping system due to the high sedimentation rate of the AAH slurry without additives. The effect is especially crucial at the bottom of long vertical pipe sections which should hence be avoided.
Based on the findings of the present project it is, as a first step, recommended to further characterize the thermal properties of the used AAH slurry. The focus of the material study should especially be on the possible creation of hydrates of lower degree which could be formed due to local fluctuations in salt concentrations. Furthermore, it is recommended to use thickeners and surfactants to decrease the high sedimentation rate of the AAH slurry, which significantly increases the risk of a blockage of the piping system. An alternative would be the usage of a different PCS with a lower density difference between solid crystals and liquid phase. The risk of (thermally) unsolvable piping blockages could furthermore be completely avoided by the usage of a PCS with a phase change temperature below room temperature.
In a second step, after the possible modification/change of the PCS, the development of the test-rig should be continued. A second heat exchanger should be installed to allow a continuous, steady-state operation of experiments as presented in the appendix. Using this approach, steady-state conditions could be adjusted more precisely, without the time constraint of a batch. Afterwards, the proposed crystallization enhancement methods such as the usage of an ultrasonic sonotrode should be investigated. Finally, it is recommended to install turbidity sensor to quantify the presence of solid crystals in the PCS before and after the heat exchanger(s).

6. Techno-economic Analysis

Along with the physical characteristics and performance of the phase change slurry, it is also crucial to develop an understanding for the potential investment costs of a slurry storage system. Therefore, a techno-economic analysis was carried out in order to assess a slurry storage system in terms of its economic viability.

6.1. Process used for the case study

A fictive process served as a basis for comparing the financial performance of the slurry storage system to a conventional water storage system. Figure 59 shows the scheme of the process used for the techno-economic analysis.

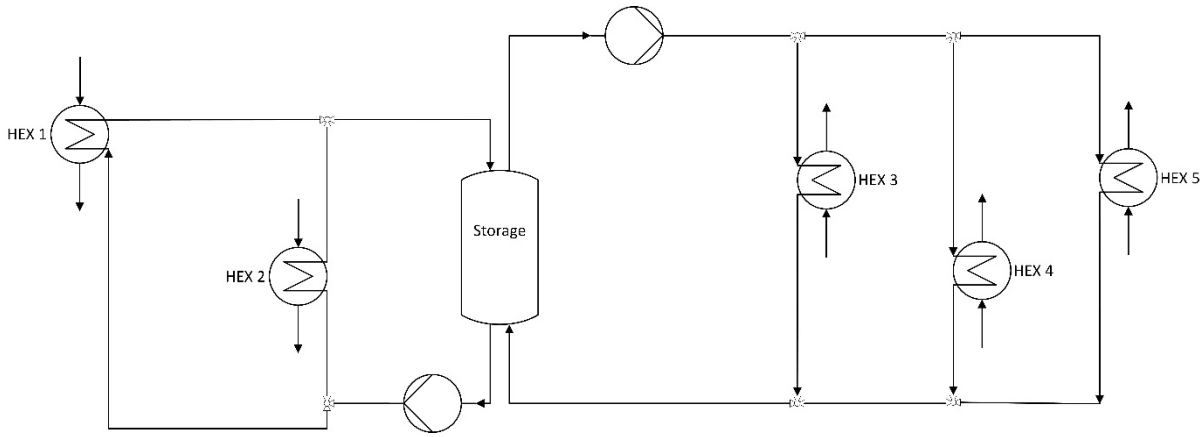

Figure 59. Scheme of the fictive process used for the techno-economic analysis

The scheme depicts the intermediate loop used for the heat recovery within a batch process. In a first step, heat is recovered at heat exchanger 1 (HEX 1) and heat exchanger 2 (HEX 2) since both process streams running through these heat exchangers have to be cooled down. After the complete heat recovery, the storage reaches its high temperature level. In a second step, the recovered heat is released to the process streams running through heat exchangers 3-5 (HEX 3-5) since these streams need to be preheated. The process streams in HEX 2-5 are water streams, which need to be preheated or cooled down respectively. The process stream running through HEX 1 is a stream of water vapor. After one complete cycle the storage reaches the same temperature level as at the starting point. For the techno-economic analysis, both, water and the PCM slurry aluminum ammonium sulfate dodecahydrate are used as a heat transfer fluid in the intermediate loop. The heat transfer fluids are compared to each other in terms of their financial viability.Base Case (Water as Sensible Storage Medium)

A base case was defined using water as the heat transfer fluid. The temperature levels within the storage are based on a real process. The heat recovered in HEX 1 and HEX 2 is equal to

the sum of the heat transferred to the process streams in HEX 3-5. The temperature levels of the various process streams were set accordingly. The power of the various heat exchangers was determined by specifying a time limit for each process stream in which the batch has to be cooled down or preheated. Subsequently, the resulting mass flows could be determined. Figure 60 illustrates the process scheme for the base case with the corresponding temperature levels. As it can be seen, the vapor stream in HEX 1 is condensing at a temperature of 74°C.

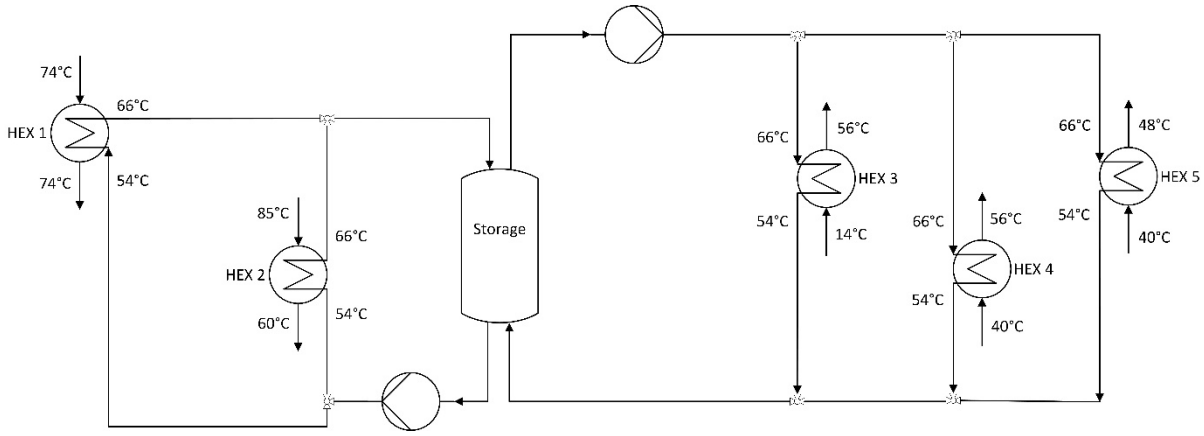

Figure 60.Scheme with temperature levels of the base case

For the base case, a heat transfer coefficient of $1000\ \frac{W}{m^2K}$ was assumed for all heat exchangers. Using these assumptions, the resulting mass flows, the storage volume and heat exchanger areas could be determined. Table 12 shows some of the important characteristics of the intermediate loop. T_{hot} and T_{cold} indicate the high and low temperature level of the storage. P_{HEX1-5} show the power of the various heat exchangers and $\dot{m}_{HEX1-5}$ the mass flows of the intermediate loop streams running through the different heat exchangers.

Total heat recovery	50 kWh
Volume Storage	3550 l
Total heat exchanger area	36 m^2
T_{hot}	66 °C
T_{cold}	54 °C
$\Delta T_{storage}$	12 K
cp_{water}	4.184 kJ/(kg·K)
P_{HEX1}	125.7 kW
P_{HEX2}	70.7 kW
P_{HEX3}	32.7 kW
P_{HEX4}	116.9 kW
P_{HEX5}	139.8 kW
$\dot{m}_{HEX1}$	2.5 kg/s
$\dot{m}_{HEX2}$	1.4 kg/s
$\dot{m}_{HEX3}$	0.65 kg/s
$\dot{m}_{HEX4}$	2.33 kg/s
$\dot{m}_{HEX5}$	2.78 kg/s

Table 12. Intermediate loop characteristics for base case

Two cases with different assumptions were defined for the intermediate loop using the slurry as the heat transfer fluid. For the first case, case 1, the assumption was made that the slurry in the intermediate loop has the same mass flows as in the base case. For the second case, case 2, it was assumed that the temperature levels of the storage are equivalent to the temperature levels in the base case. Furthermore, a slurry with 45 wt% aluminum ammonium sulfate dodecahydrate had to be chosen for case 1 and case 2 since otherwise the melting temperature would have been too low. The data showed in Figure 13 were used to determine the relation between the temperature and the hydrate fraction of the slurry. The figure shows that a 45 wt% slurry has a melting temperature (liquidus line) of approximately 63°C whereas the melting temperature of a 35 wt% slurry is approximately 51°C. Looking at the temperature levels of the storage one clearly sees that a melting temperature of 51°C would be too low and thus a 45 wt% slurry was chosen.

Choosing an adequate heat transfer coefficient for slurry represents a rather large uncertainty. No literature values were found. The CC TES has great experience with phase change dispersions (PCDs), which exhibit similar behavior and characteristics as the phase change slurries. Hence, a conversion factor for the heat transfer coefficient of water and PCD was created. This conversion factor was subsequently applied to the heat transfer coefficients used in the base case to obtain a reasonable approximation for the slurry (slurry medium). However, since this approach is still subject to some degree of uncertainty a sensitivity analysis was carried out. To obtain an upper (slurry high) and lower (slurry low) value for the heat transfer coefficient, ± 50% were added to the conversion factor. The results are shown in Table 13.

Medium	**Heat transfer coefficient** $[\frac{W}{m^2K}]$
Water (base case)	1000
Slurry medium	703
Slurry high	1054.5
Slurry low	351.5

Table 13. Heat transfer coefficients

6.2. Case 1 – Constant Mass Flow

Figure 61 depicts the scheme of the intermediate loop of case 1. Since the mass flows and the lower temperature level of the storage are the same as in the base case but the specific heat capacity does change, the higher temperature level of the storage will change too. The temperature change was calculated by determining the specific enthalpy change of the slurry at a respective ΔT.

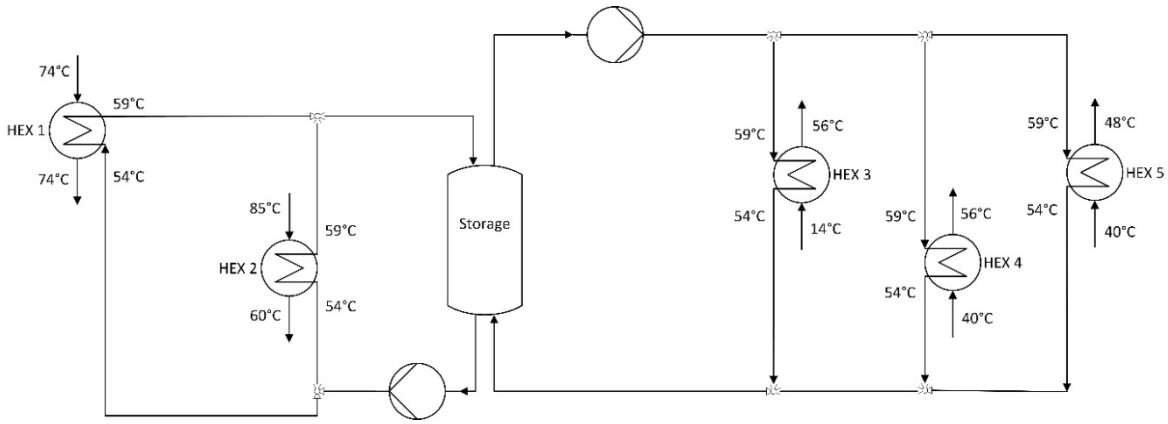

Figure 61. Scheme of case 1

The resulting characteristics of the intermediate loop of case 1 are shown in Table 14. As one can see, the mass flows and the lower temperature level of the storage did not change. Furthermore, the total heat recovery and the power of all heat exchangers are the same as in the base case too. The upper temperature level of the storage decreased to 59°C. Since the specific enthalpy change of the slurry is larger than the specific enthalpy change of water in the base case, the required storage volume decreased by approximately 14%.

Total heat recovery	50 kWh
Volume Storage	3060 l
T_{hot}	59 °C
T_{cold}	54 °C
$\Delta T_{storage}$	5 K
Δh_{pcs}	50.2 kJ/kg
P_{HEX1}	125.7 kW
P_{HEX2}	70.7 kW
P_{HEX3}	32.7 kW
P_{HEX4}	116.9 kW
P_{HEX5}	139.8 kW
$\dot{m}_{HEX1}$	2.50 kg/s
$\dot{m}_{HEX2}$	1.41 kg/s
$\dot{m}_{HEX3}$	0.65 kg/s
$\dot{m}_{HEX4}$	2.33 kg/s
$\dot{m}_{HEX5}$	2.78 kg/s

Table 14. Intermediate loop characteristics for case 1

Since in this case the power and the mass flows are given (and therefore indirectly also the change in temperature), the change in the heat transfer coefficient results in heat exchanger areas which differ from the base case. Table 15 shows the resulting heat exchanger areas for the three different heat transfer coefficients of the slurry. The table clearly shows that the value of the heat transfer coefficient has a large influence on the resulting HEX areas. For the medium value, where just the conversion factor is applied, the use of a phase change slurry leads to a 63% increase of HEX area. In case of the low heat transfer coefficient value the area increase is approximately 272%. The HEX area increases about 9% compared to the base case if the heat transfer coefficient is as high as $1054.5\ \frac{W}{m^2K}$.

	Heat transfer coefficient [$\frac{W}{m^2K}$]	Total heat exchanger area [m^2]
Slurry medium	703	59
Slurry high	1054.5	39
Slurry low	351.5	118

Table 15. Resulting total heat exchanger areas with different heat transfer coefficients case 1

6.3. Case 2 – Constant Storage Temperature Level

The scheme of the intermediate loop of case 2, same storage temperatures as in the base case, is the same as for the base case depicted in Figure 61. The specific enthalpy change of the slurry was determined using the same basic procedure as in case 1. However, in case 2 the temperature difference was already given and was not determined in an iterative manner as in case 1. Table 16 shows the characteristics of the intermediate loop of case 2. Again, the total heat recovery as well as the power of the heat exchangers are equivalent to the base case. The resulting mass flows were determined with the help of the specific enthalpy change of the slurry and the pre-defined power of the heat exchangers. One can see that the respective mass flows are all lower than in the base case, since the specific enthalpy change is rather high. The high specific enthalpy change is also the reason why there is a substantial reduction of the storage volume of approximately 58%.

Total heat recovery	50 kWh
Volume Storage	1478 l
T_{hot}	66 °C
T_{cold}	54 °C
$\Delta T_{storage}$	12 K
Δh_{pcs}	103.9 kJ/kg
P_{HEX1}	125.7 kW
P_{HEX2}	70.7 kW
P_{HEX3}	32.7 kW
P_{HEX4}	116.9 kW
P_{HEX5}	139.8 kW
$\dot{m}_{HEX1}$	1.21 kg/s
$\dot{m}_{HEX2}$	0.68 kg/s
$\dot{m}_{HEX3}$	0.31 kg/s
$\dot{m}_{HEX4}$	1.12 kg/s
$\dot{m}_{HEX5}$	1.34 kg/s

Table 16. Intermediate loop characteristics for case 2

The total heat exchanger area for the different heat transfer coefficients is depicted in Table 17. Since most of the logarithmic mean temperature differences of the heat exchangers are higher in case 2, the total HEX area is smaller compared to case 1. However, compared to the base case the area increases for the medium and low heat transfer coefficient about 44% and 184% respectively. Only in the case of a high heat transfer coefficient the HEX area decreases about 5%.

	Heat transfer coefficient [$\frac{W}{m^2K}$]	Total heat exchanger area [m^2]
Slurry medium	703	52
Slurry high	1054.5	34
Slurry low	351.5	102

Table 17. Resulting total heat exchanger areas with different heat transfer coefficients case 2

6.4. Comparison Investment Costs

The investment costs for the storage system comprise the following components:

- Storage tank
- Pumps
- Controls
- Valves
- Heat exchangers
- Pipes
- Stirrer
- Aluminum ammonium sulfate dodecahydrate (AAH)

The last two points only apply to the slurry storage system. Table 18 shows the total investment costs for the different cases. The costs of the heat exchanger of the slurry storage system, case 1 and case 2, were determined using the medium heat transfer coefficient. Some of the component costs such as pipes or controls were assumed the same for every case, no matter which heat transfer fluid is used. The costs of the storage tank for the slurry are considerably higher as for water, even with a reduction of the storage volume of 58% as seen in case 2. The reason for this is the need of stainless steel as storage material when slurry is used (compared to normal steel for water). The low price difference of the pumps results from the use of different pump types. Impeller pumps are used for the slurry and centrifugal pumps for water. The price of the AAH depends on the required mass for the 45%wt slurry and since the storage volume of case 1 is higher than in case 2, the amount of AAH increases respectively.

	Base case [CHF]	Case 1 [CHF]	Case 2 [CHF]
Storage tank	6’900	16’200	9’600
Pumps	2’660	2’410	2’410
Controls	10’000	10’000	10’000
Valves	2’500	2’500	2’500
Heat exchangers	9’133	13’765	12’221
Pipes	2’000	2’000	2’000
Stirrer	-	4’000	4’000
AAH	-	6’633	3’200
Total	33’209	57’525	45’952

Table 18. Investment costs for the different cases (medium heat transfer coefficient)

As mentioned above, the costs of the heat exchangers in Table 18 were determined using the medium heat transfer coefficient. The costs for the heat exchangers and the total investment costs will change accordingly, if the lower and higher value of the heat transfer coefficient is

used. This can be seen in Table 19 where the investment costs per kWh of all cases including the different heat transfer coefficient values are depicted. The results show that heat transfer coefficient can have a considerable impact on the investment costs, negative or positive. However, even with optimistic assumptions are the costs for the slurry system considerably higher as for a water storage system.

	Heat transfer coefficient slurry	Investment Costs [CHF]	Investment Costs [CHF/kWh]
Base Case		33'209	671
Case 1			
	Low	69'531	1'404
	Medium	57'525	1'162
	High	53'583	1'082
Case 2			
	Low	56'353	1'138
	Medium	45'952	928
	High	42'458	858

Table 19. Investment costs for the different cases with the different heat transfer coefficients

6.5. Summary & Conclusions

Comparing the investment costs of slurry and water as a heat transfer fluid in an intermediate loop revealed that water is likely to be more favorable from a financial point of view in general, even if optimistic assumptions are considered. The case study also showed that it is crucial that a high hydrate fraction is melted/solidified during the process. This is evident if one compares case 1 and 2. In case 2 a much larger hydrate fraction is melted which results in a higher specific enthalpy change of the slurry. This again favors a smaller storage volume. Furthermore, it is also important that the storage exhibits a rather large temperature difference between fully loaded and unloaded storage. Case 1 illustrates that a low storage temperature difference results in a large financial penalty. Other disadvantages when using a slurry include the need of stainless steel, the rather high price of the AAH and the need of a stirrer. Thus, although there might be certain cases where the use of slurries is favored, e.g. if there is a restriction in space, the use of slurries should not be restricted to pure energy applications. Making use of the "quality aspect" in processes, which need constant temperature (e.g. food, pharmaceutical) could offer a promising business case. Finally, it must be stated that the results of the case study cannot be considered as a general conclusion. That means for really assessing whether the slurry would be more favorable than water in a specific process, a more detailed storage integration analysis would be needed. The result should rather be considered as an initial assessment for deciding whether to generally proceed further in this field of application or not.

7. Conclusions and Outlook

In this work, the continuous production of a slurry at 63 °C could be demonstrated. This is the first time that the continuous production of a phase change slurry has been reported in

literature. The material evaluation lead to the choice of aluminium ammonium sulfate dodecahydrate (AAH) ($NH_4Al(SO_4)_2 \cdot 12H_2O$) as the most promising PCM for the temperature range of 60-90°C. Key criteria for this decision were the favourable thermo-physical properties of the particular salt hydrate, its extended characterization documented in literature and the possibility to adapt its melting point with the addition of water to cover the whole temperature range of interest. Further evaluation of the material at HSLU revealed that the material presents a high supercooling and segregation behaviour which make the material characterization with standard equipment particularly challenging. Extensive studies were performed to supress the undesired properties by the use of additives (surfactants and thickeners). The segregation could be delayed significantly in comparison to the untreated material but further investigation is required to ensure a robust sample preparation that would be meaningful for industrial applications.

The first techno-economic considerations showed that this technology can achieve a high volume reduction of the storage tank (up to 50%) in comparison to water with an increase in the investment costs in the order of 39%. Since the economics are at the moment unfavourable for the case of PSC in comparison to water, the target industrial processes should be the ones that have high space restrictions and/or high requirements in temperature stability (“precision applications”). In such processes, the PCS would offer an extra added value in comparison to water which was not taken into account in the present techno-economic analysis.

To conclude, the potential and feasibility of Phase Change Slurries for industrial process could be demonstrated at 63 °C. The Technology Readiness Level of PCS for heating applications is significantly lower than the one for cooling applications and further research should be conducted before commercialization. More specifically the following goals are defined for the next research steps:

- The factors that influence supercooling and the triggering of crystallization should be better understood. An effective crystallization trigger should be developed that would allow for the controlled crystallization start at a specified location

- The material should be better characterized. Larger scale calorimetric techniques should be developed that allow for the determination of phase change enthalpy and melting temperature at larger volumes and with continuous stirring of the slurry

- The influence of surfactants, thickeners and their combination on phase separation, supercooling and thermo-physical properties of the PCS should be further investigated. An modified slurry composition should be developed that ensures sedimentation delay for several hours and is robust enough to be suitable for industrial applications.

8. Literature

[1] S. Bachmann, R. Scherer, P.A. Salamin, M. Ferster, J. Gulden, Energieverbrauch in der Industrie und im Dienstleistungssektor-Resultate 2012, 2013. http://www.bfe.admin.ch/themen/00526/00541/00543/index.html?lang=de&dossier_id=00775.

[2] S. Frisch, M. Pehnt, M. Nast, Prozesswärme im Marktanreizprogramm Zwischenbericht zu Perspektivische Weiterentwicklung des Marktanreizprogramms FKZ 03MAP123, 2010. http://www.dlr.de/tt/Portaldata/41/Resources/erneuerbare_energien_allgemein/Prozesswaerme_im_MAP.pdf.

[3] R. Kuder, Energieeffizienz in der Industrie - Modellgestützte Analyse des effizienten Energieeinsatzes in der EU-27 mit Fokus auf den Energiesektor, 2014. http://d-nb.info/1049260554/34.

[4] C. Lauterbach, B. Schmitt, K. Vajen, U. Jordan, Das Potential solarer Prozesswärme in Deutschland, 2011. https://www.uni-kassel.de/maschinenbau/fileadmin/datas/fb15/Potential_solarer_Prozesswaerme_in_Deutschland.pdf.

[5] F. Mauthner, M.H.C. Fink, C. Brunner, L. Scheller, Angepasste solare Prozesswärmekonzepte für Brauereien, in: AEE - Institut für nachhaltige Technologie, 2011.

[6] P. Zhang, Z.W. Ma, R.Z. Wang, An overview of phase change material slurries: MPCS and CHS, Renew. Sustain. Energy Rev. 14 (2010) 598–614. doi:http://dx.doi.org/10.1016/j.rser.2009.08.015.

[7] M. Kauffeld, M. Kawaji, P.W. Egolf, Handbook on ice slurries: Fundamentals and engineering, 2005.

[8] J.-P. Bédécarrats, T. David, J. Castaing-Lasvignottes, Ice slurry production using supercooling phenomenon, Int. J. Refrig. 33 (2010) 196–204. doi:http://dx.doi.org/10.1016/j.ijrefrig.2009.08.012.

[9] M. Kauffeld, M.J. Wang, V. Goldstein, K.E. Kasza, Ice slurry applications, Int. J. Refrig. 33 (2010) 1491–1505. doi:http://dx.doi.org/10.1016/j.ijrefrig.2010.07.018.

[10] Marino Grozdek, Load Shifting and Storage of Cooling Energy through Ice Bank or Ice Slurry Systems - modelling and experimental analysis, Royal Institute of Technology Stockholm, 2009.

[11] P.W. Egolf, M. Kauffeld, From physical properties of ice slurries to industrial ice slurry applications, Int. J. Refrig. 28 (2005) 4–12. doi:http://dx.doi.org/10.1016/j.ijrefrig.2004.07.014.

[12] J. Bellas, I. Chaer, S. a. Tassou, Heat transfer and pressure drop of ice slurries in plate heat exchangers, Appl. Therm. Eng. 22 (2002) 721–732. doi:10.1016/S1359-4311(01)00126-0.

[13] M.N.A. Hawlader, M.A. Wahed, Analyses of ice slurry formation using direct contact heat transfer, Appl. Energy. 86 (2009) 1170–1178. doi:http://dx.doi.org/10.1016/j.apenergy.2008.11.003.

[14] E. Oró, C. Barreneche, M.M. Farid, L.F. Cabeza, Experimental study on the selection of phase change materials for low temperature applications, Renew. Energy. 57 (2013) 130–136. doi:10.1016/j.renene.2013.01.043.

[15] H. Suzuki, N. Wada, Y. Komoda, H. Usui, S. Ujiie, Drag reduction characteristics of trimethylolethane hydrate slurries treated with surfactants, Int. J. Refrig. 32 (2009) 931–937. doi:10.1016/j.ijrefrig.2008.11.003.

[16] S. Wenji, X. Rui, H. Chong, H. Shihui, D. Kaijun, F. Ziping, Experimental investigation on TBAB clathrate hydrate slurry flows in a horizontal tube: Forced convective heat transfer behaviors, Int. J. Refrig. 32 (2009) 1801–1807. doi:10.1016/j.ijrefrig.2009.04.008.

[17] X.J. Shi, P. Zhang, Cold storage by tetra-n-butyl ammonium bromide clathrate hydrate

slurry generated with different storage approaches at 40 wt% initial aqueous solution concentration, Int. J. Refrig. 42 (2014) 77–89. doi:http://dx.doi.org/10.1016/j.ijrefrig.2014.02.002.
[18] M. Darbouret, M. Cournil, J.-M. Herri, Rheological study of TBAB hydrate slurries as secondary two-phase refrigerants, Int. J. Refrig. 28 (2005) 663–671. doi:http://dx.doi.org/10.1016/j.ijrefrig.2005.01.002.
[19] H. Suzuki, T. Itotagawa, Y.S. Indartono, H. Usui, N. Wada, Rheological characteristics of trimethylolethane hydrate slurry treated with drag-reducing surfactants, Rheol. Acta. 46 (2006) 287–295. doi:10.1007/s00397-006-0119-x.
[20] H. Hidaka, M. Yamazaki, M. Yabe, H. Kakiuchi, M. Kubota, F. Watanabe, H. Matsuda, Evaluation of trimethylolethane trihydrate containing additives lower-ing the melting point for cold heat storage, Kagaku Kogaku Ronbunshu. 33 (2007) 59–64. doi:10.1252/kakoronbunshu.33.59.
[21] M. Yamazaki, C. Sasaki, H. Kakiuchi, Y.T. Osano, H. Suga, Thermal and structural characterization of trimethylolethane trihydrate, Thermochim. Acta. 387 (2002) 39–45. doi:http://dx.doi.org/10.1016/S0040-6031(01)00821-8.
[22] H. Mehling, Verfahren zum Einsatz schlecht kristallisierender Salzhydrate als Latentwärmespeichermaterial, 2009.
[23] H. Schmit, M. Frank, C. Rathgeber, S. Hiebler, Investigation of K2HPO4·6H2O as Phase Change Slurry (PCS), in: 11th IIR Conf. Phase Chang. Mater. Slurries Refrig. Air Cond., Karlsruhe, 2016: pp. 217–225.
[24] H. Suzuki, T. Kishimoto, Y. Komoda, H. Usui, Investigation of Thermal Properties of Na2HPO4 Hydrate Slurries for Evaluating Their Use as a Coolant in Absorption Chillers, J. Chem. Eng. JAPAN. 43 (2010) 34–39. doi:10.1252/jcej.09we069.
[25] R. Hidema, T. Tano, H. Suzuki, M. Fujii, Y. Komoda, T. Toyoda, Phase Separation Characteristics of Ammonium Alum Hydrates with Poly Vinyl Alcohol, J. Chem. Eng. JAPAN. 47 (2014) 169–174. doi:10.1252/jcej.13we085.
[26] R. Hidema, H. Suzuki, T. Tano, Y. Komoda, With Surfactants As Drag-Reducers and With Polyvinyl Alcohol As Stabilizers, in: Proc. 15th Int. Heat Transf. Conf., Begellhouse, Connecticut, 2014: pp. 1–14. doi:10.1615/IHTC15.fcv.009469.
[27] H. Suzuki, T. Konaka, Y. Komoda, T. Ishigami, Flow and heat transfer characteristics of ammonium alum hydrate slurries, Int. J. Refrig. 36 (2013) 81–87. doi:http://dx.doi.org/10.1016/j.ijrefrig.2012.09.013.
[28] R. Hidema, H. Suzuki, H. Sato, Y. Komoda, K. Nakamura, Particle Sedimentation Depression with Stabilizers and Surfactants on Phase Change Materials, in: 11th IIR Conf. Phase Chang. Mater. Slurries Refrig. Air Cond., 2016.
[29] H. Mehling, L.F. Cabeza, Heat and cold storage with PCM, Hand Book, Publ. Springer, Ger. (2008).
[30] K. Pielichowska, K. Pielichowski, Phase change materials for thermal energy storage, Prog. Mater. Sci. 65 (2014) 67–123. doi:http://dx.doi.org/10.1016/j.pmatsci.2014.03.005.
[31] A. Sharma, V. V Tyagi, C.R. Chen, D. Buddhi, Review on thermal energy storage with phase change materials and applications, Renew. Sustain. Energy Rev. 13 (2009) 318–345. doi:http://dx.doi.org/10.1016/j.rser.2007.10.005.
[32] B. Zalba, J.M. Marín, L.F. Cabeza, H. Mehling, Review on thermal energy storage with phase change: materials, heat transfer analysis and applications, Appl. Therm. Eng. 23 (2003) 251–283. doi:http://dx.doi.org/10.1016/S1359-4311(02)00192-8.
[33] M. Kenisarin, K. Mahkamov, Salt hydrates as latent heat storage materials:Thermophysical properties and costs, Sol. Energy Mater. Sol. Cells. 145 (2016) 255–286. doi:10.1016/j.solmat.2015.10.029.
[34] S.D. Sharma, K. Sagara, Latent heat storage materials and systems: a review, Int. J. Green Energy. 2 (2005) 1–56.
[35] M.M. Farid, A.M. Khudhair, S.A.K. Razack, S. Al-Hallaj, A review on phase change energy storage: materials and applications, Energy Convers. Manag. 45 (2004) 1597–

1615. doi:http://dx.doi.org/10.1016/j.enconman.2003.09.015.
[36] L.F. Cabeza, A. Castell, C. Barreneche, A. de Gracia, A.I. Fernández, Materials used as PCM in thermal energy storage in buildings: A review, Renew. Sustain. Energy Rev. 15 (2011) 1675–1695. doi:http://dx.doi.org/10.1016/j.rser.2010.11.018.
[37] Y. Marcus, V. Dangor, S. Lessery, The phase diagram of magnesium bromide and chloride hexahydrate mixtures, Thermochim. Acta. 77 (1984) 219–226. doi:10.1016/0040-6031(84)87061-6.
[38] S.I. Sandler, Chemical, Biochemical, and Engineering Thermodynamics, 4th ed., John Wiley & Sons, 2006.
[39] T. Kousksou, A. Jamil, Y. Zeraouli, Enthalpy and apparent specific heat capacity of the binary solution during the melting process: DSC modeling, Thermochim. Acta. 541 (2012) 31–41. doi:10.1016/j.tca.2012.04.027.
[40] H. Suzuki, T. Konaka, Y. Komoda, T. Ishigami, Flow and heat transfer characteristics of ammonium alum hydrate slurries, Int. J. Refrig. 36 (2013) 81–87.
[41] G.A. Lane, Solar heat storage: Latent heat materials. Volume II. Technology, CRC Press, 1986.
[42] L.F. Cabeza, G. Svensson, S. Hiebler, H. Mehling, Thermal performance of sodium acetate trihydrate thickened with different materials as phase change energy storage material, Appl. Therm. Eng. 23 (2003) 1697–1704. doi:http://dx.doi.org/10.1016/S1359-4311(03)00107-8.
[43] B. Nesbitt, Handbook of Pumps and Pumping, Elsevier Science & Technology Books, 2006.
[44] ZUWA, Flexible Impeller Pumps one design - four types, 2017.
[45] F. Bernhard, Technische Temperaturmessung, 2004. doi:10.1007/978-3-642-18895-4.
[46] Natiaonal Instruments, Callendar-Van Dusen Equation - NI-DAQ™mx Help - National Instruments, (n.d.). http://zone.ni.com/reference/en-XX/help/370466AC-01/measfunds/callendarvandusen/ (accessed August 30, 2017).
[47] B. Nehr, Auslegung, Bau und Inbetriebnahme eines PCM-Slurry Teststandes f¨ ur Di-Kaliumhydrogenphosphat-Hexahydrat, 2009.
[48] Mathworks, 1-D digital filter - MATLAB filter - MathWorks Switzerland, (2006). https://ch.mathworks.com/help/matlab/ref/filter.html#buagwwg-2 (accessed September 3, 2017).
[49] VDI-Gesellschaft Verfahrenstechnik und Chemieingenieurwesen, VDI-Wärmeatlas, 11. Auflag, Springer-Verlag, Berlin Heidelberg New York, 2013.

9. Appendix

9.1. Modified Sample Preparation for Material Characterization

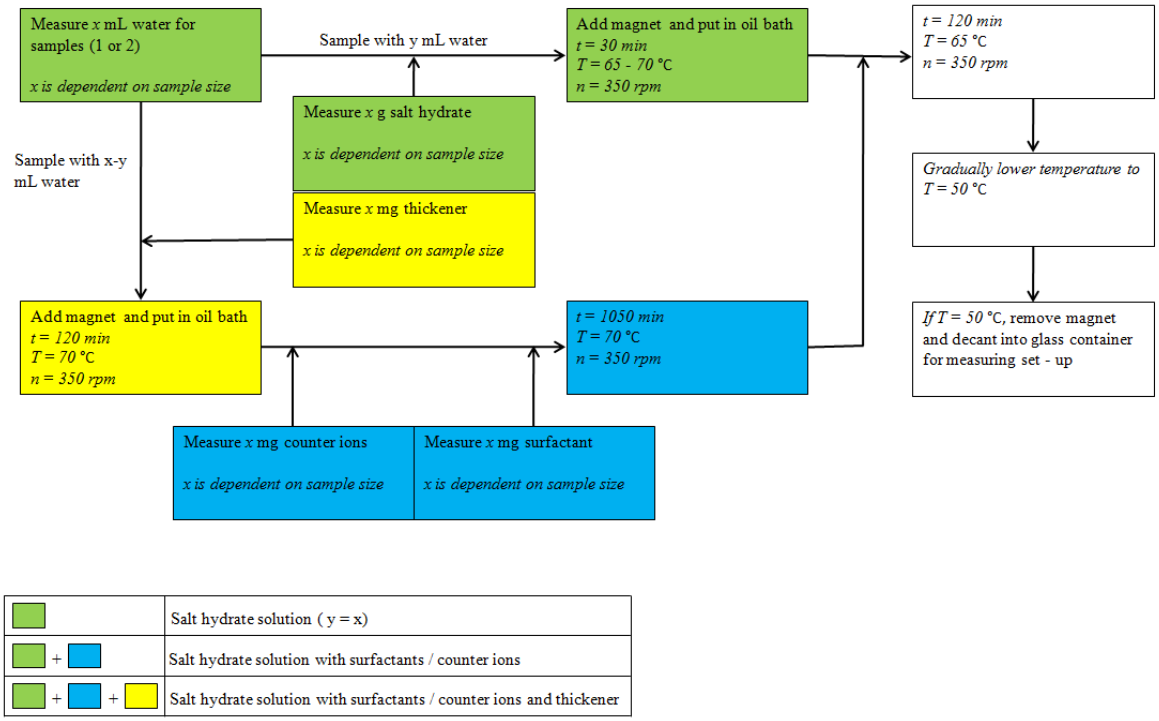

Schematic overview of the procedure to make slurry with a 35 wt% of salt hydrate in water. This procedure is used for samples that contain only the salt hydrate and water, but also for the solutions with additives

9.2. Dimensioning

Pipe diameter

The pipe diameter was determined as follows. Firstly, the PCM tank 1 volume which is given by the tank adopted from the baseline setup amounts to approximately $V_{PCS,T1}$ =15 L. The minimal batch time was set to t_{min} =3 min based on the experience made with the preliminary setup. The resulting maximal volume flow rate can simply be calculated as follows:

$$\dot{V}_{PCS,max} = \frac{V_{PCM,1}}{t_{min}} = 5\ Lmin^{-1} \quad (11)$$

Sedimentation can lead to a blockage of the piping system and should be taken into consideration in the piping design. For ice slurries, Kauffeld et al. recommend following empirically determined minimum flow velocity for horizontal tube sections in order to avoid phase segregation [24]:

$$v_{min} = 1.4 \cdot \sqrt{g \cdot D \left(1 - \frac{\rho_l}{\rho_s}\right)} \quad (12)$$

In Figure 62, the minimum flow rate required with a safety factor of two, which is recommended in by Kauffeld et al. in [7], is plotted against the inner tube diameter d_i. As shown, the critical tube diameter $d_{i,max}$ for a flow rate of 5Lmin^{-1} amounts to approximately 13.5mm. If the tube is dimensioned with a larger diameter, it must be expected that the resulting flow velocity with a flow rate of 5\Lmin^{-1} is too slow and hence sedimentation might occur.

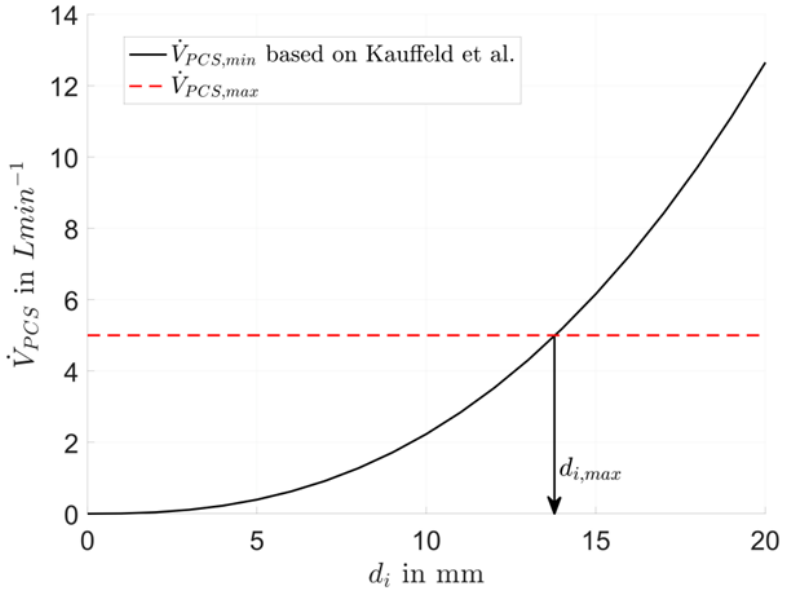

Figure 62: Red dashed line: maximal flow rate to achieve the min batch time required. Black line: minimal required flow rate to avoid sedimentation depending on the inner tube diameter d_i.

Due to the ratio between tube outer surface and cross-section area of the tube, it is in terms of thermal losses desirable to maximize the pipe diameter. Hence, based on the results shown in the plot above and with an additional safety margin, the inner tube diameter in the preliminary setup was set to **12mm**.

Pressure drop

The pressure drop in internal pipe flows Δp is in general described by following mathematical relation [49]:

$$\Delta p = \zeta \cdot \frac{l}{d_i} \cdot \frac{\rho \cdot v_i^2}{2} \quad (13)$$

where l is the length of the pipe, ρ the density of the fluid, v_i the velocity of the flow in the pipe and ζ the drag coefficient which is directly related to the reynolds number Re_i. For inner pipe flows Re_i is mathematically describes as:

$$Re_i = \frac{v_i \cdot \rho \cdot d_i}{\eta} \quad (14)$$

η is the dynamic viscosity of the fluid. For laminar flows, the drag coefficient ζ for smooth pipes is commonly defined as follows:

$$\zeta = \frac{64}{Re_i} \quad \textbf{(15)}$$

and according to Blasius for turbulent flows, the drag coefficient between $Re_i \approx$ 3'000 and $Re_i \approx$ 100'000 following simple relation is valid:

$$\zeta = \frac{0.3164}{\sqrt[4]{Re_i}} \quad \textbf{(16)}$$

Based on the material properties of AAH determined by Suzuki et al. in [40] and using the simple relation stated in Equation 16 for the calculation of the slurry density, the reynolds number and pressure drop can be calculated.

$$\rho_{PCS} = \frac{1}{\frac{x_H}{\rho_s} + \frac{1-x_H}{\rho_l}} \quad \textbf{(17)}$$

As previously mentioned, x_H describes the mass fraction of hydrate crystals in the solution. As illustrated in Figure 63, the reynolds number decreases with increasing hydrate fraction in the AAH solution. For an inner tube diameter of d_i=12mm and a volume flow rate of 5Lmin^{-1}, the flow regime is in the transition zone if the hydrate fraction x_H is close to zero. However, the flow regime becomes laminar if the hydrate fraction in the fluid is increased. This can be explained by the proportional relationship between the hydrate fraction and the viscosity of the slurry.

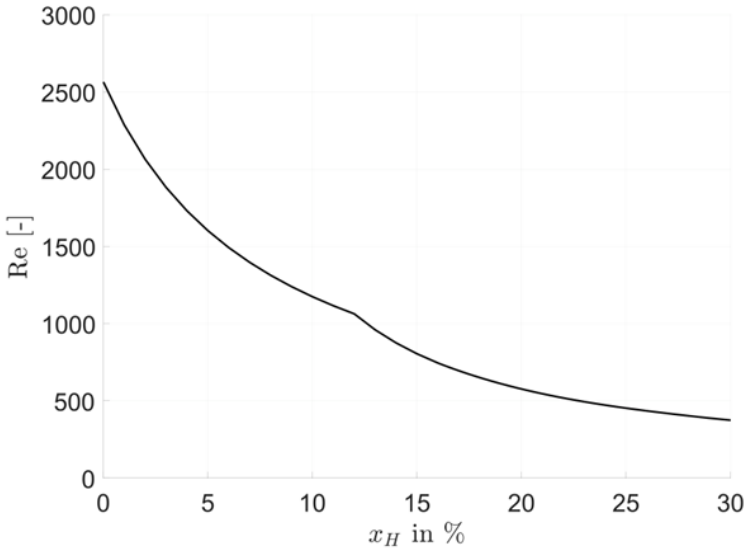

Figure 63: Reynolds number as a function of the hydrate mass fraction in the slurry. Due to the increased viscosity of the slurry with higher hydrate fraction, the reynolds number drops with increasing hydrate fraction.

In Figure 64, the resulting pressure drop as a function of the slurry flow rate and the hydrate fraction x_H is plotted. The tube length used in the calculations amounts to 5 m. It is furthermore assumed that the slurry has the same hydrate fraction in the entire pipe. As shown, for a volume flow of 5 Lmin^{-1} the expected pressure drop for a hydrate fraction of 30% in the entire tube is approximately 0.3 bar. If the pressure drop across the HEX and all valves is assumed to

be approx. 1 bar, the total pressure loss over the entire setup might amount to 1.3 bars which is relatively small. It must be mentioned, that due to the limited data available in literature, the viscosity values used to determine the pressure drop are based on a 35 wt% slurry. A slightly higher pressure drop might be expected for a 45 wt% slurry for an equivalent hydrate fraction and flow rate.

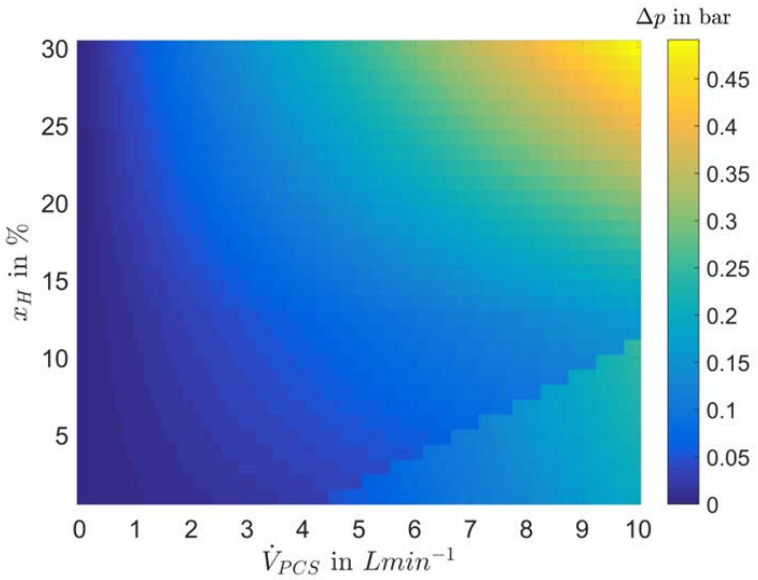

Figure 64: Pressure drop as a function of the hydrate fraction x_H and the flow rate of the ammonium alum hydrate slurry for a pipe with a length of 5m and inner diameter of 12mm.

9.3. Pump characteristics

The pump characteristic curves for different rotation speeds are plotted in Figure 65. The maximum pressure difference amounts to 5bar which is smaller as the max. pressure difference of the gear pump used in the preliminary setup. Regarding blockage of the system, this might be considered as a major disadvantage of the flexible vane pump. However, it is worth mentioning that Nehr used the similar pump type in a slurry test-rig using the salt hydrate K_2HPO_4 * $6H_20$ [47].

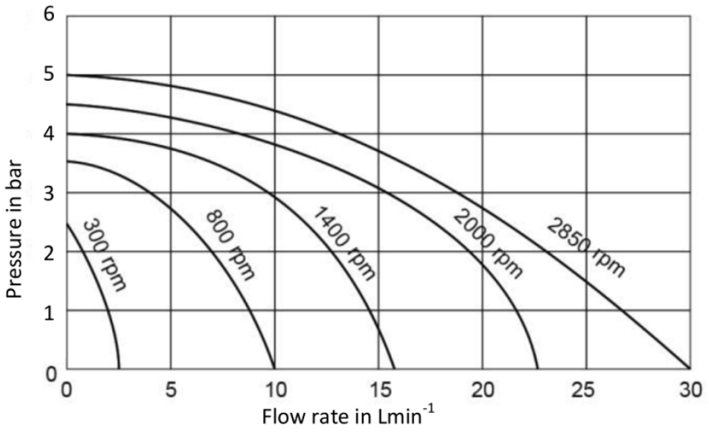

Figure 65: Pump characteristic curves of the used pump model *Nirostar 2001-A* with an NBR impeller for different rotation frequencies.

9.4. Measurement sensors

Measurement point	Symbol	Sensor type	Range	Measurement-uncertainty
Temperature of PCS in Tank 1	TI01 / $T_{PCS,T1}$	PT-100, Class A, Type TR1c R2108	-40 - 140 °C	$\pm(0.15\text{K} + 0.02T)$
Temperature of PCS at HEX inlet	TI02 / $T_{PCS,in}$	PT-100, Class DIN 1/5, Type TR1c R2108	-40 - 140 °C	$\pm(0.06\text{K} + 0.01T)$
Temperature of PCS at HEX outlet	TI03 / $T_{PCS,out}$	PT-100, Class DIN 1/5, Type TR1c R2108	-40 - 140 °C	$\pm(0.06\text{K} + 0.01T)$
Temperature of water at HEX inlet	TI04 / $T_{W,in}$	PT-100, Class DIN 1/5, Type TR1c R2108	-40 - 140 °C	$\pm(0.06\text{K} + 0.01T)$
Temperature of water at HEX outlet	TI05 / $T_{W,out}$	PT-100, Class DIN 1/5, Type TR1c R2108	-40 - 140 °C	$\pm(0.06\text{K} + 0.01T)$
Ambient temperature	TI06 / T_{Amb}	PT-100, Class DIN 1/5, Type TR1c R2108	-40 - 140 °C	$\pm(0.06\text{K} + 0.01T)$
Temperature of PCS in Tank 2	TI07 / $T_{PCS,T2}$	PT-100, Class DIN 1/5, Type TR1c R2108	-40 - 140 °C	$\pm(0.06\text{K} + 0.01T)$
Temperature of HEX surface front	TI08 / $T_{HEX,S1}$	PT-100, Class B, Type P0K1.232.2l.B.050	-50 - 200 °C	$\pm(0.3\,\text{K} + 0.005T)$
Temperature of HEX surface back	TI09 / $T_{HEX,S1}$	PT-100, Class B, Type P0K1.232.2l.B.050	-50 - 200 °C	$\pm(0.3\,\text{K} + 0.005T)$
Volumetric flow rate of PCS	FI01 / $\dot{V}_{PCS}$	Inductive, FLOMID 0 FX, Wisag SN: BH06896	10 - 1000 L/h	±0.5 % of reading value
Volumetric flow rate of water	FI02 / $\dot{V}_{W}$	Inductive, Promag 33A, Endress & Hauser SN: 1H 458908	54 - 1810 L/h	±0.5 % of reading value

Table 20: Sensors used in the experimental setup.

9.5. Solidification with 30°C water inlet temperate and blockage of the piping system

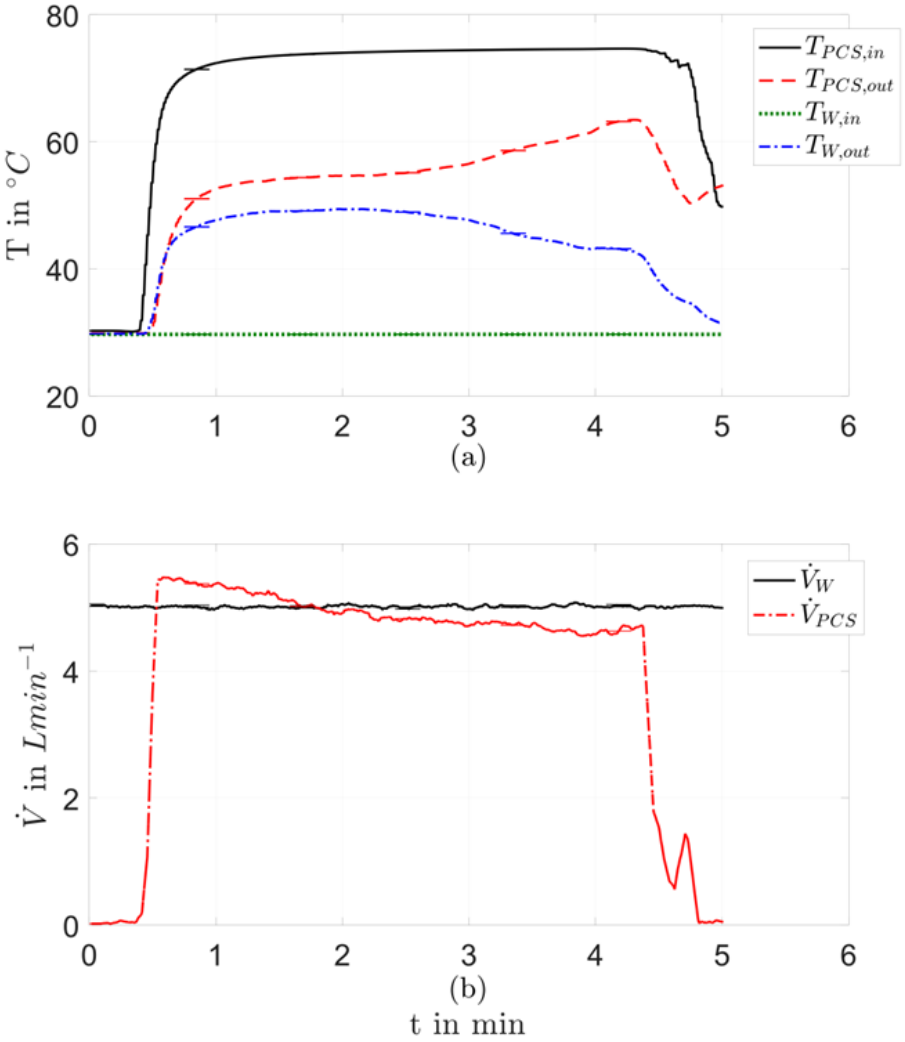

Figure 66. Heat exchanger in- and outlet temperatures (a) and flow rates (b) as a function of time for the 45wt% experiment with 30°C water inlet temperature. Due to the starting blockage of the test-rig, steady-state conditions could not be met.

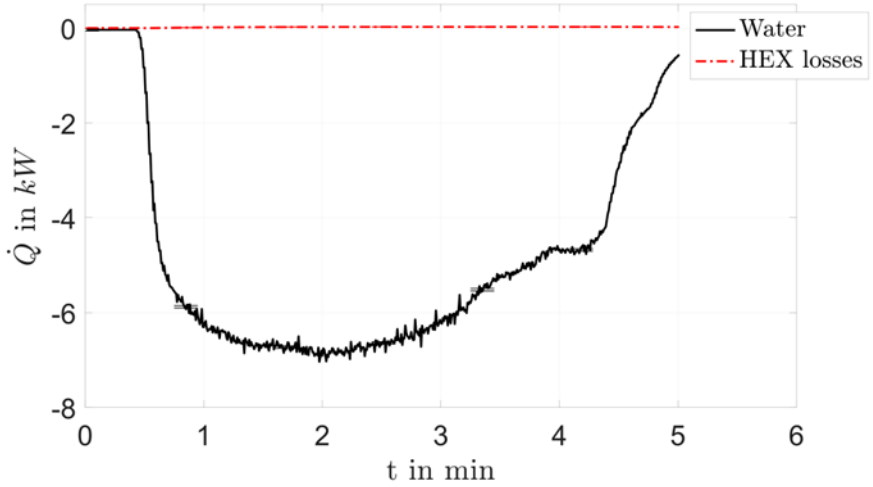

Figure 67. Heat flow rate determined by the water temperature change and flow rate in the HEX as well as heat losses in the heat exchanger as a function of time for experiment C3. After 2min a the heat flow rate starts to decrease to the blockage of the system.

9.6. Further development of test-rig

To improve the ability to investigate both, the crystallization and the melting of the PCS, a modification of the test-rig is proposed. In the present projects, the conduction of batch mode experiments was necessary to achieve steady-state conditions in the process. However, this condition could also be achieved in a continuous process if a second heat exchanger is installed as shown in Figure 68. Hence, in the first heat exchanger, the PCS could be cooled below the melting temperature using thermostat 1. An (optional) crystal releaser could be placed after the outlet of HEX 1. The crystallized PCS could then be heated up again in HEX 2 using the second thermostat. By the use of this approach, a continuous, accurate investigation of the crystallization and melting processes with less effort in comparison to batch experiments could be achieved. Furthermore, PCM tank 2 would become obsolete and the rig could be simplified.

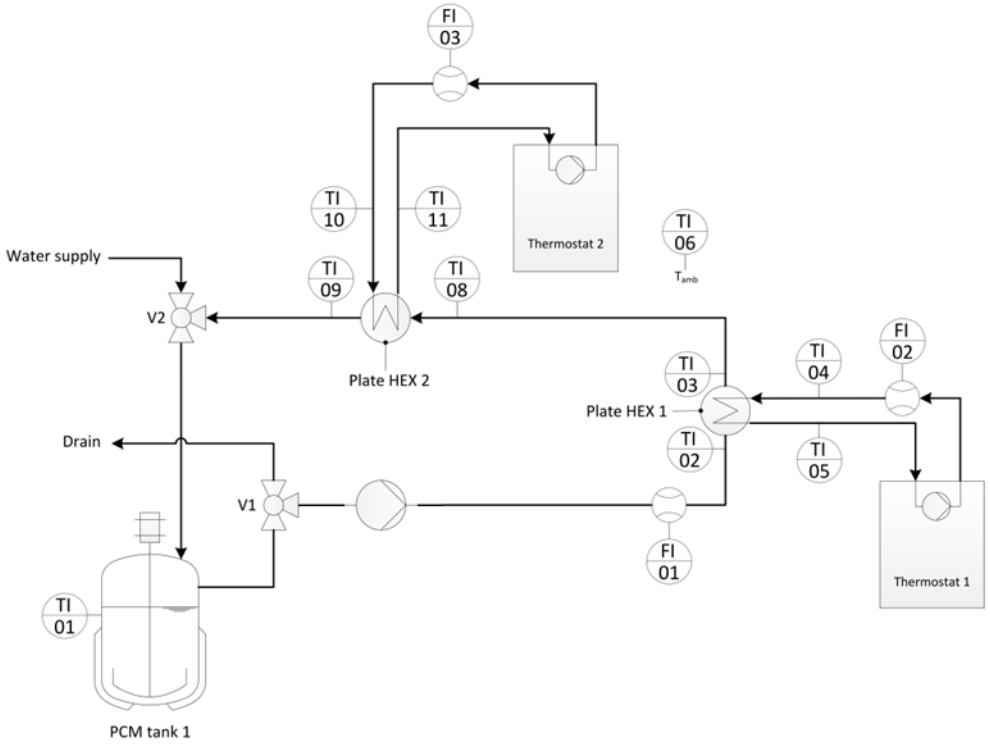

Figure 68: Proposed hydraulic scheme of the test-rig for future investigations.